Summer 2022

# Hybrid Theory-Machine Learning Methods for the Prediction of AFP Layup Quality

Christopher M. Sacco

# HYBRID THEORY-MACHINE LEARNING METHODS FOR THE PREDICTION OF AFP LAYUP QUALITY

by

Christopher M. Sacco

Bachelor of Science
Presbyterian College, 2017

Masters of Science
University of South Carolina, 2019

---

Submitted in Partial Fulfillment of the Requirements

For the Degree of Doctor of Philosophy in

Mechanical Engineering

College of Engineering and Computing

University of South Carolina

2022

Accepted by:

Ramy Harik, Director of Thesis

Subramani Sockalingam, Committee Member

Roudy Wehbe, Committee Member

Elizabeth Gregory, Committee Member

Federico Gasco, Committee Member

Tracey L. Weldon, Vice Provost and Dean of the Graduate School

# DEDICATION

To my Gramps. Our moments of joy are made bittersweet in the absence of the ones we love. Find rest and comfort in the eternal glory of the Lord.

# ACKNOWLEDGEMENTS

I would be remised if I failed to thank the many individuals and groups that have allowed me to participate in what has been an incredibly worthwhile period of research. Firstly, I would like to thank my advisor, Dr. Ramy Harik, for his steadfast encouragement and engaging instruction on this project. My dear friend, Anis Baz Radwan, has likewise contributed greatly to this research. I would like to acknowledge The Abnormal Corner. Without their patient instruction in all manner of software development and coding, I would not be to programmer and researcher I am today. The many undergraduates who contributed to this project deserve much praise for their efforts, many of which made contributions that directly helped this research. They include Nick Johnson, Drew Sander, Ian Ross, and Matthew Godbold. My friend and sage advice giver, Florentius-Johannes Van Zanten has been an excellent candidate for challenging questions. My former mentors, Dr. Chad Rodekohr, Dr. Eli Owens, and Dr. Clinton Harshaw were instrumental in forming my approach as a researcher and my experiences under their instruction were beyond valuable. Lastly, I must thank my supervisors, friends, and fantastic colleagues at Relativity Space for allowing me the opportunity to complete this course of study while beginning an exciting new adventure. Dave Leiphon and Jeff Campbell have been incredibly understanding and encouraging throughout this process and I doubt I would have found the end of this saga without their patience.

# ABSTRACT

The advanced manufacturing capabilities provided through the automated fiber placement (AFP) system has allowed for faster layup time and more consistent production across a number of different geometries. This contributes to the modern production of large composite structures and the widespread adaptation of composites in industry in general and aerospace in particular. However, the automation introduced in this process increases the difficulty of quality assurance efforts. Industry available tools for predicting layup quality are either limited in scope, or have extremely high computational overhead. With the advent of automated inspection systems, direct capture of semantic inspection data, and therefore complete quality data, becomes available. It is therefore the aim of this document to explore and develop a technique to combine semantic inspection data and incomplete but fast physical modeling tool into a comprehensive hybridized model for predicting and optimizing AFP layup quality.

To accomplish this, a novel parameterization of Gaussian Process Regression is developed such that nominal behavior is dictated through theory and analytic models, with latent variables being accounted for in the stochastic aspect of the model. Coupled with a unique clustering approach for data representation, it is the aim of this model to improve on the current state of the art in quality prediction as well as provide a direct path to process parameter optimization.

# TABLE OF CONTENTS

# LIST OF TABLES

# LIST OF FIGURES

# LIST OF ABREVIATIONS

ACSIS…….Advanced Composite Structure Inspection System

AFP……Automated Fiber Placement

ANN……..Artificial Neural Network

BO…….Bayesian Optimization

CAPP……..Computer-Aided Process Planning

CFRP……Carbon Fiber Reinforced Polymer

CNN……..Convolutional Neural Network

ECT…….Eddie Current Testing

ELM……Extreme Learning Machine

ELU…….Exponential Linear Unit

FCN…….Fully Convolutional Network

FPGA……..Field Programmable Gate Array

FRP……...Fiber Reinforced Polymer

GA……Genetic Algorithm

GAN……...Generative Adversarial Network

GFRP……...Glass Fiber Reinforced Polymer

GP…….....Genetic Programming

GPR…….....Gaussian Process Regression

GPU……..Graphical Processing Unit

IMT…….Ingersoll Machine Tools

JSON……...JavaScript Object Notation

KNN……...k-Nearest Neighbor

ML……Machine Learning

MLE……..Maximum Likelihood Estimation

MWUT……...Mann-Whitney U Test

NDT……Non-Destructive Testing

PINN…….Physics-Inspired Neural Network

PLC……Programable Logic Controller

PSO……..Particle Swarm Optimization

SVM……Support Vector Machine

ReLU……Rectified Linear Unit

RNN…….Recurrent Neural Network

RTM…….Resin Transfer Molding

UI…….User Interface

VARTM……...Vacuum Assisted Resin Transfer Molding

VCP…….Vericut Composites Programming

# CHAPTER 1

# INTRODUCTION

## 1.1 AN INTRODUCTION TO COMPOSITES

Composite materials are any material set consisting of a non-homogenous mix of two or more material types. This is typically done to augment the properties of both materials by engineering interactions on the material scale. In structural design, most often this is manifest in the development of anisotropic materials, or materials where properties vary depending on the direction traversed through the material. For most use cases, and especially in aerospace design, composites are almost always intended to refer to fiber reinforced polymers (FRPs)[1].

FRPs can come in a multitude of flavors, but primarily consist of a fiber material, usually either glass, aramid, or carbon-graphite, embedded within a polymer matrix [Figure 1.1]. The fiber takes the majority of the load, while matrix helps set shape and redistributes load among the fibers. Matrix materials can vary, with two general classes of thermoplastics and thermosets. Thermoplastic matrix materials are currently outside of the scope of this document, however it is useful to note that they have a number of desirable material properties and manufacturing characteristics. Thermosetting matrix materials vary

[1] Throughout this document, composites and FRPs will be used interchangeably.

widely with application, but common matrix materials include epoxy resins and vinyl ester resins.

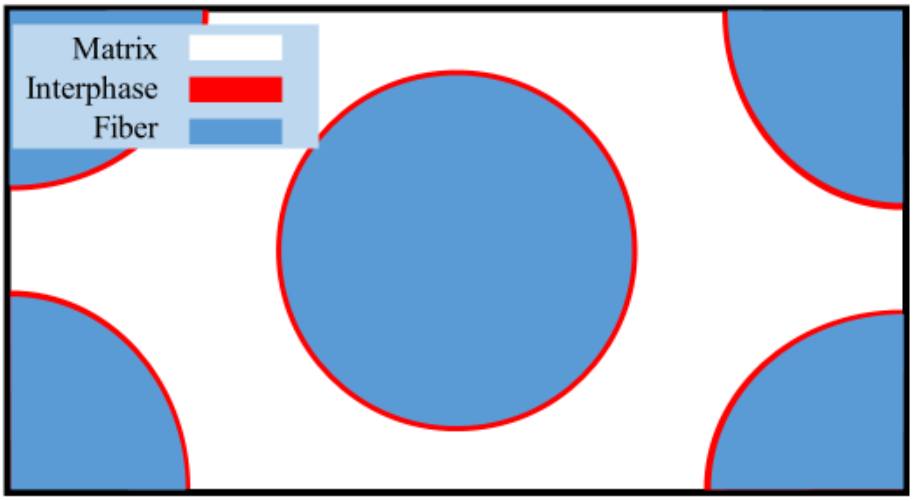


Figure 1.1: A Cross Section of an FRP Material

Much of the manufacturing of these types of composites centers around the cure process for the resin system. Simplistic cure mechanisms such as open air curing in a hot press can be used, but are generally abstained from in favour of more sophisticated techniques. Various infusion and cure methods have been developed, including Resin Transfer Molding (RTM) and Vacuum Assisted Resin Transfer Moulding (VARTM), where dry fiber is infused with matrix and then allowed to cure under vacuum, often at room temperature. A common vacuum bag setup can be seen in Figure 1.2.

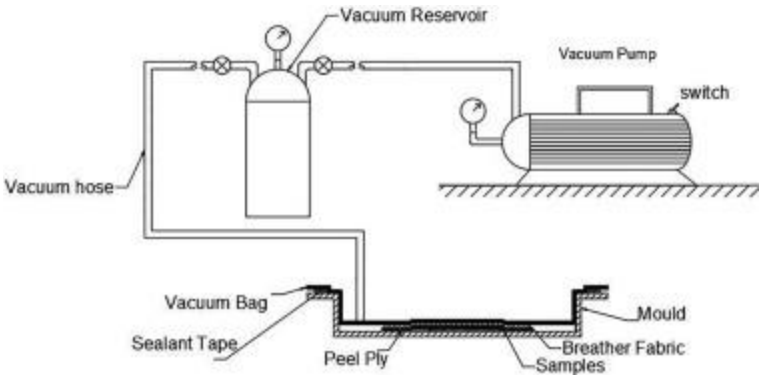


Figure 1.2: A Vacuum Bagging Setup Common in VARTM [1]

For large aerospace structures using a thermosetting material, the cure cycle requires additional pressure and heat for proper material consolidation and cure. Therefore, it becomes necessary to use an industrial autoclave. Parts are bagged in a similar fashion to VARTM curing and placed in the autoclave [Figure 1.3], where heat and pressure are applied to the part over the duration of the cure.

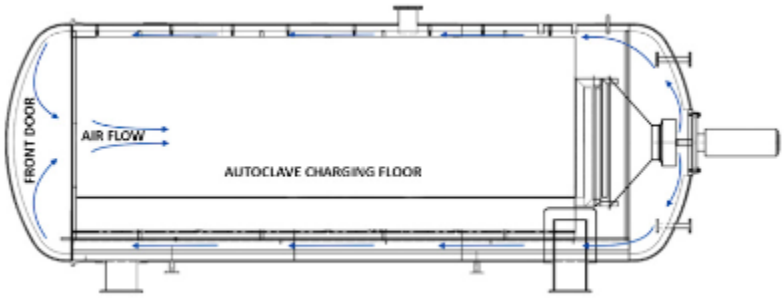


Figure 1.3: Autoclave Model for Curing of Composite Prepregs [2]

## 1.2 AN OVERVIEW OF AUTOMATED FIBER PLACEMENT

Automated Fiber Placement (AFP) marries advanced robotic placement with composites manufacturing to produce and additive manufacturing process that has a higher rate of production and is more consistent than hand layup. As an additive manufacturing process, AFP requires the deposition of composite material on a tool surface. This material is typically thermosetting, but thermoplastics have been an increasing source of curiosity

over the last decade [3]. The AFP machine has a few common features: a material feeding mechanism, a heater that increases the pliability and tackiness of the material prior to deposition, some type of actuation system, and a compaction mechanism that ensures proper adherence of the material to the surface. Multiple approaches exist for developing each component of an AFP machine, with various mixing and matching among the accepted standards for each component. One AFP configuration can be seen in Figure 1.4, however the look and function of AFP machines can vary dramatically between manufacturers [4].

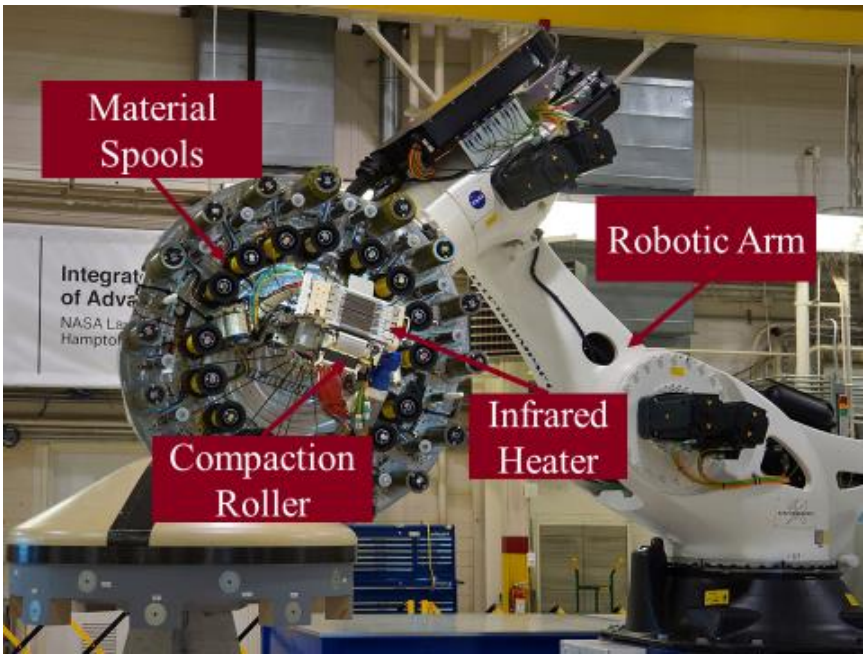


Figure 1.4: ISAAC AFP Machine at NASA Langley with Robotic Arm, External Material Spools, and an Infrared Heater [5]

AFP deposits strips of material, denoted as tows, in groups call courses onto a tool. Consecutive courses placed next to each other constitute a ply. Multiple plies laid on top of one another create a completed part [Figure 1.5]. By articulating where the head is placed during deposition or controlling placement of where the tows are cut, differing stiffness properties can be tailored across the part.

This variable stiffness approach is most commonly represented is steered fiber laminates [6], [7], where AFP material deposition is done in such a way that courses are placed on curved paths. Therefore, stiffness and strength properties can be continuously tailored for the part, rather than discretized or constant properties. This has the potential to greatly reduce the weight of the overall structure [8] and has been the focus of intense investigation for aerospace applications. Removed from explicitly tailoring the stiffness properties of a part using steered placement, complex geometries often necessitate steering of some kind. Thus, understanding dynamics in fiber steering is necessary for layup across any general geometry, even when explicit stiffness tailoring is not necessary.

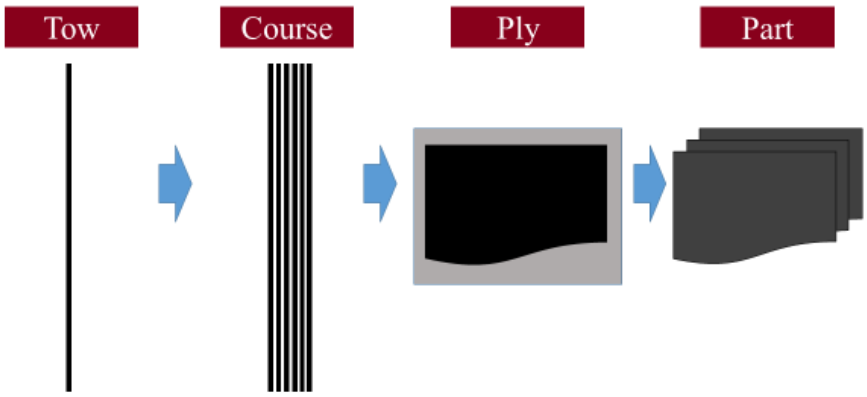


Figure 1.5: Components Constituting an AFP Manufactured Composite Part

### *1.2.1 Automated Fiber Placement Defects*

AFP, while an effective and efficient way of producing a composite structure, has a number of drawbacks. Critically, the sensitivity of input parameters and the physical restrictions of the machines themselves frequently result in defects during layup. These defects can manifest in several ways and are characterized extensively in literature. The quality of the final AFP-manufactured part is directly correlated with the number and

severity of these defects. A significant enough concentration of defects in a structure can have a notable effect on the overall structural performance of the part [9], [10]. The author has extensive experience in the inspection of AFP manufactured composites, with an eye towards in-situ inspection such that defects can be identified and corrected early in the manufacturing process [11]–[13].

## 1.3 RESEARCH OBJECTIVE AND OUTLINE

AFP has become a standard tool in the manufacturing of large-scale composites structures. The marrying of composites manufacturing with high-precision robotic placement has yielded an additive manufacturing technique that has found success in the aerospace field.

The automated nature of AFP has come with large problems of complexity in the manufacturing process. AFP as an additive process involves the complex interaction of many physical phenomenon. The inhomogeneity of the material requires the consideration of micro-mechanics models. The tensioning and feeding of the tows during laydown is the purview of macro-mechanics. Heating elements for the tacking of the material to the tool is a thermodynamic and heat transfer problem. Depending on materials systems, viscous flow of resin must also be taken into account. Thus, the modelling of the AFP process is incredibly complex, often resulting in physical models that are either inadequate, or have run times considerably longer that what is acceptable for more dynamic production environments.

The gap between physics-based models and real-world practice in AFP is apparent in the strategies utilized in industry for the identification of optimal processing windows or defect predictions for a given geometry. Typical methods for determining part quality

in industry are simply a function of experiment and experimental design. Often months of tests and tweaks are required to adequately produce a part of acceptable quality.

Table 1.1: A Collection of Notable Defect Types Identified by Harik et. al. [14]

| Defect | Description | Cause |
|---|---|---|
| Gap | Unoccupied space between tows | Steering errors or layup on a complex tool |
| Overlap | Placement of a tow onto an adjacent tow | Steering errors or layup on a complex tool |
| Wrinkle | Wavy pattern at the boundaries of a tow resulting on only partial tool contact | Small steering radius; Overfeeding material |
| Twist | A tow rolled axially 180 on itself and then compacted by the roller | Friction between guide holes or overly tacky tows; Fold propagation |
| Missing Tow | An entire tow falls off the tool or is never applied | Material feed error; Adhesion problems |
| Splice | Two tows are joined end-to-end so that they overlap | Result of finite length slit tape for forming tows |
| Pucker | Lifting up of a tow from the tool surface along the tow width | Overfeeding material; Machine error |

Tools exist for the prediction of part quality, such as Vericut VCP [15]. However, these tools are often only concerned with part geometry, which limits the predictive power in the context of the manufacturing process as whole. There currently exist no widely available tools to evaluate part quality over a range of defects with respect to geometry *and* manufacturing parameters. Numerical codes exist to compute structural responses of individual tows using finite element methods. However, the scope of these models are fundamentally limited and run times are lengthy.

The limitations identified in the above are indicative of the need for a new approach to predicting part quality and even optimizing aspects of the AFP process. Thus, any attempt at such a problem must be able to address the creation of a model with the following attributes:

- Low run time
- The ability to quantify uncertainty
- Interpretability
- Ability to be used for further process optimization

### *1.3.1 Inspection and Inspection Informed Manufacturing*

The adoption of machine learning (ML) and other data analysis techniques over the last decade has greatly increase the amount of useable *semantically informed* data. Accelerating this trend is the transition to industry 4.0, with a multitude of data sources available for analysis. Management of these data sources, including organization and pipelining, create an ecosystem through which rapid decisions can be made on the shop floor [16].

In the context of AFP, several automated inspection strategies have allowed for the rapid evaluation of a part in manufacturing time, creating a source for qualitative data about the overall quality of the part being produced. Profilometry enabling rapid height profiling [17], and thermography using the residual heat from the laydown process [18], [19] are leading data acquisition methods for the evaluation of AFP parts during manufacturing. Coupled with ML-based computer vision algorithms, these systems can precisely quantify defect production. Already, small scaled experiments have demonstrated that automated inspection systems can directly inform the manufacturing process [20].

This begs the question: can an inspection system somehow aide in the discovery of governing mechanics in AFP?

### *1.3.2 Pure Data Approaches*

The newfound quantitative quality data afforded by the automated inspection systems leads to a potential new direction of exploration; that of the statistically or ML-driven approach to discovery of governing mechanics through a pure data approach. Those who have worked in depth with many of the out-of –the-box ML or statistical methods are painfully aware of the need for many testing and training samples. In classical areas of use for ML, such as natural language processing and computer vision, many training samples can be gathered quickly and cheaply. In addition, it is often applicable to bootstrap previously successful models for a new application provided the datasets have a similar distribution.

In the case of predicting the responses of large industrial processes, such as AFP, material and equipment costs coupled with a significant time investment for experimentation places a fundamental limit on the amount of data that can be collected.

Millions of samples would be impossible; thousands might be achievable through massive coordination across industry and academia. More realistically, manufacturers and labs are siloed off from one another implying that, at best, a few hundred parts could be run over the course of months or years. Further, the data generated must be of the proper distribution to generalize enough to be widely applicable.

It has been noted, especially when considering neural networks and deep learning, that current ML approaches are incredibly sensitive to the distribution of training samples. This means that while many ML approaches are fantastic engines for interpolation, they fundamentally lack when considering new samples that are significantly different from the training set. Additional problems such as overfitting in more complex models further compound on the issue.

Using pure ML approaches to derive relationships between the AFP process and defect production contains fundamental challenges from multiple perspectives. The availability of data, the distribution of data, and inability to account for radical deviations from previous samples would appear to doom the "Machine Learn Everything" approach. What is needed is an entirely new approach that, while able to usefully account for experimental data, can also incorporate other sources of knowledge to aide in the learning process.

### *1.3.3 Hybrid Physics-Data Models*

This coupling between knowledge systems and experimental data can take a number of forms. However, the representation ability of ML should not be casually thrown away without attempt at incorporation. What is concluded then is that a new paradigm not reliant solely on a single information source should be developed for the prediction of AFP

defects. Hybrid models capable of adjusting imprecise analytic models with stochastic data from experiments represents a fundamental change towards the ongoing shifts in AFP manufacturing. By leveraging all available knowledge sources, the problems in both a purely analytic model and a purely data driven model can potentially be overcome.

Hybrid models can account for mean behavior using the physics-embedded knowledge, while accounting for both stochastic fluctuations in real-world systems and undiscovered latent variables. Nosie parameters and unknown physics account for a large part of failed modelling attempts.

What these types of models can also potentially provide is a degree of interpretability and insight that would be previously difficult in “black-box” machine learning approaches. The hesitancy in many industry settings in the adoption of large-scale machine learning applications stems directly from this lack of interpretability. Thus, by embedding physics-enabled knowledge, many qualms from machine operators may be reduced, as the reasons for system decisions become obvious. In the applications of certain hybridization approaches, uncertainty quantification can also be performed, further aiding in offering explainable modelling approaches.

## 1.4 PROCESS IMPROVEMENT

Accurate, efficient, and explainable modeling of predictive AFP layup quality should also come with a corollary of enabling process improvement through the explicit modeling of system dynamics. Optimization should naturally follow knowledge representation with a goal of improving the key response features. This is where past inspection data should become particularly useful, with the ability to define a quasi-distance metric to allow for direct comparisons between proposed manufacturing

configurations and past manufacturing data. In this case, complex representations (i.e., neural-style solutions) may not be required to express this, instead relying on aspects of metric theory, topology, and probability theory to identify paths from previous experiments to new, better configurations.

## 1.5 OVERVIEW OF DOCUMENT

The information contained in this document will be referenced with the necessary flow of information indicative of how this research was conducted. Chapter 2 will expound upon the concepts and techniques of model hybridization across multiple disciplines, with a particular eye towards past applications in composite materials. Joining these discussions will be the presentation of the current state of the art for defect prediction in AFP, and some relevant methods in machine learning that have become popular. Chapter 3 outlines a theoretical methodology for the hybrid approach to defect prediction. This includes rational for why certain common industry tools should provide a good representation of mean behavior in the system. Chapter 4 will present an argument based on experiment that would indicate that geometric arguments are suitable for the mean function definition for the hybridized model. Chapter 5 will present data collection mechanisms and an experiment to collect samples that will then be used to train and validate a hybridized ML model. Final results and some notes on implementation will be shown in Chapter 6. Lastly, a final conclusion will be offered including situating this work in the larger project of closing the loop in AFP and indications where the next phase of this work could be pushed.

# CHAPTER 2

# LITERATURE REVIEW

The advent of modern computing tools in engineering applications

## 2.1 INTRODUCTION

The incorporation of hybrid data-physics models is well documented in literature. Something as simple as an empirically set parameter in a model has been a consistent feature of attempts to predict behavior of systems that are often too complex to represent by purely analytical methods. With the advent of machine learning, strong representative abilities of learning through data meant that hybridization could take on a different form to empirically determined parameter values. Hybridized models tackle two problems representative of analytic and data driven models. In analytic models, should the system dynamics or mechanisms not be fully understood, then either the use of the model must be restricted to those situations where the poorly understood mechanisms have minimal influence, or a loss in predictive accuracy and generalization of the model. Purely data driven models have several significant limits that are currently preventing extension to broad fields.

## 2.2 MACHINE LEARNING

### *2.2.1 Algorithms and Techniques*

Machine learning is a set of processes and their respective algorithms that automatically create relationships between sets of data. These algorithms can be extended

for use on classification tasks, clustering, and even image and signal processing. Algorithms such as Artificial Neural Networks (ANN) [21], [22], [Figure 2.1] and Support Vector Machines (SVM) [23] have allowed greater generalization of tasks. Particularly in industry, *supervised learning processes* are utilized to develop accurate and high generalization systems. The latter are then trained on a set of input data and are expected to produce a desired output when shown a similar data sample. The great advantage of machine learning systems is that they can take highly dynamic and non-linear data sets spread among a large number of features and find relations between inputs and desired outputs. Hornik et al. showed that multilayer networks are capable of approximating any non-linear function given enough hidden layers[24].

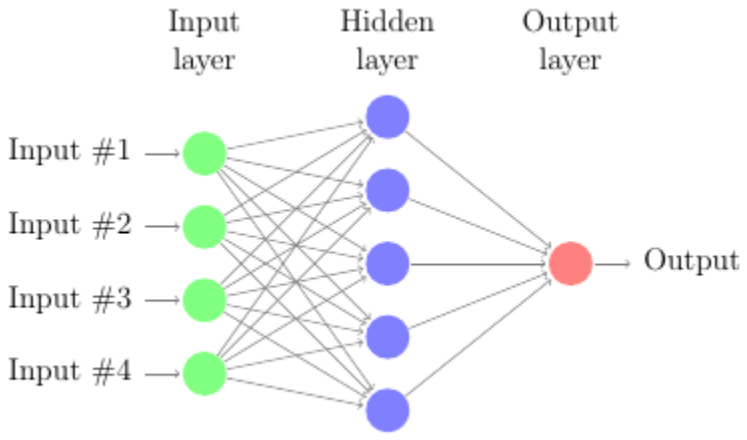


Figure 2.1: A schematic of a basic neural network

Nerual Networks consist of general computing nodes that sum the inputs into the nodes, pass the summation into a function, *A*, known as the activation funciton, to skew the output, and then passes that output onto other nodes using a weight, *w*, to scale the output [Figure 2.2**Error! Reference source not found.**]. Ocassionally an additional term know as a bias, *b*, will be added into the input. In general, a single neuron of a Neural

Network can be expressed in Equation 2.1. It can be noted that in the case where *A* is the unit function or provides a linear output, then the neruon reduces to a linear regression model. Commonly, activation functions avoid learization of outputs and seek to either scale or gate outputs. Popular activation functions include Sigmoid [Equation 2.2], ReLU [Equation 2.3], and ELU functions [Equation 2.4].

$$o_j = A\left(\sum W_{ij}x_i + b_i\right) \quad 2.1$$

$$Sigmoid(i) = \frac{1}{1 + e^{-i}} \quad 2.2$$

$$ReLU(i) = \begin{cases} i \leq 0 \; then \; 0 \\ i > 0 \; then \; \alpha o \end{cases} where \; \alpha \in R \quad 2.3$$

$$ELU(i) = \begin{cases} i \leq 0 \; then \; \alpha(\exp(i) - 1) \\ i > 0 \; then \; i \end{cases} where \; \alpha \in R \quad 2.4$$

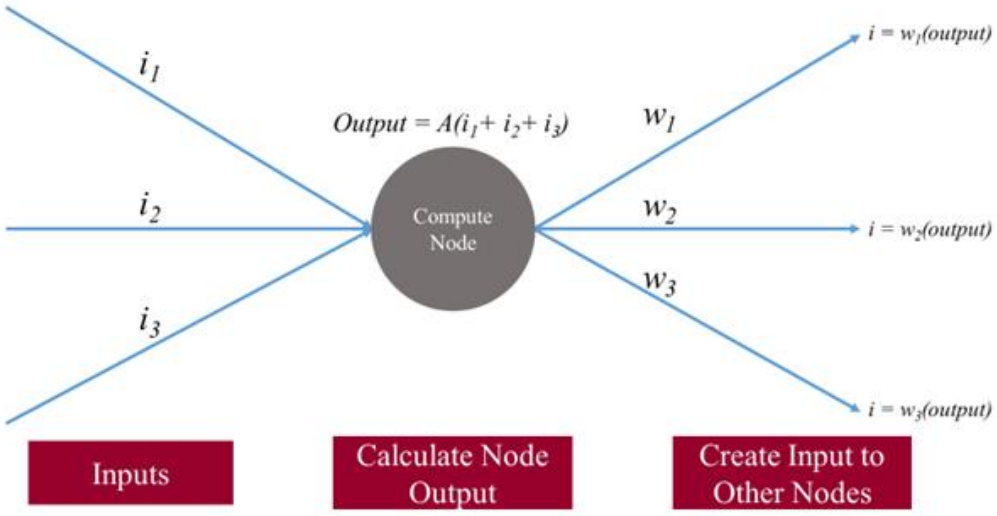


Figure 2.2: A Neural Network Compute Node

In addition to the techniques listed above, algorithms such as the Single Hidden-Layer Feedforward Neural Network Extreme Learning Machine (ELM) [25] , k-Nearest Neighbor (KNN) [26], and decision trees have also found acceptance as useful tools in the ML community. Each respective algorithm has specific tasks for which it was constructed [Table 2.1].

There are two common techniques by which ML algorithms are trained on data: (1) supervised learning and (2) unsupervised learning. Supervised learning implies that the ML model infers relational information through minimizing the difference between labeled training data and network predictions. If an algorithm were to be trained to classify pictures, an input picture would be given to the algorithm, which would make a prediction. This prediction would be then compared to a true labeling of the image, and the properties of the algorithm would be updated to correct the errors of the initial prediction. In ANNs, this is usually accomplished through a gradient descent approach with using the backpropagation algorithm. Unsupervised learning implies that the ML algorithm is allowed to explore a solution space until a generalized solution is reached. This idea is connected to a number of ML tasks including reinforcement learning and autoencoders. As a result of data labeling often being the most intensive portion of creating a machine learning model, unsupervised learning has become an area of enormous potential and could allow for the development of true online learning systems.

Table 2.1: Some ML Algorithms and Their Respective Objectives

| **Algorithm** | **Task** |
|---|---|
| KNN | Classification, Regression |
| SVM | Classification |
| Neural Nets | Classification, Regression |
| Principle Component Analysis | Dimensionality Reduction |
| Self-Organizing Map | Clustering |
| ELM | Classification, Regression |
| Naïve Bayes | Classification, Probability Density |
| Maximum Likelihood Estimation | Probability Density |
| K-Means | Clustering |

Each ML algorithm is attempting to create a model for the mapping of an input vector $I$ to an output vector $o$ according to a list of model parameters $\theta$ such that

$$o = F(I|\theta) \tag{2.5}$$

In non-parametric learning models, such as KNN, these parameters are intrinsic to characteristics of data itself. Thus, the concept of "training", or using data to infer $\theta$, is simply a matter of adding additional data to the model. In these cases, the interpretation of the model is typically straightforward, however the need to observe the properties of each data instance can be both computationally and memory intensive.

In algorithms such as Neural Networks, the goal is to explicitly model a probability distribution without knowing any of the priors. Thus, updating the parameters of these models becomes an exercise in defining the error $E$ between the observed target distribution

*r* and the distribution output from the model *y*. The latter has a fundamental dependence on model parameters, and thus it is possible to define $E$ in terms of $\theta$. In order to find the change in $\theta$ for the optimal model, one may simply observe the error gradient from each training instance between targets and outputs in terms of $\theta$ [Equation 2.6].

$$\Delta\theta = \eta \frac{\partial E}{\partial \theta} \tag{2.6}$$

Where the total update for model parameters for the sequential step s becomes

$$\theta(s+1) = \theta(s) + \Delta\theta \tag{2.7}$$

Where $\eta$ is the learning rate, or the size of step that is taken over the gradient in moving towards the optimum. This technique is known as gradient descent. $\eta$ does not need to be a constant. Several variations of the algorithm have been developed to allow for an adaptable $\eta$. These included Adagrad [27], ADADELTA [28], and AMSgrad [29] algorithms.

In the case of non-differentiable evaluation functions, different update rules must be derived. For Decision Trees, impurity measures are used to determine model complexity and parameters.

*2.2.2 ML Objectives*

ML can be used for a number of tasks. Firstly, classification has become an area where ML has begun to dramatically change what is possible in industry. With the advent of AlexNet in 2012 [30], image classification accuracy was improved to a point where it began to rival human testers in some tasks. Classification can also be viewed as a subset of interpolation and extrapolation. Therefore, regression similarly falls under the domain of potential ML applications. Thus, as the reader will discover in later sections, ML can be

utilized as a powerful tool for generating additional data points without having to rely on laborious computations.

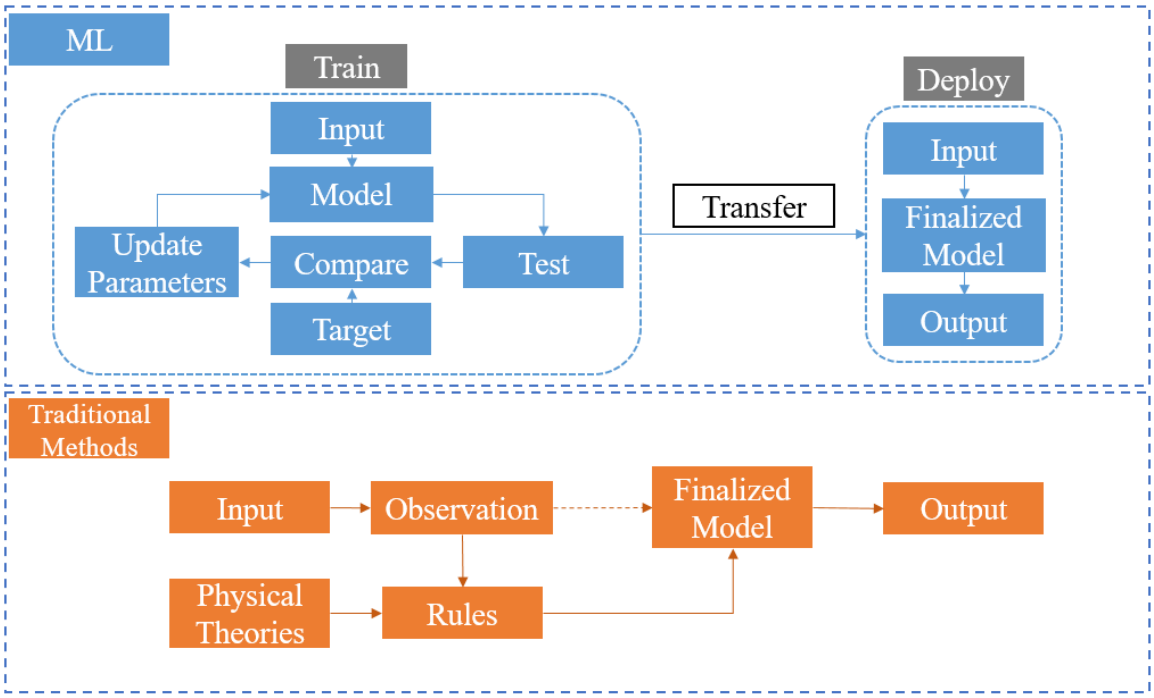


Figure 2.3: Machine Learning Comparison to Traditional Modeling Methods

In addition to classification, representation has become a unique field that ML has begun to broach in recent years. A Generative Adversarial Network (GAN) is a remarkable training structure that has the capacity to produce a representation of most datasets. In the computer vision field, GANs have been used to generate entirely new and unique data that can show complex scenes [31]. In doing this, GANs learn a number of low level features that can either be used as a pre-training phase for a classification network or leveraged for understanding the key feature components of data through feature extraction. Autoencoders [32], a neural network structure that embeds semi-semantic meaning of a data instance into a low-dimensional latent space, also has application to representation. By providing inputs directly into the latent space, one can render new original examples in the original feature space the autoencoder was trained on.

Clustering is another task that ML can have direct application to. Neural network strategies such as the self-organizing map [33] can accomplish clustering in an unsupervised learning task. The K-Means algorithm [34] can be utilized as a clustering algorithm that is non-parametric.

Reinforcement learning is one of the oldest subsets of ML. Conceptually, a network is trained to maximize a reward generated through making decisions in an environment. This demonstrates reinforcement learning as an optimization algorithm, capable of developing policies that generate the largest rewards possible. This structure has been used to learn complex tasks; occasionally in a beyond human capacity [35]–[37]. While playing the Atari 2600 games referenced in [38] at a grandmaster level is an interesting way to prove the viability of reinforcement learning based task solving, one can clearly see its application in any general setting involving choice-based optimization. There are a number of interesting attempts to integrate reinforcement learning into scheduling and intelligent control of machines [39].

Table 2.2: ML Types and Common Tasks

| **Supervised Learning** | **Unsupervised Learning** | **Reinforcement Learning** |
|---|---|---|
| • Classification<br>• Regression | • Clustering<br>• Dimensionality Reduction | • Decisions Under Uncertainty |

*2.2.3 Notes on Hardware Implementation*

One of the developments that has most recently allowed ML to come to the forefront of data analysis is the development or incorporation of dedicated hardware into

ML training and operation. The Graphical Processing Unit (GPU) has become a notable addition to the ML researcher's toolkit in recent years. It allows for faster training and operation on increasingly broad ranges of data [40], [41]. This stems from the ease with which the common matrix algebra in ML is run in parallel on GPU. Another hardware implementation of ML that has recently gained traction is the Field-programmable Gate Array (FPGA). The latter are effectively programmable silicon, allowing for individual logic gates to be moved in such a manner that the ML architecture is physically embedded on the circuit. They have a number of advantages in ML implementation including faster operating speed and lower power consumption [42]–[44].

### *2.2.4 Other Artificial Intelligence Techniques*

There are a number of noted statistical optimization techniques adjacent to the ML field that are worth mentioning. Often, these techniques include a number of properties that are distinct from pure ML, but the underlying concept of creating system models from pure data is shared between the two methods. One of the most widely used class of algorithms exhibiting this behavior are the evolutionary approaches. Genetic Algorithms [45]–[47] and Genetic Programming [48]–[51] can yield complex structure through a mixing of solution properties that mimics biological evolution. Other heuristic statistical problem solving techniques include Particle Swarm Optimization [52]–[56], similarly mimics biological systems by simulating the behavior of flocking animals.

## 2.3 COMPOSITE MATERIAL INSPECTION TOOLS

Due to their low contrast, the imaging of composite materials for defects has proved difficult in the past. Surface and subsurface defects manifest in a number of ways, and thus finding methods for imaging analysis must be equally as broad. Generally, conventional

visual spectrum images are not viable as an inspection technology. The low contrast, particularly of carbon composites, makes feature identification challenging. However, laser profiling, thermal imaging, eddy current inspection, and a number of other additional non-conventional imaging techniques have had great success in the non-destructive testing (NDT) process.

Thermographic-based composite inspection begins with the excitation of material through a heat source. This is typically accomplished through the use of a halogen lamp, however LED heat sources have also been used [57]. The propagation of heat through a structure is almost entirely dependent on material properties, and thus where those properties have changed due to damage[2] heat transfer will occur differently from the background material. As this transfer is taking place, thermal cameras capture the differences and produce an image of the structure under inspection. Two variations of the thermographic techniques are lock-in and long pulse thermography. Lock-in implies that detection and excitation are happening simultaneously in a pulsed pattern, which results in higher quality IR images [58]. Long pulse thermography involves the extended excitation of the structure, which can be useful in poorly conducting materials such as composites [59]. [60] notes that thermography struggles in identifying deep subsurface defects or defects across complex geometries.

[2] Such as the production of voids or delaminations.

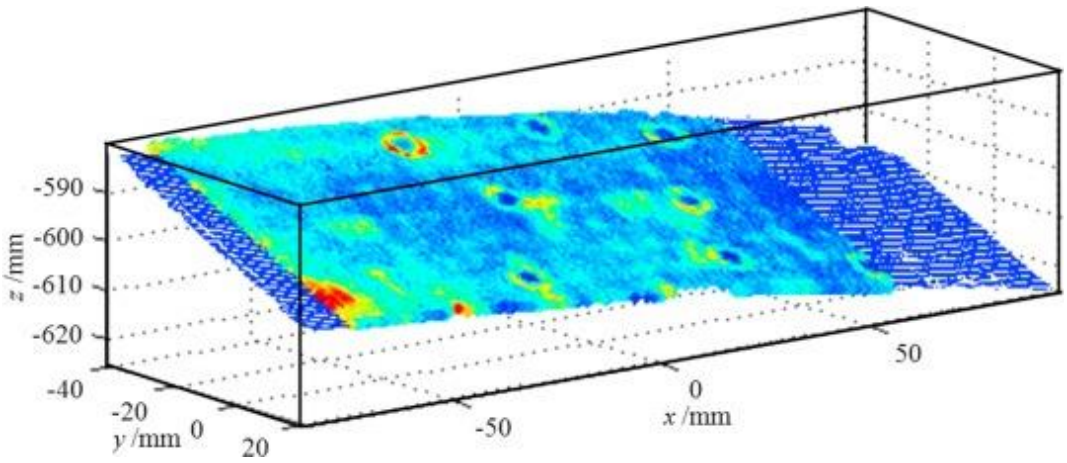


Figure 2.4: Thermography Data from CFRP Part [61]

[62] uses three infrared cameras operating at different wavelengths to create a complete scan of a composite aircraft structure. [63] examines a number of advanced image processing techniques to improve the inspection of a composite plate with hand-placed cracks. [64] demonstrates the use of Sparse Principle Component Analysis in Thermography for the structural health monitoring of a CFRP plate with induced defects.

Profilometry is another popular NDT technique most often utilized in the 3-dimensional rendering of a surface. A laser pattern is projected down onto a surface, through which surface features are inferred from deviations in the pattern [65]. The advantage of profilometry is the rapid profiling of a surface without the need to take surface contrast into account. However, [11] observes that material type in AFP inspection can have a direct effect on data loss and artifact production. Ultrasonic inspection has become a leading NDT technique in composite materials. Ultrasonic project sound waves into a test article and look for inference patterns in either the return echo[3] or the sound waves

[3] Known as Pulsed Echo Technique

propagated through to the other side of the structure[4] [66]. There are a number of parameters that can affect both the resolution and penetration depth of an ultrasonic signal such as frequency [67].

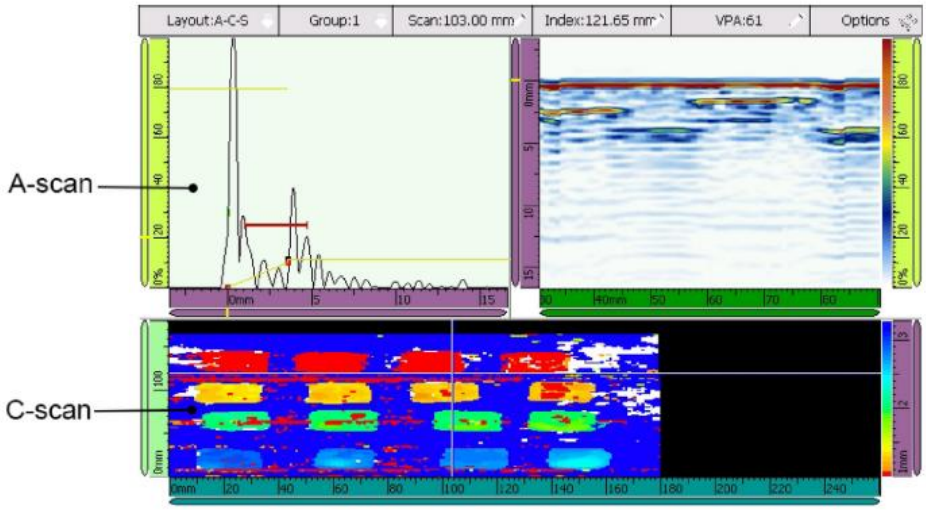


Figure 2.5: Ultrasonic Inspection Scans from Meng et al. [68]

Eddy current testing (ECT) has gained notice in the last several years for their ability to detect deep sub-surface defects in composite structures without the need for contact with the structure [69]. ECT measures the electrical properties of a sample. Using the electrical impedance sampled in ECT, it is possible to identify local changes in the reference material. ECT can be particularly useful in determining fiber angle error post-manufacturing, which makes it adept at identifying gaps and waves in a given composite part [70].

[4] Known as Through Transmission Technique

## 2.4 ML IN INSPECTION

The general complexity of composite manufacturing ensures that defect will inevitably be produced in some manner. Composite materials, specifically CFRP and GFRP laminates will have material properties dramatically affected by manufacturing defects. Thus, screening for said defects in an efficient and effective manner can be a key stage in the production of composite parts. The often dynamic and visual nature of inspection processes dictates that, until recently, human expertise had to be used for accurate results [71]. Thus, a number of studies have leveraged machine learning to perform various inspection tasks on composites.

[72] proposes a system by which several sensor systems are integrated with ML algorithms to detect defects resulting from the drilling of carbon fiber composites for aircraft wing assemblies. A three step process of data collection, feature extraction, and data analysis was constructed. Optical and thermal systems were used for the inspection process, but the author makes note that a host of additional sensors such as eddy current sensors could be added. [73] use SVM to predict 4 defect types in ultrasonic inspection.

[74] shows how feature extraction from thermographic inspection and processed through an ML algorithm can be used for process parameter optimization. [75] examined the identification and characterization of defects in both a flat and curved CFRP laminate using reference free thermal contrast. They used three ML models: Multi-layer Perceptron (MLP), SVM, and Radial Basis Function Networks. Patch classification was performed to segment the entire thermographic image into its defect and non-defect components.

[76] looks at using ML methods for the classification of defects based on eddy current inspection on aircraft structures. The researchers evaluated a number of ML

algorithms including U-BRAIN algorithms that showed promise. Feature extraction methods also had a heavy emphasis placed and a series of feature extractors were validated through each of the ML algorithms evaluated. MLP and U-BRAIN performed particularly well when trained using Fast Fourier Transform extracted features.

[68] demonstrates ultrasonic signal classification using a convolutional neural network (CNN) as a feature extractor to be fed into a SVM for later classification. The system was trained to find voids and delaminations in a CFRP plate. The CNN was used principally as a feature extraction method. Ultrasonic A-scans were processed and used as the input data for the ML system. As the classifications were made, C-scans were taken and used to create 2-dimension and 3-dimension renderings of the defect areas.

Utilizing pulsed thermography, [77] trained and evaluated three sets of classifiers to find surface and subsurface defects. Several preprocessing steps were taken such as median filtering. Decision Trees, an Ensemble Decision Trees, and a standard and weighted version of the k-Nearest Neighbor (KNN) classifiers were used. [78] used two ANNs to determine first the novelty index of the sensing of Lamb waves through a GFRP part, and then a classification of the type of defect based on the second ANN. It should be noted that PCA played a principle role in reducing dimensionality and locating major features. The specific defects investigated were introduce by heating and chemical products.

[79] built an ANN to determine structural health in GFRP beams. An impulse load was applied to the beam and a microphone recorded the resulting acoustic signals. The input of PCA was fed into the ANN.

[80] created a convolutional neural network and trained it to perform patch classification on X-Ray computed tomography (CT) scans of CFRP plates. The network

produced a rough segmentation of delaminations in the composite part. Applying similar principles, [11] used a fully convolutional neural network (FCN) proposed by [81] with ResNet architecture outlined in [82] to segment profilometer scans of AFP courses to detect and identify AFP defects.

## 2.5 MODELING AND PREDICTION OF COMPOSITE MANUFACTURING WITH ML

Composite manufacturing often involves highly expensive modeling procedures that, while effective and insightful, are a drain on both resources and time. In the instances where computational requirements exceed what is available in terms of processing power or run time, ML has often been utilized as a potential solution due to the relatively low computing requirements for many of the ML algorithms available. The coupling of numerical simulations with ML algorithms in such a manner has been utilized for considerably faster optimization as well as rapid confirmation of design changes. Such concepts have been applied to optimization of Resin Transfer Moulding (RTM) gate and vent locations [83] and allowed for a control loop in the AFP process through ML-enabled fast modeling of the compaction roller [84].

In this space, many of the parametric models, such as neural networks, SVM, and SVR find use due to their low memory requirements by deriving a model that has no need to calculate priors directly from the training data. Instead, models are created as representations of these priors and thus training data can be disposed of after the initial training session. This also makes these types of algorithms ideal for online processes.

In the instance where a large experimental dataset is available with a limited understanding of the physical processes that are occurring in a system, ML enabled

modeling has made a number of interesting progressions forward in the manufacturing space. Efforts to model the drilling of composite plates to infer the production of delaminations have shown promise [85], [86] . Patel et al. [87] used ANNs to investigate process parameter effects on heat affected zone (HAZ) in the laser cutting of GFRP materials and demonstrates an ad- vantage with ANN over a second order regression model developed on the same data. Stamopoulos et al. [88] ANNs to link autoclave pressure, porosity, and mechanical properties of unidirectional CFRP laminates using X-ray Tomography. Seyhan et al. [89] shows how a three layer ANN can be used to predict the compressive strength of composite parts produced by the Vacuum Assisted Resin Transfer Molding (VARTM). The researchers focused on three parameters they identified as key to the VARTM process to train the ANN. Caggiano et al. [37] presented a machine learning based model to predict the need for replacement of drilling tools in CFRP drilling. A novel feature extraction method based on fractal analysis was utilized to train the ANN. Spoerre et. al. [90] uses a Cascading Correlation Algorithm (CCA) to create a network that can model void content, strength, and mold cycle time for the RTM process.

Golkarnerenji et al. [91] investigated and validated the use of ANN and Support Vector Regression, a subset of SVM that accomplishes regression tasks, as modeling techniques for the stabilization process in the production of carbon fiber. A GA was subsequently used to optimize the energy usage during the process. Wilcox et al. [92] used ANNs to model how various processing parameters in the pultrusion process affected the overall part quality as measured in flexural strength and density. Pfrommer et al. [93] modeled the shear angle in the composite textile draping process using a very deep neural

network in an attempt to optimize the tension gripper position to minimize wrinkling defects.

## 2.6 SHORTCOMINGS OF ML AND PURE DATA METHODOLOGIES

Many of the modern variants of data-driven methodologies are extremely data dependent. This manifests itself in poor generalization if the data set is not large enough, nor has a wide enough distribution of samples with which to train on. In deep learning, models of several million parameters are not uncommon, requiring extremely large datasets to train effectively. In the context of many environments where repeated experimentation is prohibitively expensive, this is simply not practical. The hope of hybridized models is that by combining the input of often limited physical or analytical models with the representative power of statistical or machine learning techniques, the nominal physical behavior of the system can be described with the analytic models with stochastic and uncertain behavior is added through the data driven component.

Table 2.3: Data Challenges in Key Areas Identified by Lwakatare et. al. [94].

| Adaptability | Scalability | Privacy |
|---|---|---|
| • Unstable data dependencies and data quality problems<br>• Difficult Feature Engineering | • Cold start and sparse data problem<br>• Limited access to training data<br>• Manual data labeling | • Difficult data exploration in private datasets<br>• Difficult debugging without access to underlying data<br>• Incompleteness of training data |

### *2.6.1 ML Objectives*

ML can be used for a number of tasks. Firstly, classification has become an area where ML has begun to dramatically change what is possible in industry. With the advent of AlexNet in 2012 [30], image classification accuracy was improved to a point where it began to rival human testers in some tasks. Classification can also be viewed as a subset of interpolation and extrapolation. Therefore, regression similarly falls under the domain of potential ML applications. Thus, as the reader will discover in later sections, ML can be utilized as a powerful tool for generating additional data points without having to rely on laborious computations.

Sculley et. al. [95] highlighted the additional technical debt incurred in the development of ML systems. This includes difficulty maintaining multiple ML models against changing feature sets and understanding the ecosystems that both depend on and feed into these systems. Most importantly, the paper argues that we should not think of the representational power of ML as coming for free. There are real technical debts, or long-term consequences to the cost of moving quickly in software engineering, that must be paid through the entire lifecycle of the adoption of ML applications.

### *2.6.2 Shortcomings of Neural Networks*

Even for very shallow neural network architectures, the optimal structure to generalize properly to a given dataset is not clear. Lawrence et. al. as early as the mid-90s note that the ability for neural networks to accurately approximate a function is both highly dependent on function complexity, even in a 1-dimensional case, and that in a real-world scenario, backpropagation can struggle to find global optimums [96]. This work predates

the advent of the modern deep networks, but it does give an indication of some of the fundamental limitations that persist in more sophisticated ML approaches.

As an overview of deeper network models, the fundamental issue with building large neural networks is the potential for (a) overfitting to the dataset, particularly when "not enough" data is used, and (b) the possibility of the backpropagation algorithm slowing down over complex features in the neural network solution space. The problem of neural network accuracy is inherently linked to data distribution [97], with theoretical measures of the complexity of a dataset bounding the performance of a neural network model. This makes some intuitive sense, as the dataset becomes increasingly sparse in the domain, it becomes more difficult to infer the behavior of the function that generated the dataset.

## 2.7 COMMON METHODS FOR MODEL HYBRIDIZATION

Hybridization approaches can be varied based on application. In computational fluid dynamics, deep learning approaches combined with a first-principles informed structure have allowed for the development of models that give a computational boost from machine learning, while avoiding the peril of learning sparse data representations [98]. This physics-constrain neural network architecture appears to have strong generalization to a number of partial differential equation problems [99].

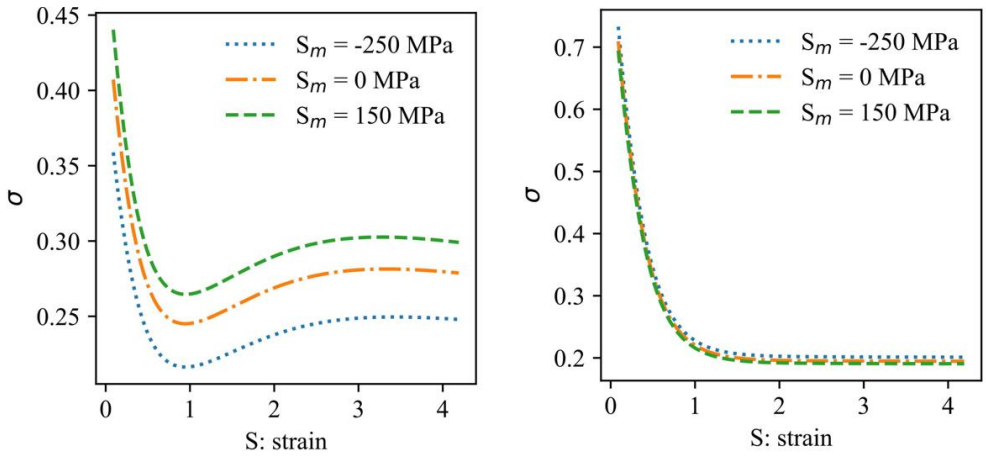


Figure 2.6: Stress and strain variance for a physics-informed neural network (right) and a standard neural network (left) for the prediction of fatigue

Another potential approach for hybridization is to use physical knowledge to perform feature engineering before a given dataset is processed through a machine learning algorithm. One can use physically relevant descriptors as inputs into traditional ML architectures [100], which causes the ML models to learn a physics-relevant representation of the data. Using first-principle calculations as a filtration mechanism to either cull poor training examples or to restrict the domain that an ML model must operate on [101] is another approach that can improve the robustness of the ML model. Wu et. al. [102] used this strategy quite effectively to best the current standards for predicting turbulent flow through the modeling of Reynold's stresses using neural networks coupled with reduced, physically relevant feature sets. The generalization of the models to new flow regimes indicated that the models learned physics-relevant representations rather than just fitting data.

Direct influence of a physical or mathematical equation embedded within a model itself can be accomplished with a great degree of success as well. First principle models can be augmented through simple weighted addition to the output of a machine learning

model, with the difference between the analytical model and the true value being corrected through the ML algorithm [103]. In this case, the model can be considered a case-specific, tunable correction factor for the physical model

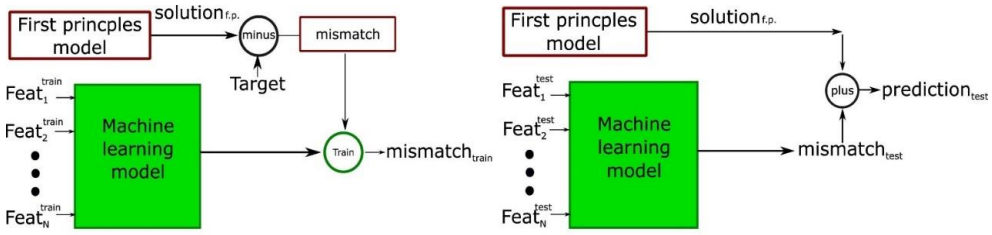


Figure 2.7: A Hybridized ML-Physics Model for the Augmentation of First Principles Equations in Bikmukhametov and Jaschke [103].

Certain models can incorporate stochastic metrics such as uncertainty quantification into this process as well. Gaussian Process Regression (GPR) has been widely used to express model uncertainty when evaluating away from previously observed points and refining the predictions of mechanistic models [104].

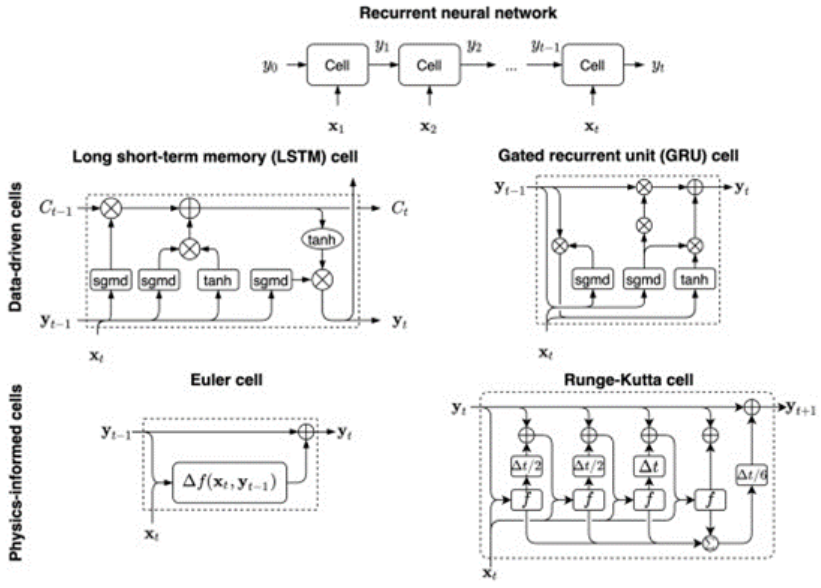


Figure 2.8: PINN Architectures and Their Traditional Counterparts

*2.7.1 Physics-Informed Neural Networks*

There are a class of neural networks known as Physics Inspired Neural Networks (PINN). Though the formalization of this approach and terminology have yet to be completely set, the essential element of the approach is to reformulate common algorithms for solving ordinary and partial differential equations into a form similar to the structure of a neural network. Nascimento et. al. [105] uses Euler and Runga-Kutta algorithms reformulated to be similar to certain recurrent neural network (RNN) approaches [Figure 2.8]. This was then used to examine time series data in the same style that RNNs would be utilized. Though it can be shown that these approaches have validity, it begs the question whether such a solution is really learning a solution representation rather than just nesting ODE solvers together. In other words, does such an approach truly count as machine learning? The author believes this answer is no.

A considerably more sophisticated approach to the PINN project is to use neural networks as the DE solver itself, allowing for the learning of a physics guided representation while also allowing for the substitution of data from tests. Rao et. al. [106] uses this principle to solve for fluid flow simulations by using a neural network to map spacio-temporal inputs to a mixed-variable field. The auto-differentiation capabilities of the model were used to compute the results of each prediction in an analytically differentiable manner, leading to a direct formulation of the Navier-Stokes equation in terms of model parameters. Then, a loss function consisting of physics loss, essentially ensuring that the equations balanced and that boundary conditions were met, and a data loss was constructed [Equation 2.8].

$$\{\mathbf{w^t}, \boldsymbol{b^t}\} = argmin\{J_d(w,b) + \alpha J_p(w,b)\} \quad 2.8$$

### *2.7.2 White-Box Machine Learning*

Table 2.4: A Summary of Various Approaches to Physics-ML Hybridization

| Problem | Approach | Study |
|---|---|---|
| Model Efficiency | Learned model reduction | [107], [108] |
| Poor Training Dataset | Physics-informed feature engineering | [100]–[102] |
| | Physics-inspired network architecture | [98], [99], [105], [109] |
| | Incorporate first principle models into loss function | [103], [109] |
| | Use of first principles to explain nominal behavior | [104], [109] |
| Uncertainty Quantification | Stochastic modeling of system dynamics | [104] |
| Physics Discovery | Learn physics-relevant representations rather than raw output | [102], [110] |
| | Regression using a library of governing dynamics terms | [111]–[113] |

Other attempts to merge physics and machine learning together include attempts to predict reliable governing dynamics through data. SINDy [112] has become one of the

leaders in the space. By using sparse regression and a library of potential solution components, SINDy has been shown to accurately predict flow dynamics and reconstruct Lorentz Systems.

### *2.7.3 Hybrid Models in Composite Materials*

Pure physics approaches to modeling of composites, while often effective, are notorious for both heavy computational overhead, and imperfect physics assumed into the model. Many of the common composite failure criteria rely on material strength properties and to not take into account material inhomogeneity [114]. Many failure criteria came under increased scrutiny in the early 2000s with the results of the World Wide Failure Exercise [115], [116] and the discovery that many of the purely analytical approaches to laminate failure prediction were fundamentally lacking in generalization. In the realm of fatigue many of the more successful theories are highly numerical [117], [118] and thus have the capability to incur large computational overhead. Failure models have a long history of using empirically influenced models as well, attempting to make up for holes existing in the understanding of fatigue mechanisms [118] . Clearly, there already exists space in the composites community to include the influence of experimental data. The additional of better representational ability afforded by many of the hybrid methodologies discussed in the previous section could alleviate the problems of incomplete physics and high computational cost in a new and unique way.

Pure data-driven approaches have been demonstrated some success, but often require massive amounts of data, are difficult to train properly, and have limited use beyond speeding up existing simulation tools [119] . It becomes apparent that without some form of precise feature engineering model performance can suffer [120] . In the case of an

investigation into an artificial designer for composite voxels, Gu et. al. [121] required the generation of tens of thousands of training examples to have the level of representation required to properly predict performance properties in the structure. Often, testing thousands of potential designs, both in simulation and in experiment is simple not practical. The requirements of feature selection and the requirement to reduce data usage are both strong hints that the introduction of physics-knowledge influences might be appropriate for the composites domain.

For composites specific applications of hybrid or first-principles influenced learning models, there exists a remarkably small amount of work. A new paradigm, Theory-Guided Machine Learning (TGML), has shown some promise in reducing the total number of tests required to accurately train a machine learning model [122] . Wei et. al. [123] used Gaussian process regression to determine thermal properties of a composite material, but unfortunately kept the hybridization approach limited to selection of physics relevant input features rather than including a physics-inspired mean function.

Finding acceptable models of the purely data or physics variety is uniquely challenging in composite materials due to the many material variations that can be used in production. The many different material types expand to potential distribution of training data, making pure data-driven models limited in generalization. Certainly, one could theoretically conceive of an incredibly effective first-principles model that could account for all material variations. However, this model may be prohibitively expensive to develop and computationally complex. While hybridized models may not have the pure predictive power that a theoretical universal first-principles model may have, it is quickly constructible and it potentially requires a much smaller dataset that the pure data approach.

For hybridized models, there may two potential paths forward: (1) a reduction of many material variables into a limited set of input parameters through feature engineering, or (2) augmentation of a limited physical model with a limited training set for calibration to a new material system. This second option seems the most likely, given that a combination of input features that might be able to be reduced in such a way that the model could be fully generalized seems a stretch. While this does expose a potential drawback in hybridization, it should be noted that a relatively small dataset (somewhere on the order of 10n – 50n where n is the number of input features) can be quickly achieved should the proper apparatuses for data collection exist. This calibration step could also theoretically leverage transfer learning [124], [125] or other meta-learning strategies to retain key hierarchical features relevant to all material systems while learning additional representations for the new material systems. In the case of neural networks, this could take the form of frozen bottom layers of the network while only the top few parameters are trained, drastically reducing the number of trainable parameters in the system so as to reduce data requirements.

## 2.8 DEFECT PREDICTION IN AFP

Explicit modeling of defect production in AFP has principally taken the form of physics or geometry descriptors of the process, with particular emphasis on the geometric properties of the part.

### *2.8.1 Gaps/Overlaps*

A standard form of analysis in the prediction of part quality is to examine the course and tow trajectories during a layup and performing a simple analysis of where tow collisions will occur due to the geometry of the layup. This is approach is most commonly

manifested in AFP process planning tools such as Vericut VCP [15] and Ingersoll Composites Planning Software (ICPS). Often, the production of gaps and overlaps from a purely geometric view comes from the use of constant angle paths over a complex surface that requires steering [126].

*2.8.2 Wrinkles*

Pure geometry arguments of wrinkle formation are based on the mismatch between the length of a tow and the length of the path that it is steered over [127], [128] [Figure 2.9]. It represents a good first approximation for identifying problem areas in layup, though there is a lack of many of the more important physical behaviors such as tack behavior.

Wehbe et. al. [129] attempted to characterize wrinkling potential of a layup through a geometrical argument by examining the geodesic curvature of the tow path and updated the wrinkling models through experimental measurement to empirically determine the critical steering radius of a tow material. This pure geometry with empirical updates strategy has the benefit of fast run time and very interpretable results, potentially leading to definitive mitigation strategies. However, these models have only limited capacity to include process information, with a design of experiment to determine critical steering radius the only current method available.

Other approaches modeled the physics of the system, with finite element modeling of the material deposition process [130]–[132]. It should be noted that while these modeling approaches have good agreement with the experimental results they are compared to, these studies are primarily limited to layup of a single tow in a constant curvature arc on a flat plate. For these explicit modeling approaches to become useful for

the quality prediction of an entire layup, the scope of the modeling approaches needs to dramatically improve.

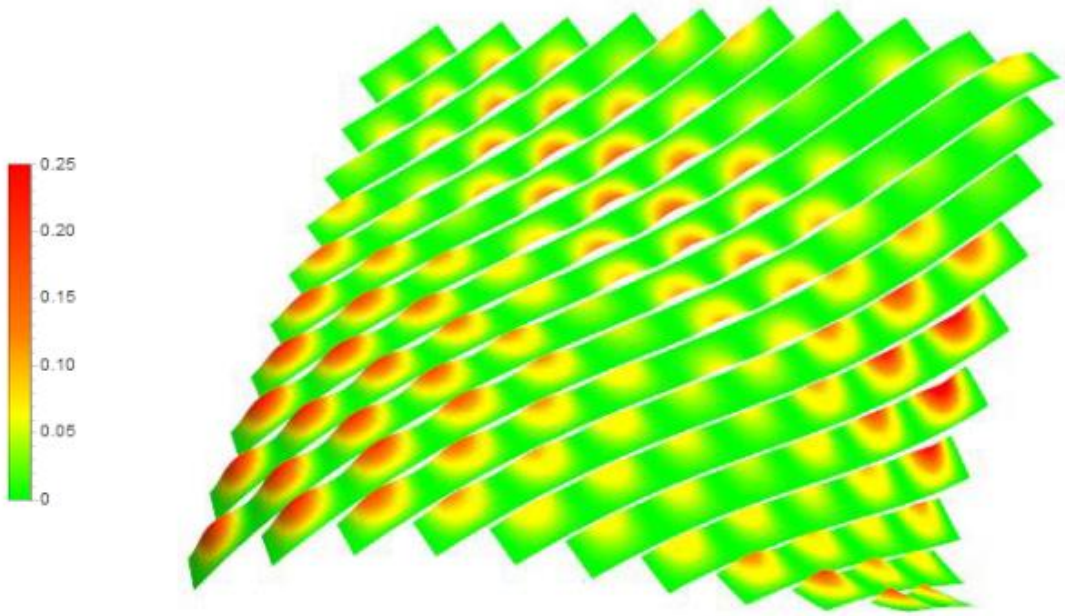


Figure 2.9: The Result of a Geometrical Model of Wrinkling on a Surface [127]

Wrinkling also has a unique dependence on material properties which makes system dynamics a particular challenge to understand. Prepreg tack is a subject of intense debate, with wildly varying approaches to measurement. Some have suggested that simple probe testing is enough [130], [133]. Sreehari et. al. [134] noted that fracture mechanics may be a more appropriate way of determining surface separation in fiber steering and designed experiments to determine various important fracture parameters.

Some of the results of these models, particularly regarding the sensitivity of wrinkling to certain parameters, proves extremely useful to the further understanding of the wrinkle formation process. Hutten et. al. [132] gave an indication that wrinkling is particularly sensitive to the ABD matrix parameter $D_{11}$ and the separation energy. Therefore, tack parameters and fiber stiffness are significant factors in driving the

governing dynamics behind wrinkle development. The purely geometric descriptions of wrinkling have indicated the importance of the geodesic curvature of the tow path [135]–[137]. We will return to this discussion in latter chapters when considering the down selection of features to include in the stochastic portion of the hybridized models.

## 2.9 CONCLUSION

One may make note of how a number of the studies examined here date from almost 20 years ago, with a wide gap of publications through the mid-2000s. This is indicative of the ML solutions forwarded from this time being more of a ‘buzzword’ rather than an actual tool. Dedicated training hardware had yet to be employed, and deep learning had not emerged to offer greater generalization. Thus, while ML showed promise, the slow training times and tedious data labeling exercises meant that such systems were difficult to implement through traditional means.

Why the emergence of ML once again? If the author must forward a suggestion, the great swath of data that is collected in modern manufacturing settings mean that the ML ability to infer correlation and connection through a large feature domain can be brought to bear. Particularly in the image analysis space, ML has made considerable strides due to the advances of both the convolutional neural network, and the parallelization of training with GPUs. In the span of a few years, ML algorithms went from being one of a competing number of object recognition algorithms to a clear and away favorite rivaling human accuracy in many challenges. Data driven decisions become far easier when enough information is at the disposal of whichever analytics system that one chooses to use. ML also represents an acceptable approach to online data driven inferencing [138], thus extending use into a live environment. This is particularly useful when discussing

manufacturing applications. When considering the applications of ML to a specific domain of composites manufacturing, the ability to immediately use information coming from a manufacturing apparatus can be a strong indicator of the applicability of the system.

The progress of ML and AI in the last 10 years has shown that ML is a long term trend in the age of big data. For the greater number of cases with extremely large data can be a first approach in generating a model with high accuracy. In the case of composite inspection, the soft boundaries that various objects of interest are identified with coupled with the large amount of data created in manufacturing leaves ML as the only approach with significant potential. The numerous impressive results in numerous object identification tasks support the use of ML in AFP based inspection. With the ability to accurately make case-based decisions, the composites manufacturing space has begun to take notice of how ML can be applied in the hopes of bridging a number gaps in the knowledge base of many of the engineers controlling and developing the current spectrum of composite inspection processes.

# CHAPTER 3

# MODEL HYBRIDIZATION THROUGH GAUSSIAN PROCCESS REGRESSION

## 3.1 GAUSSIAN PROCESS REGRESSION

GPR is a probabilistic regression method that assumes a given function is normally distributed with a mean $\mu_0$ and a covariance matrix $\Sigma_0$. If a vector of test points along the function is expressed as

$$f(x_{1:n}) = [f(x_1), f(x_2), \cdots, f(x_n)] \quad 3.1$$

Then

$$f(x_{1:n}) \sim \mathcal{N}(\mu_0(x_{1:n}), \Sigma_0(x_{1:n}, x_{1:n})) \quad 3.2$$

Suppose that $f$ is measured without noise. Consider a new point $f(x_k)$ that is not included in the original set of test points. To estimate the response of $f$ at this point, consider a stochastic expression for the distribution of $f$ and compute the conditional value at $x_k$ such that

$$f(x_k)|f(x_{1:n}) \sim \mathcal{N}\big(\mu_n(x_k), \Sigma_n(x_k)\big) \quad 3.3$$

Where

$$\mu_n(x_k) = \Sigma_0(x_k, x_{1:n})\Sigma_0(x_{1:n}, x_{1:n})^{-1} * \big(f(x_{1:n}) - \mu_0(x_{1:n})\big) + \mu_0(x_k) \quad 3.4$$

$$\Sigma_n(x_k) = \Sigma_0(x_k, x_k) - \Sigma_0(x_k, x_{1:n})\Sigma_0(x_{1:n}, x_{1:n})^{-1}\Sigma_0(x_{1:n}, x_k) \quad 3.5$$

It has been noted previously that $\Sigma_0$ is a matrix. This matrix is contains a kernel that computes the distance between two given sets of input features. $\Sigma_0$, true to its name as the covariance matrix or covariance function, represents the dispersion of data points in the dataset. There is open choice in the selection of the kernel function for the covariance matrix, so long as the resulting matrix is positive and semi-definite. This typically is represented in the form of a Gaussian and Matern kernel. The two kernels can respectively be expressed as

$$\Sigma_g(x, x') = \alpha_0 \exp\left(-\|x - x'\|^2\right) \tag{3.6}$$

$$\Sigma_m(x, x') = \alpha_0 \frac{2^{1-\nu}}{\Gamma(\nu)} \left(\sqrt{2\nu}\, \|x - x'\|\right)^{\nu} K_\nu \left(\sqrt{2\nu}\, \|x - x'\|\right) \tag{3.7}$$

Where $K_\nu$ is the modified Bessel function and $\Gamma(\nu)$ is the Gamma function. Typically, the norm value is the weighted L2 norm of the difference between x and x'. Note that x' is a separate test point from x and not the derivative of x.

Note that there are an assortment of hyper-parameters, such as $\alpha_0$ and $\nu$, that can inform the behavior of the kernels, and therefore improve or decrease the prediction accuracy of the GPR model. To set these values, one can take a variety of routes including performing cross validation or calculating the parameter values with the maximum likelihood to explain the data.

The mean function $\mu_0$ also has freedom for selection. The mean function is most consistently set as a constant, almost always zero, under the absence of information about the behavior of the original function to be modelled. However, there are a few cases where the mean function can be expressed as a generalized collection of basis functions [3.8],

where $\Psi_i$ can be any of a number of shape functions such as tanh or a Radial Basis Function.

$$\mu_0(x) = \mu + \sum_{i=1}^{\nu} \mathrm{B}_i \, \Psi_i(x) \tag{3.8}$$

This mean function gives some freedom for the modeller to work with subject experts to give a general idea about the behavior of the function of interest. It will later be discussed that smart choices for this mean function represent a clear path towards model hybridization, with the mean function becoming the best available model for the prediction of layup quality.

*3.1.1 Noise and Scale Invariant GPR*

The standard approach to developing stochastic behavior through GPR is to assume that the scaling of the distribution of the model, defined through the covariance function, can be tuned through a careful inspection of training data. In other words, there exists a scalar parameter $\tau^2$ such that the covariance of the model can be tuned to better fit the observed data [3.9].

$$f \sim \mathcal{N}(\mu_n, \tau^2 C_n) \tag{3.9}$$

In addition, consider if the observations of layup quality are governed by either poorly understood chaotic behavior or additional stochastic parameters. If this is the case, then perfect interpolation between testing points could be considered overfitting, as repeated tests at similar points in the solution space could yield varying system responses. It is therefore necessary to relax the interpolative nature of GPR to give the model an ability to determine nominal behavior from noisy observations through smoothing. Let us consider a set of observed system responses Y(x)

$$Y(x) = f(x) + \epsilon \tag{3.10}$$

Where f(x) is the nominal system behavior and ε is a noise parameter. Suppose that the nominal behavior and noise parameter are independent and normally distributed. For multivariate normal distributions, this means that f(x) and ε can be expressed as

$$f(x) \sim N(\mu_f, \tau^2 C_n)$$
$$\epsilon \sim \mathcal{N}(\mu_\epsilon, \tau^2 C_g) \tag{3.11}$$

The sum of normally distributed variables is also normally distributed with the means and covariances summed together. Therefore

$$Y(x) \sim \mathcal{N}(\mu_f + \mu_\epsilon, \tau^2 (C_n + C_\epsilon)) \tag{3.12}$$

Assume that the mean of the noise parameter is centered at 0. Intuitively, this choice of mean for the noise parameter indicates that the nominal behavior of the model is unbiased by the noise parameter. This will become important in later sections, as the choice of mean function for the final GPR model is determined from outside knowledge, and therefore is independent of any noise that is induced through the actual manufacturing of the part. Finally, it is assumed that the distribution of the noise parameter is independent among the variables constructing the multivariate normal distribution and that the standard deviation is equivalent between all of these variables and is controlled by $\sigma^2$. What results is a common expression for a function defined by a noise and scale invariant Gaussian Process [3.13].

$$Y(x) \sim \mathcal{N}(\mu_f, \tau^2 (C_n + \sigma^2 \mathbb{I}_n)) \tag{3.13}$$

The two parameters $\tau^2$ and g can be determined through the calculation of the maximum likelihood explanation (MLE), cross validation, entropy calculations, and a

number of other approaches. In this application, the MLE calculation for both parameters is selected in an attempt to preserve training data that would otherwise need to be held out for cross validation and the interpretability of the result. Therefore, the final expressions for the GPR model with noise and scale invariance are

$$\mu_n(x_k) = \Sigma_0(x_k, x_{1:n})(\Sigma_0(x_{1:n}, x_{1:n}) + \sigma^2 \mathbb{I}_n)^{-1} * \left(f(x_{1:n}) - \mu_0(x_{1:n})\right) + \mu_0(x_k) \quad (3.14)$$

$$\Sigma_n(x_k) = \tau^2[\Sigma_0(x_k, x_k) - \Sigma_0(x_k, x_{1:n})(\Sigma_0(x_{1:n}, x_{1:n}) + \sigma^2 \mathbb{I}_n)^{-1}\Sigma_0(x_{1:n}, x_k)] \quad (3.15)$$

*3.1.2 Geometric Arguments for Mean Function*

If the reader will recall an earlier discussion in this document, it was noted that there are a few fast but imprecise tools to predict the formation of gaps, overlaps, and wrinkles for the layup strategy of a given part. These tools, while lacking in the more robust descriptions of layup behavior, are generally accepted in industry as a good first approximation of layup quality. Figure 3.1 demonstrates the results of a layup analysis from the toolpathing software VCP for determining potential gaps and overlaps displayed in the CAPP process planning tool [139].

This first approximation from toolpath generation and process planning tools are useful for a human operator to refine the manufacturing strategy on a number of levels, including seed point placement optimization and selecting the tow propagation strategy. For the purposes of the model hybridization approach, such an initial check on system response is a perfect candidate to set nominal behavior in a predictive model. Analysis of raw toolpaths is a common step in determining the manufacturing strategy, and therefore has precomputed data available and ready to be used. The process planning tools extend

import and export of this data out of the software, allowing it to be easily incorporated with third party applications such as the hybrid model proposed in this document.

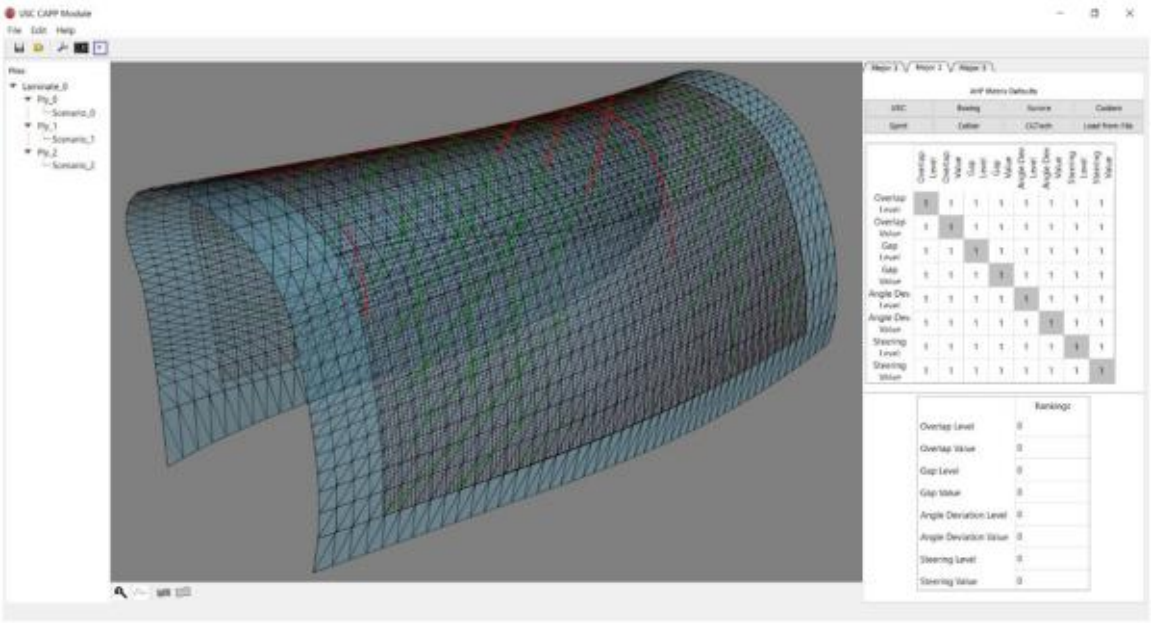

Figure 3.1: Gaps (Green) and Overlaps (Red) Predicted through VCP for a Saddle Part [139]

More importantly, geometric arguments in future chapters will be shown to be an effective predictor in the quality of layup. In Chapter 4, it will be demonstrated that the curvature of a given course was the single largest influence on the quality of the layup. If it is assumed that this curvature argument holds for extensions from 2D part curvature to 3D part curvature, then it is reasonable to declare geometry-based predictions from process planning and toolpath generation as a worthy candidate to include as the mean function for the GPR modeling approach.

## 3.2 FEATURE SELECTION

A particularly important discussion in the implementation of GPR models is the limit on the number of input features that can be effectively utilized. To a certain degree, this problem is present in nearly all ML approaches and is commonly referred to as the

"curse of dimensionality". However, because GPR is a method based more in statistical or probabilistic representation, the ability to process information from high-dimensional domains is limited. An image, audio, or time-frequency input has some difficulty being distilled into an efficient representation as a probability distribution. Therefore, it is important that the predictive models described in this chapter have a reduce set of input features selected due to their importance in part quality and the lack of influence in the physics-based model composing the mean or nominal behavior function.

This section will present a discussion on the feature set to be included in the quality prediction model and the rationale behind why each feature was selected as well as why other important features were left out. Subsections will be focused on groups of input features including material properties, part features, and processing parameters. The complete list of input features can be found in Table 3.1.

*3.2.1 Selection of Material Property Features*

There are a host of material properties that may have relevance to part quality. Any number of material stiffness qualities including $E_1$, $E_2$, and $G_{12}$ are all relevant to the mechanical response of the material. In addition, material tack and the viscous flow properties of the resin in green state prepreg have influence on the ability for the material to stick to the tool surface. As mentioned in Section 2.8.2, parametric studies with Finite Element models have indicated that the single most important aspects of material properties contributing to wrinkle development are $D_{11}$ and material tack. Recall that for a uniaxial composite material consisting of a single ply

$$D_{11} = \int Q_{11} z^2 dz \tag{3.16}$$

$$Q_{11} = \frac{E_{11}}{1 - \nu_1 \nu_2} \tag{3.17}$$

Note that Poisson terms are typically bounded between 0.3 and 0.5 and that when considering a single ply, the height z will remain constant. Therefore, it can be concluded that bending stiffness $D_{11}$ is dominated by material stiffness in the fiber direction. Finally, observe that $E_1$ is primarily controlled by the fiber stiffness and the fiber volume fraction $V_f$ if it is assumed that $E_f$ is significantly larger than the matrix modulus $E_m$. This holds if one is considering a typical thermosetting resin.

$$E_1 = E_f V_f + E_m V_m \tag{3.18}$$

For the purpose of creating the hybridized GPR model, this means that the most relevant feature to include from the material stiffness properties would be $E_1$. In the context of creating a testing regiment to determine the model input features, this is significant due to $E_1$ being a relatively simple property to determine through a straightforward test that can be conducted just prior to the material being loaded into the machine. It is certainly possible to also use the raw $E_f$ values provided by the manufacturer without testing This approach will be investigated in later chapters. However, fluctuations in $V_f$ across various batches of material may have a detrimental effect on model performance, and therefore should be determined through test when convenient.

The second feature to be included in material property feature set is the tack of the material. As noted, there are a number of ways to define and determine tack. However, an advantage afforded by the GPR model approach avoids much of this messiness and debate. Recall that the kernel for the covariance function in GPR is effectively a weighted distance measure. This means that as long as a given input feature is consistent across testing examples, that is as long as the difference between two feature properties can be

represented by the distance between them in the hyperspace, then different definitions or measures on an input feature can still be effectively represented by the model. For this reason, tack for the purposes of this document is defined as separation energy between two tows determined by probe testing. This can be parameterized by considering separation energy at different temperature values.

The final selection of features consisting of material properties will consist of a parameterized form of material tack measured through probe testing, and $E_1$ of the material.

### *3.2.2 Selection of Part Design Properties*

Several design features may contribute to overall layup quality. The Gaussian curvature of the part has been discussed in prior work. In addition, the geodesic curvature of the individual AFP tows is a significant contributor to wrinkling. This is further reinforced through the experimental work presented in Chapter 5. In essence, there is need to determine the degree of steering and surface curvature required in the part design. To accomplish this, the instantaneous geodesic curvature of the tow at a given point on the surface will be used. By calculating this geodesic curvature values, the surface geometry as well as direct steering of the part can be accounted for.

### *3.2.3 Selection of Processing Parameters*

Previous discussions introduced a number of experimental observations involving the relationship between the production of defects on steered courses and various processing parameters. From this work, it can be observed that among the three key manufacturing parameters, feed rate, temperature, and compaction pressure, has indirect rather than direct effects on layup quality. This makes some intuitive sense, as long as the control mechanisms for the tensioning and feed systems in the machine can keep up with

layup speed, then one would expect higher rates of material deposition would have a smaller effect on the overall layup quality. The effect of layup speed is instead derived from the interaction between layup speed and nip point temperature and roller compaction dwell time. Both of these effects can be compensated for by running at higher compaction pressures and heater powers. However, there exist several potential arguments for the inclusion of layup speed in the feature set. Most notably, it is easier for a potential optimization scheme to directly optimize on a set layup speed rather than nip point temperature values and compaction setting and then generating an appropriate matching speed.

Table 3.1: Features to Be Included in the Data Driven Component of the Hybridized Model

| Parameter | Support for Inclusion |
|---|---|
| **Part Gaussian Curvature** | Literature |
| **Fiber Angle/Geodesic Curvature** | Literature, Experimental Measurements |
| **Heater Power/Temperature** | Experimental Measurements |
| **Compaction Pressure** | Experimental Measurements |
| **Layup Speed** | Analytical Arguments, Future Optimization |
| **Material Tack** | Literature |
| **$E_1/E_f$** | Literature, Analytical Arguments |
| **Defects in Previous Layer** | Analytical Arguments |

### *3.2.4 Defects in Previous Layers*

It can be seen anecdotally in through scan examples that a significant factor in the creation of nucleation sites for future defect production, particularly with respect to wrinkles and puckers, is the presence of defects in the previous layers that disrupt the smooth layup surface. It can be hypothesized that defects such a nature as to effectively increase or reduced the layers of material would be the most detrimental. Namely gaps, missing tows, twists, folds, splices, and overlaps would theoretically serve a being the most dangerous for the formation of defects in subsequent plies.

## 3.3 FEATURE REPRESENTATION

### *3.3.1 Problems with Raw Input Data*

To discuss the influence of certain parameters on defect production, it is important to consider the analysis of local areas of the part rather than point measurements. If one considers a potential point measurement before during and after a defect is produced, it is difficult to consider what and where the input parameters directly caused a defect to form. If one considers an energy model of defect production, then one can consider the defect to be a release of previously accumulated stress in the tow. Therefore, measurements of parameters during and immediately following a defect may in fact only contain a small amount of information regarding what manufacturing and design features produced the defect.

Rather, it should be more useful to consider points immediately proceeding the defect. However, this raises another important question: where should this measurement take place?  Perhaps a series of point measurements could be integrated and used as an

input vector. This would capture a continuum of information surrounding the defect, but choosing the start of this integration point is tricky.

A potential solution to this problem which will be given a more firm theoretical foundation in the next section is to perform part discretization using a clustering algorithm and take an average of local features rather than point measurements. This eliminates the problem of choice in which local measurements to incorporate into the predictive model. An averaging of the features within these discretized elements would capture some of the behavior suggested by the integration strategy above.

*3.3.2 Part Discretization*

Consider a given AFP part with defects placed across the surface. One could begin by discretizing the part and noting the given area of the discretized elements occupied by defects. Noting the ratio of defect to no-defect areas, one can arrive at the average distribution of defects across the element. Similarly, take the field of all parameters the modeler wishes to incorporate into the model on the element and perform averaging. Assume that each element Q holds a state that is uncovered by a state retrieval function S, and that the set of all element states can be expressed as $\{S(Q_1), ..., S(Q_n)\}$. Suppose that the state of each element is approximately independent of other states or

$$P(S(Q_K)) \approx P\left(S(Q_k)\middle|S(Q_1), \dots, S(Q_n)\right) \tag{3.19}$$

If one then assumes each element is identically distributed from its nominal function input parameters, then by the central limit theorem, a large enough (<25) random sampling of the support will give an approximately Gaussian Distribution.

Let's spend some time justifying this assumption that the defect distribution of each element is independent of other elements. Certainly, in the context of the field distribution

across the face of the part, this is not the case. A wrinkle is directly influenced from a point earlier in the tow where stress concentrations build until separation of the tow from the substrate surface occurs. In wrinkle modeling literature, this is referred to as a local approach [129], [140], [141]. However, a smart discretization procedure may alleviate this problem. Consider a simplified model of defect production on a single tow with an arbitrary element Q with boundary locations $Q_1$ and $Q_2$ [Figure 3.2].

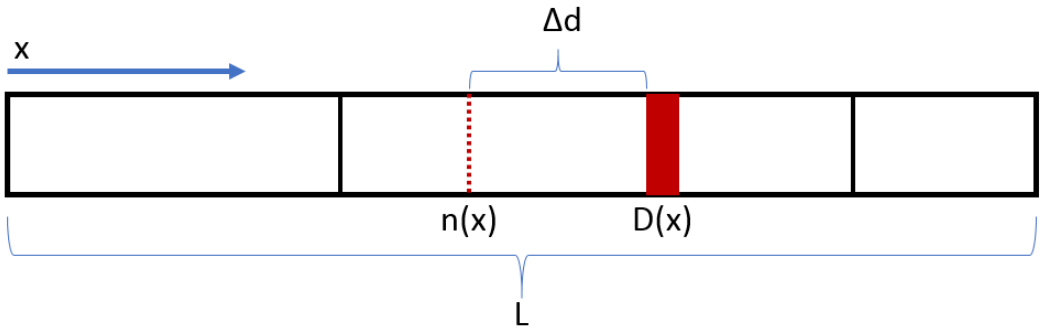


Figure 3.2: A Schematic of Defect Production on a Discretized Tow

Suppose a defect at location D(x) is caused by some perturbation of layup parameters a length Δd before the defect at a point n(x). Let this defect appear on the tow with a probability that is uniformly distributed. What can be first observed is that the probability of a defect appearing such that the nucleation point is within the element boundary is

$$P(Q_1 < n(x) < Q_2 - \Delta d) = \frac{Q_2 - \Delta d - Q_1}{L} = \frac{\Delta Q - \Delta d}{L} \quad 3.20$$

Similarly:

$$P(Q_1 \in \Delta d) = P(Q_1 - \Delta d < n(x) < Q_2 + \Delta d) = \frac{2\Delta d}{L} \quad 3.21$$

$$P(Q_1 + \Delta D < D(x) < Q_2 | D(x) \in [Q_1, Q_2]) = \frac{\Delta Q - \Delta d}{\Delta Q} \quad 3.22$$

Where L is the length of the entire tow and $\Delta Q$ is the size of the element. In essence, what is measured with equations 3.20, 3.21, and 3.22 is the probability that a given defect in the element will have a perturbation from another element as an influence. Note that the influence of previous elements in the discretization can be controlled through the size of elements and the size of the part. If $\Delta Q >> \Delta d$ and $L >> \Delta d$ then the probability that a defect inside of the element was caused by a perturbation from the previous element approaches zero as a result of equation 3.22. While this is a somewhat simplistic model of defect production, it gives a hint that discretization is a key for independence within the part. One can further improve this idea by using the changes in part features to mark the boundaries of each element. A simple clustering algorithm can perform the discretization of a given part with consideration for potential boundaries between similar regions.

A clustering approach is necessary for a number of reasons: (1) to maintain the independence assumption for the GPR model, and (2) the local averaging component of the predictive approach is sensitive to outliers and therefore it is necessary to ensure that local differences in manufacturing and part characteristics don't cancel each other out. Should there be large fluctuations in part curvature in both the positive and negative directions, then an average of the two regions will cancel out and leave an improper representation of the features for this region.

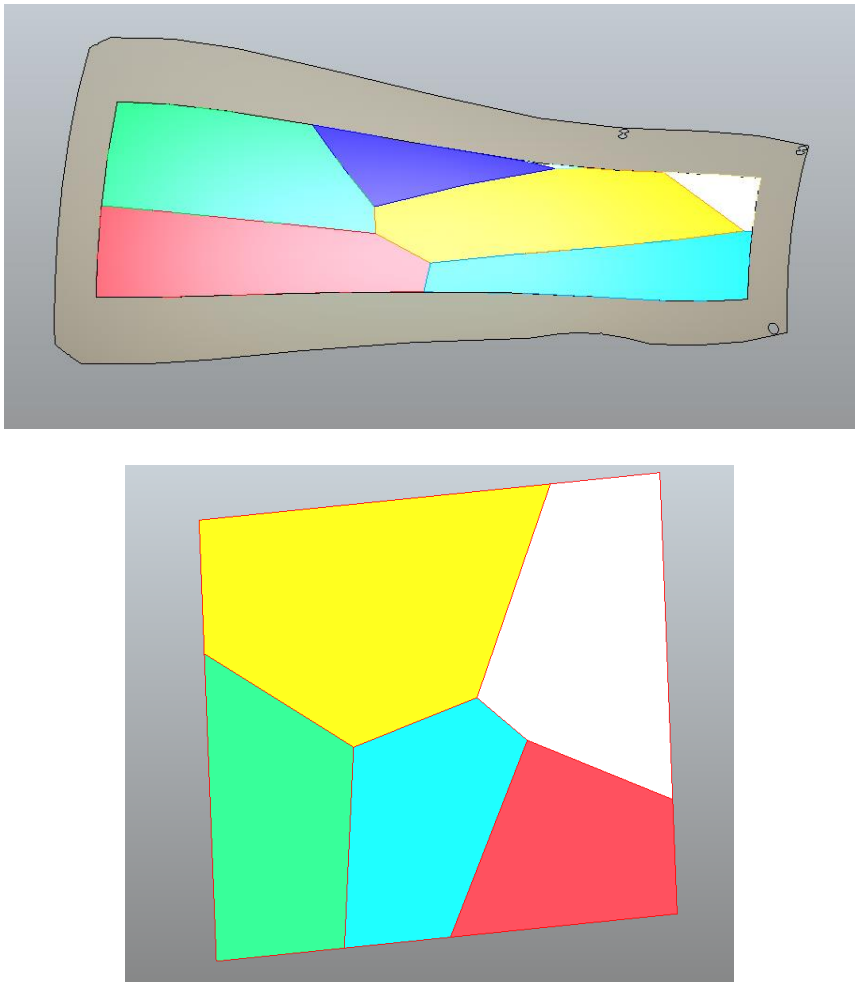

Figure 3.3: Segmented Part Surfaces by Affinity Propagation Clustering

Other attempts to merge physics and machine learning together include attempts to predict reliable governing dynamics through data. SINDy [112] has become one of the leaders in the space. By using sparse regression and a library of potential solution components, SINDy has been shown to accurately predict flow dynamics and reconstruct Lorentz Systems.

## 3.4 RESPONSE REPRESENTATION AND CONSTRAINED GPR

The final result of the discretization procedure is to have elements with a percentage of the element area occupied by a defect. This is the quality response metric that the hybridized model will attempt to predict. Note that there is a particular issue with adapting

GPR to perform predictions on the bounded domain [0,1]; GPR as a function is defined on GPR:$\mathbb{R}^n \rightarrow \mathbb{R}$. This means that GPR output is unbounded on the real numbers.

*3.4.1 Warped Output Spaces*

One way to address this, a mapping function is required to transform the predicted response values into the open domain for GPR and take the predictions from the GPR model and transform them back into the original domain space. There exists a candidate function that executes this exact type of transformation: the probit function $\Phi(x)$ [142]. The probit function is

$$\Phi(x) = \sqrt{2}\ \mathrm{erf}^{-1}(2x - 1) \tag{3.23}$$

The erf function is defined as

$$erf(x) = \frac{2}{\sqrt{\pi}} \int_0^x e^{-t^2}\, dt \tag{3.24}$$

When processing training data, the geometry/physics predictions for quality can be transformed through the probit function into the open interval (-∞, ∞), where it can be processed through the hybridized GPR model. Then predictions from the GPR model are transformed back into the restricted range [0,1] using $\Phi^{-1}(x)$. A caveat to the probit-space-warping approach is that the data must be gaussian distributed within the [0,1] domain. Consider if output values of the model come very close to one or zero. The probit function will distribute them accordingly across the real numbers, implying that dispersed data across the [0,1] interval will be mapped very far apart, limiting generalizability of the model.

*3.4.2 Constrain through Hyperparameter Tuning*

Another alternative for constraining the mean prediction of the GPR function is to construct and optimize the hyperparameters in the covariance kernel such that, when combined with the training data, the model will be forced to generate positive predictions. This can take a number of forms, however the easiest to construct is a set of hyperparameters that consist of bijections that would bound their values to the positive real numbers. Performing this on the scaling parameters that control sizing of the variances in the covariance kernel give a true positive matrix. Simple hyperparameter tuning on the observation noise value $\tau$ can then give reasonable confidence that the, when coupled with the scaling parameters, the mean predictions of the GPR model will remain bounded between zero and one. There has been prior work on the theoretical performance of constraining through hyperparameter selection and optimization [142].

## 3.5 EXPLORATION OF HYBRIDIZATION ERROR BOUNDS

To facilitate this discussion, it may be wise to explore comparisons of a theoretical hybridization approach against a more traditional mean function selection, such as a constant. Let us assume that a hybridized mean function selection has a bounded error of $\epsilon$ against the real function $f(x)$. Therefore, the total GPR model as a function of $f(x)$ and the error between the mean function and the true function can be expressed.

$$\mu_0(x) = f(x) \pm \epsilon \tag{3.25}$$

Then express the entire GPR model as a function of the difference between the mean function and the true objective function.

$$\mu_n(x_k) = \Sigma_0(x_k, x_{1:n})\Sigma_0(x_{1:n}, x_{1:n})^{-1} * (f(x_{1:n}) - (f(x_{1:n}) \pm \vec{\epsilon})) + f(x_k) \pm \epsilon \tag{3.26}$$

Recall that $\Sigma_0$ is positive and semi-definite. Note that $\vec{\epsilon}$ is the scalar vector where all elements contain $\epsilon$. Thus, the potential range of values for a given model under these conditions is

$$\mu_n(x_k) \leq \Sigma_0(x_k, x_{1:n})\Sigma_0(x_{1:n}, x_{1:n})^{-1} * (-\vec{\epsilon}) + f(x_k) + \epsilon$$
$$\mu_n(x_k) \geq \Sigma_0(x_k, x_{1:n})\Sigma_0(x_{1:n}, x_{1:n})^{-1} * (\vec{\epsilon}) + f(x_k) - \epsilon \qquad 3.27$$

Let us make one more algebraic manipulation to these equations and suggest that an important value to derive would be the error between the predicted nominal value of the model and the actual value of the real function. First, let us simplify by compacting the covariance equations such that

$$\Sigma_T(x_k, x_{1:n}) = \Sigma_0(x_k, x_{1:n})\Sigma_0(x_{1:n}, x_{1:n})^{-1} \qquad 3.28$$

Therefore

$$\Sigma_T(x_k, x_{1:n}) * (\vec{\epsilon}) - \epsilon \leq \mu_n(x_k) - f(x_k) \leq \Sigma_T(x_k, x_{1:n}) * (-\vec{\epsilon}) + \epsilon \qquad 3.29$$

Thus, the prediction error is driven by more than the actual prediction error of the mean function. In addition, the total prediction error is also either moderated or enhanced depending on the dispersion of the point of interest from the individual data points in the dataset. The closer the point of interest is to another point in the dataset, the less the expected error is between the predicted value and the true value. But as the dispersion in the data grows, the error becomes dominated by the overall prediction error between the mean function and true function. Even rough approximations of the true behavior of the system can therefore be calibrated well through the inclusion of data in the form of the GPR model. It can be easily shown that this concept can be extended to any mean function

whose error is bounded on the interval $[\epsilon_1, \epsilon_2]$. To the author's knowledge, this is a novel formulation in the context of GPR as a hybridized model.

Juxtapose this with the traditional selection of a mean function in the form of a constant function.

$$\mu_n(x_k) = \Sigma_0(x_k, x_{1:n})\Sigma_0(x_{1:n}, x_{1:n})^{-1} * \left(f(x_{1:n}) - \vec{C}\right) + C \tag{3.30}$$

Consider following a similar approach as above, allowing the reader to quickly reach an expression for the error between the constant value GPR predictions and the true value.

$$\begin{aligned} \mu_n(x_k) - f(x_k) & \\ &= \Sigma_0(x_k, x_{1:n})\Sigma_0(x_{1:n}, x_{1:n})^{-1} * \left(f(x_{1:n}) - \vec{C}\right) + C \\ &- f(x_k) \end{aligned} \tag{3.31}$$

Now consider the possible circumstances in which the constant value mean function can reach parity or outperform the hybridized approach. It becomes clear that one circumstance when this is certainly the case is when the constant value is within $\epsilon$ of the true function. In other words, when C also satisfies the conditions of the hybridization assumptions of the current scheme. This is valid for any bounded function such as sinusoidal functions. It may also be true when function domains are restricted to areas that are either approximately constant or approximately bounded across the interval. Consider a higher order polynomial function centered around zero where the domain is restricted to a small area around zero. However, it can also noted that in the general case for all potential combinations of data on any unbounded function, the hybridized approach will always outperform the constant value mean function.

## 3.6 AN OVERVIEW AND EXPLICIT FORMAULATION OF APPROACH

Many of the concepts presented in this chapter have an air of obscurity due to the language of the statistical approach. It may be somewhat difficult for the AFP practitioner to clearly see how these many moving, stackable, approach fit together in a finalized product. It is necessary to explain in plain language a "lightly-technical" overview of the many and demonstrate how to build the whole. Figure 3.4 shows a graphical overview of the approach outlined in this chapter and can be used as a general reference when considering how each individual component of the approach fits together.

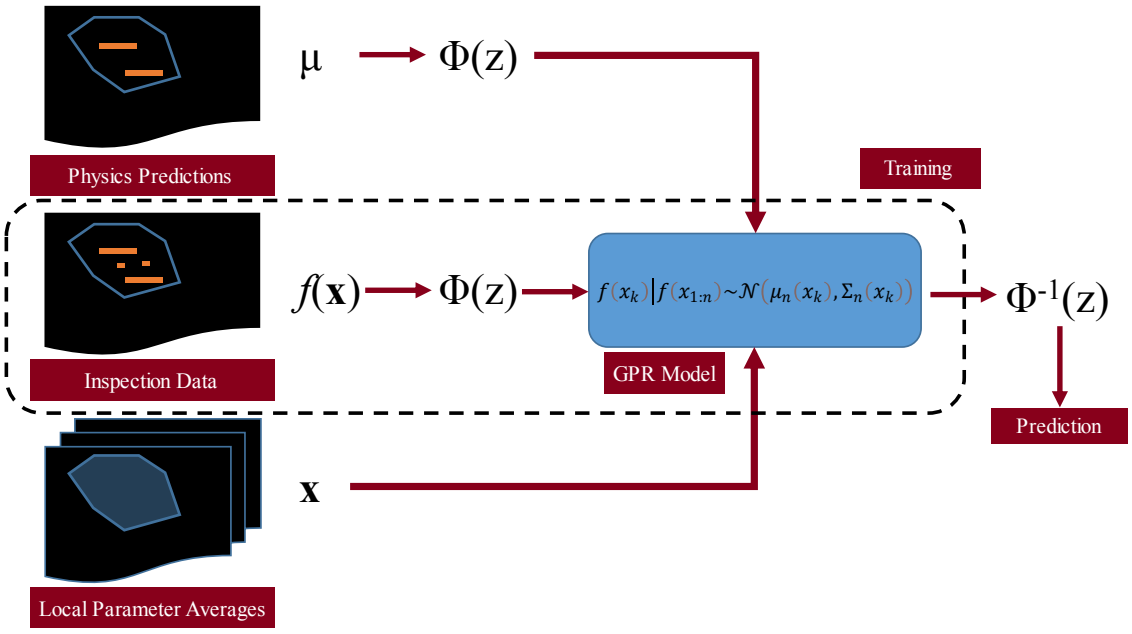


Figure 3.4: A Graphical Overview of the Model Approach

In short, our problem is that it is necessary to combine the predictive approach of explicit models with experimental semantic data to improve the prediction of layup quality in AFP. Defect data is provided from an inspection system in the form of sections of a part that are occupied by defects. In addition, physical and geometric models also provide predictions about what sections of the part contain defects. Therefore it is possible to use

the GPR Bayesian ML approach to predict future defect formation using the physical and geometric models for defect production as a mean function to indicate the nominal behavior of the system. Additional latent responses as well as the covariance of the system are predicted using the experimental data.

To properly format the inputs to the model so as to both preserve many of the nice mathematical properties of GPR as well as to create an input vector that captures all of the necessary information, the part surface is discretized according to the local design and processing parameters. This discretization takes place by generating a cloud of points across the part and then clustering those points according to the parameters at that point and the (u,v) location. What results is a segmentation of the part where local regions of similar parameters are defined. The local points in an element boundary are then averaged over all of the parameters and used as an input vector into the GPR model in addition to the physically predicted amount of defects within the element, with the predicted output vector being the percentage of the element occupied by defects.

Since the response is bounded between zero and one and GPR is unbounded on the real number line, a constrain condition must be put on the model. The probit warping function can be used to transform the output vector for training the GPR model. Once a prediction is made, the inverse probit function is used to transform the GPR model output back into a bounded range between zero and one. As an alternative, conditioning on the hyperparameter values and optimizing can also yield reasonable expectation that constraints will be met.

# CHAPTER 4

# SELECTION OF AN AFP RELEVANT MEAN FUNCTION

The following chapter will endeavour to present a comprehensive review of experiments suggesting that geometric arguments for defect production are a suitable choice for the mean function of the hybridized GPR model. Notably, this predictive strength extends beyond standard quasi-isotropic constant angle layup and can be a powerful explanatory tool for the prediction of wrinkling and tow-slippage in steered fiber plies. What will be presented is a series of experiments measuring defect responses to assorted design and process parameters. The conclusion of which is that across multiple defect types and utilizing multiple standard and non-standard metrics, geometry and design specific features are key, and possibly most importantly, well understood, predictors of defect production. Significantly, the methodology outlined in this document is completely empirical and data-driven; giving an unclouded picture about what actual occurs in laminate.

What follows is an examination of two experiments considering the influence of geometry on the production of defects in an AFP layup. In one experiment, a steered laminate is produced and all relevant process parameters are tracked including design and geometry parameters. Using an advanced feature weighting tool, it can be shown that the design and geometry parameters are a considerable influence in the production of certain defects during fiber steering. An additional experiment presented towards the end of the chapter takes these conclusions and extends them to a unidirectional layup on a doubly-

curved surface. VCP predicted defects from the layup strategy were compared with actual defects produced during manufacturing were compared with strong agreement between the VCP predictions and the experimental results.

## 4.1 INTRODUCTION

Many of the investigations into the characterization of AFP has been limited to reduced studies on single tows with limited geometry. To begin approaching the prediction of defect production on the scale of the entire physical process, it becomes necessary to attempt to characterize the production of a set of parts at the machine level. Physical modeling has yet to reach the point of performing this characterization. Thus, it is necessary to perform a series of experiments and attempt to understand the process through the collection and analysis of data. The following chapter is a presentation of work previously published by the author in a series of studies [13], [20], [143], [144].

Experiments are performed and data is collected through a profilometry-based inspection system. From this, defect formation and input parameters from both the geometry of the curve and the processing parameters are collated such that a ranking of each experimental parameter can be obtained.

## 4.2 EXPERIMENTAL DESIGN

To examine the production of an AFP manufactured part at the process level, a series of experiments were performed to lay up individual fiber steered courses on a complex shape. In the case of our experiment, this shape was a cylinder. A series of curves were chosen, with a set of process parameters varied for each course.

Course guide curves were generated in three classes: (a) constant curvature paths [Figure 4.1], (b) snakes, and (c) snails. The snakes and the snails were both generated with the aim of producing continuously variable curvatures.

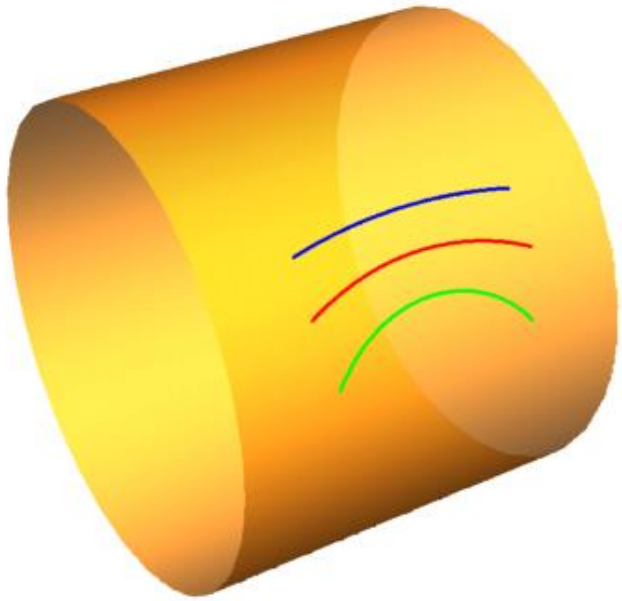

Figure 4.1: Arc Designs for Constant Curvature Paths on Cylinder

*4.2.1 Constant Curvature Paths*

For the constant curvature paths, arcs were generated at 1270, 635, and 318mm radii. In order to map the arcs to a cylindrical surface, a differential geometry approach was utilized [127]. A parametric representation of the cylinder surface can be created as a function of the cylinder length z, the radius r, and the circumference c.

$$cylinder(c,z) = \left\{r\ cos\frac{c}{r}, r\ sin\frac{c}{r}, z\right\}$$
$$0 \le c \le 2\pi r \qquad 4.1$$
$$z_{min} \le z \le z_{max}$$

To obtain the curved paths on the cylinders surface, a 2D particularization {x(s), y(s)} of the constant curvature arcs is used as follows:

$$\{x(s), y(s)\} = \{\rho \sin(as + b), \rho \cos(as + b) + e\} \qquad 4.2$$

With ρ being the circumference of the arc and a, s, b, and e as constant that are selected such as to guarantee that the curve is within the domain for layup on the cylinder. The parameter values considered for the constant curvature courses are listed in Table 4.1. The complete list of courses and associated parameters can be found in the Appendix [Table A.1].

Table 4.1: Parameter Variations for Constant Curvature Paths

| *Parameters* | *Values* | | | | | |
|---|---|---|---|---|---|---|
| *Compaction Force (N)* | 180 | 300 | 445 | 600 | 750 | |
| *Heater Voltage (V)* | 150 | | 170 | | 190 | |
| *Feed rate (%)* | 6 | 10 | 20 | 30 | 50 | 100 |

## 4.3 MANUFACTURING EQUIPMENT

### *4.3.1 AFP Machine*

The courses were deposited using an Ingersoll Machine Tools (IMT) Lynx AFP machine [Figure 4.2] at the University of South Carolina McNair Center for Aerospace Innovation. The Lynx is controlled through a Siemens 840D Powerline controller and Siemens Simatic300 PLC. It is a gantry style AFP machine with a 3+3 axis configuration,

with the first three axes being linear movement rails, and the other 3 axes being rotational axes. A 50.8mm wide roller with a hardness of 50 was used for compacting the material.

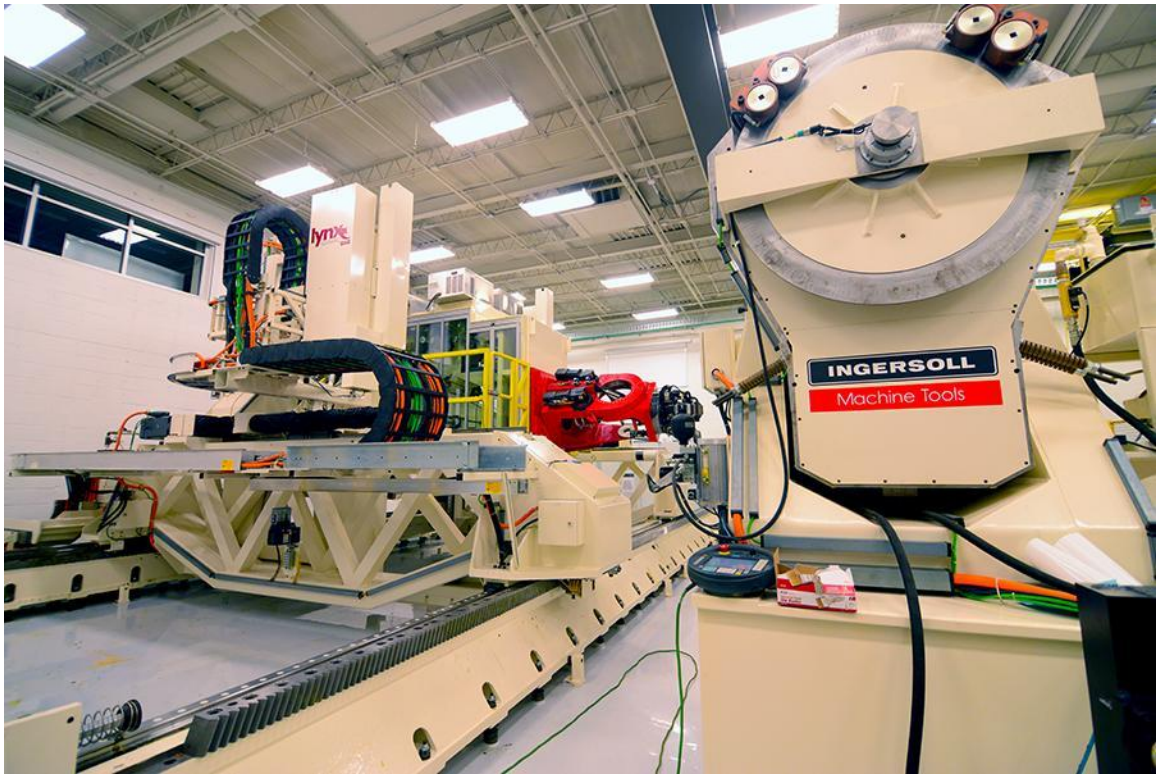


Figure 4.2: Ingersoll Machine Tools Lynx AFP Machine at McNair Center

For material heating a focused pulsed-light heater from Heraeus denoted as the Humm3 [Figure 4.3] was used. The Humm3 is a xenon light heater that can reach up to 6kW of power. The heat is focused a distributed across the material through a crystal.

*4.3.2 ACSIS Inspection System*

The Advanced Composite Structures Inspection System (ACSIS) is an automated profilometry-based AFP inspection system developed by IMT. It consists of 4 Keyence LJ-7080 blue light laser profilometers actuated by a Kuka KR120 robotic arm [Figure 4.4 a]. The profilometers allow for rapid height profiling and the ability to quickly asses a layup. The height maps constructed by the profilometers are embedded into greyscale images and processed to yield a clear visual representation of the part surface [Figure 4.4 b]. These

greyscale images can then be taken and analysed by ACSIS internal defect detection algorithms. ACSIS defect detection placed a box around each defect.

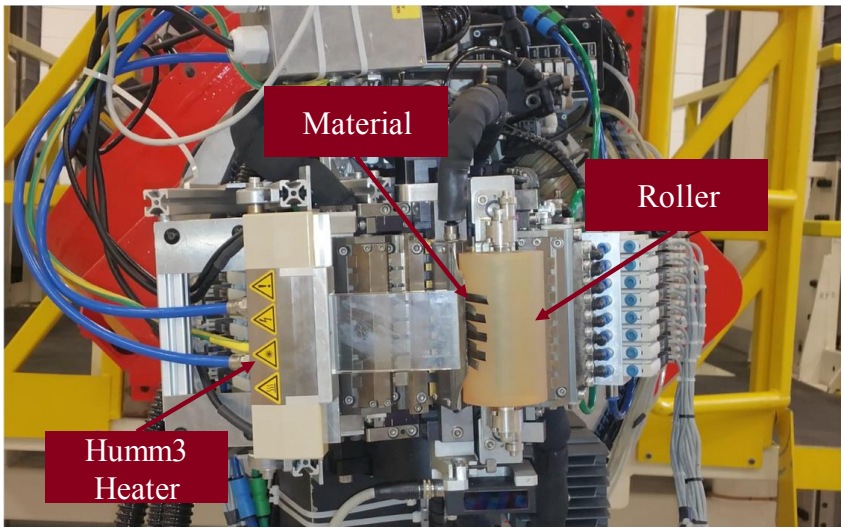


Figure 4.3: Lynx AFP Machine Head with Heraeus Humm3 Heater

ACSIS operates as a ply-by-ply scanning system with the Kuka arm placed on an external rail. When a ply is laid down, the mandrel of the AFP machine flips to expose the new ply to the ACSIS system. Scanning is then done and the mandrel rotates back into its original position.

## 4.4 DESIGN OF EXPERIMENT

The principle parameters investigated by this study is the layup speed, or feed rate (S), the compaction force (P), the nip point temperature (T), and the steering curvature (C). The feed rate is best determined by the U axis, or the speed at which material is being laid down.

To begin the experimental session, courses were laid down with varying parameters to first identify the process window of the material. A set of random parameters that would guarantee minimal course quality, essentially measuring if a majority of the tow would stick to the surface, was identified and set the bounds on which the design of experiment

would be executed. The parameter sets in Table 4.1 were settled upon as the range of parameter exploration. A complete list of courses and their respective parameters can be found in Table A.1.

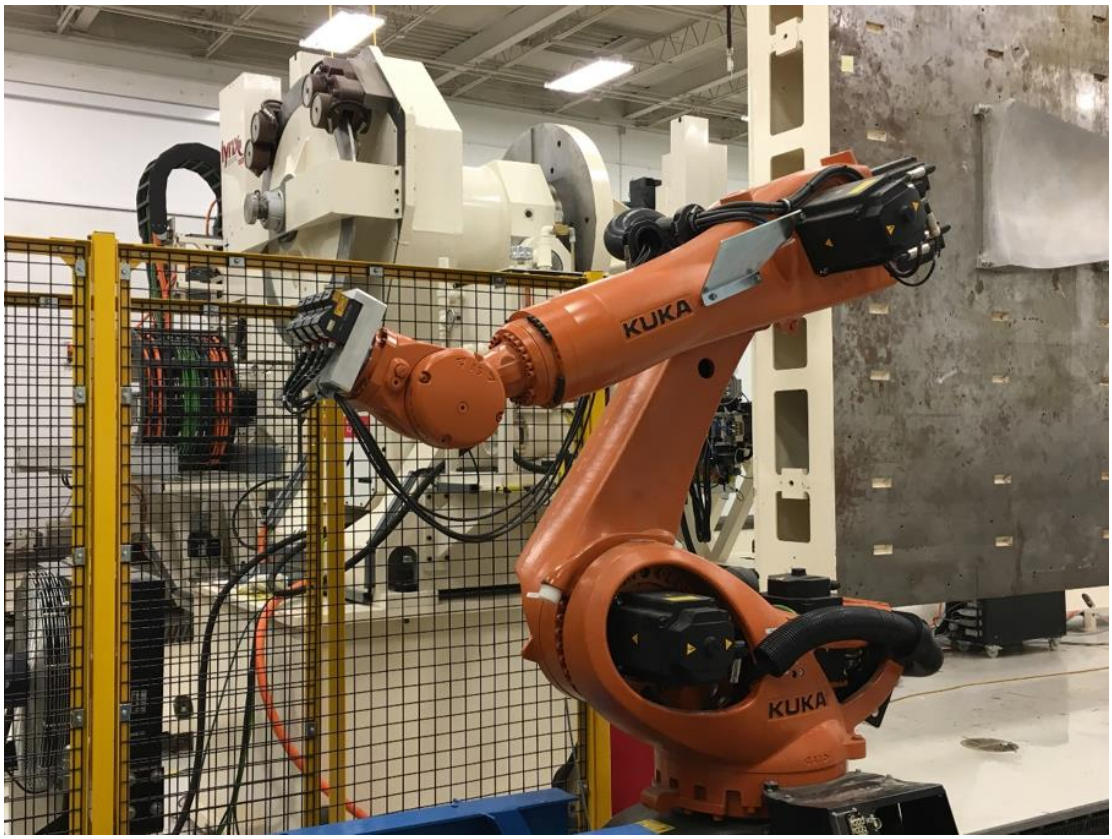


a. ACSIS Inspection System

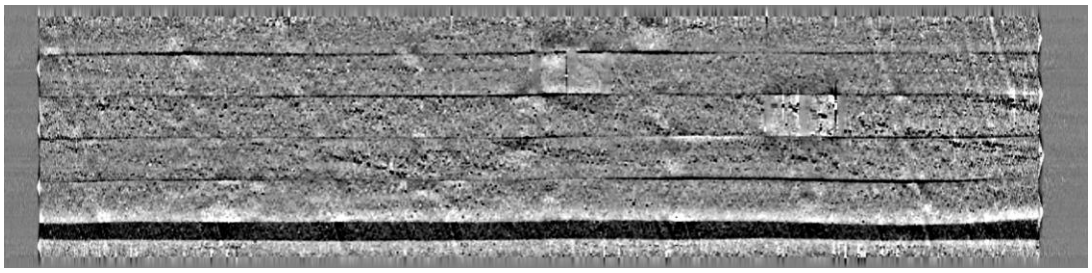

b. ACSIS Profilometry Image

Figure 4.4: ACSIS AFP Inspection System and Course Scan Image

For the process monitoring during the layup a recording of the layup speed for each course is captured to note any discrepancy between the actual speed of the layup and the

programmed one. To determine the nip point temperature, a trial 0° course is laid down with thermocouples placed under the toolpath. Varying this process at assorted layup speeds between 1500mm/min and 25000mm/min and three heater power levels of 150V, 170V, 190V allowed for the construction of an empirical model of nip point temperature as a function of heater power and layup speed. The results of this experiment can be seen in Figure 4.5.

Feed rate was captured through the recording of the machine material output. This data was subsampled to produce data at .1s intervals. Due to the internal machine parameters and head kinematics, the feed rate, despite being set so, is not a constant. Therefore, it was determined to move to a data scheme that matched data up according to course length rather than time. To attain the current position on the course, the feed rate was integrated with respect to time.

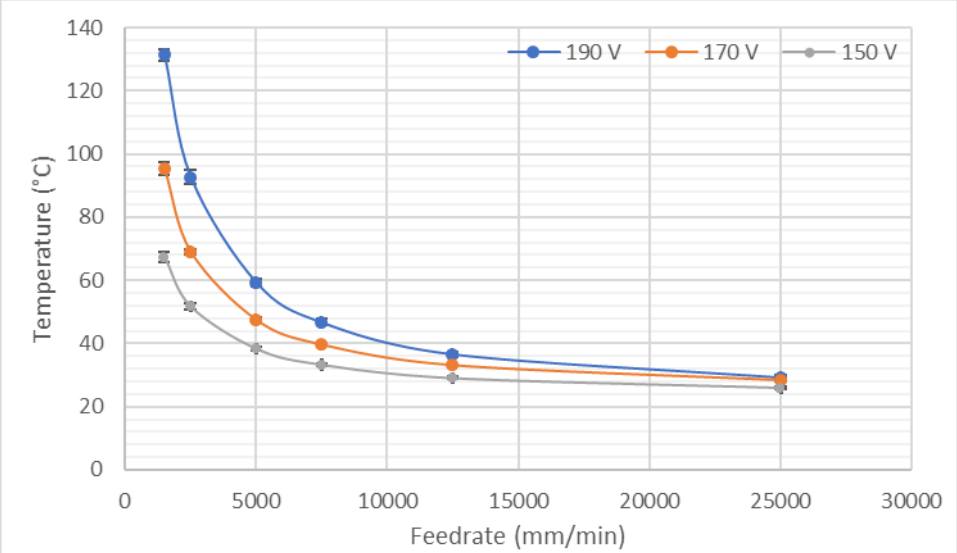


Figure 4.5: Results of Nip Point Temperature Experiments

## 4.5 DEFECT IDENTIFICATION AND COURSE QUALITY QUANTIFICATION

ACSIS scans were performed after all courses were laid up on the cylinder. To extract information relevant to defect production, a distinction between two classes of defects was made. The first class consisted of out-of-plane defects relating to wrinkles, folds, and puckers. The second class was denoted as in-plane defects and corresponded to gaps resulting from tow slippage during steering.

### *4.5.1 Automated Defect Identification*

To identify these defects on the profilometry scans, a simple observation that the two classes of defects correspond to two different heights in the scan allowed for the development of a very simple gating procedure to identify pixels corresponding to either defect type. The bottom 1% of pixel values were mapped to in-plane slippage, and the top 1% of pixel values were designated for out-of-plane deformation. After this gating procedure, small corrections were made through a UI previously developed. The final results of analysis can be seen in Figure 4.6. Green indicates in-plane defects and orange indicates out-of-plane defects. The boundaries of each course were also marked through the UI and saved for later identification of the course centreline.

As an initial investigation into the distribution of defects in the courses, the areas of the courses occupied by defects were calculated. Table 4.2 shows this preliminary evaluation of course quality for the 1270mm radius courses. A complete list of these values for all courses can be found in the Appendix.

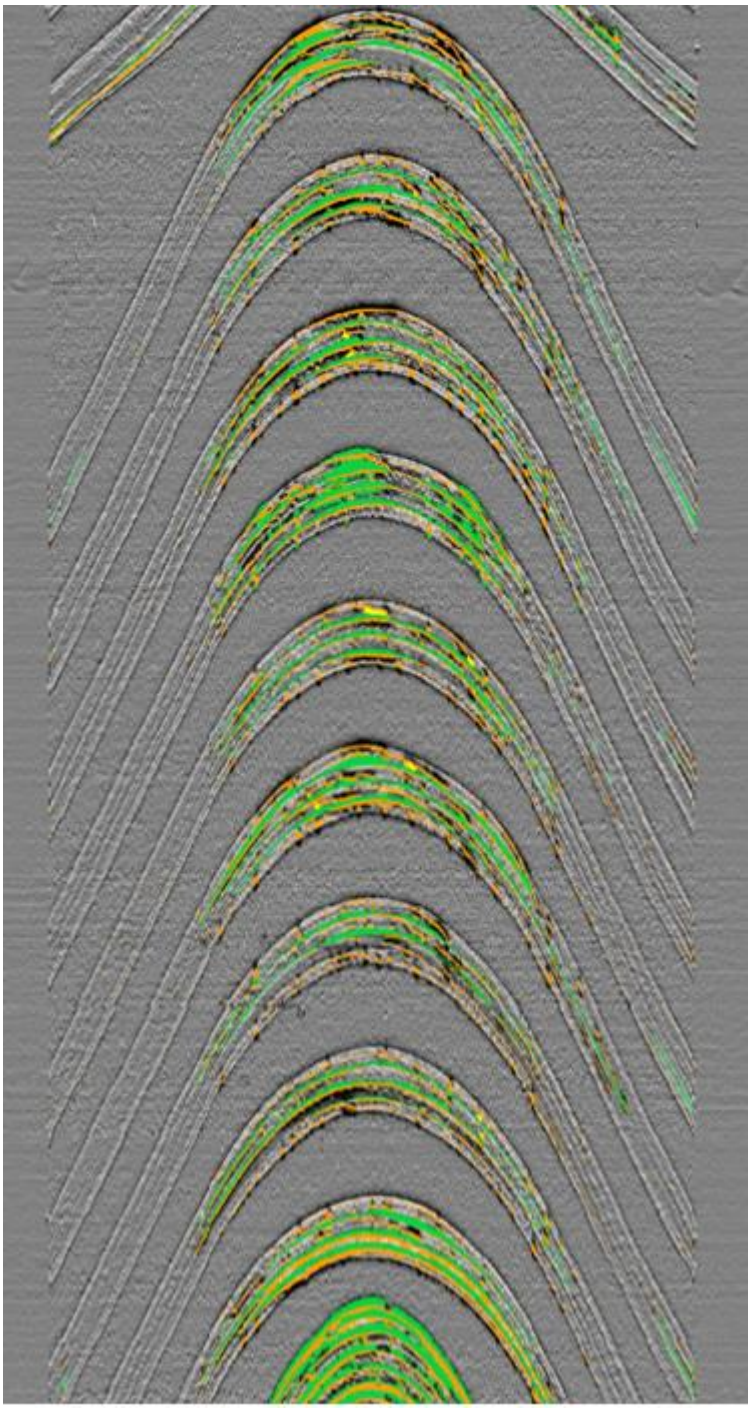

Figure 4.6: Defects Identified through Automated Defect Detection

Table 4.2: Area of 1270mm Radius Courses Occupied by Defects

| Course | Out-of-Plane (%) | In-Plane (%) | Total (%) |
|---|---|---|---|
| **130** | 6.45 | 7.51 | 13.96 |
| **131** | 3.69 | 12.67 | 16.37 |
| **132** | 5.95 | 10.73 | 16.74 |
| **133** | 5.25 | 6.13 | 11.39 |
| **134** | 4.99 | 11.16 | 16.15 |
| **135** | 5.19 | 10.12 | 15.31 |
| **136** | 5.37 | 4.59 | 9.95 |
| **137** | 10.10 | 8.58 | 18.68 |
| **138** | 7.44 | 10.23 | 17.68 |

*4.5.2 Identifying Course Centerline*

To properly represent this data in the context of the overall course, a centerline must be determined such that the defect can be placed in relation to both the course itself, and located according to the width of the course. To generate this centerline, the Voronoi Diagram [145] is created using the course boundaries as seed points [Figure 4.7].

The Voronoi produces a set of edges that can begin to be thought of as a pseudo-centerline. However, these edges must be filtered and selected from within the larger collection of Voronoi edges. Therefore, edges are filtered to only include those edges that fall within the course. The pseudo-centerline resulting from this filtering process may contain many artifacts that require more processing to remove.

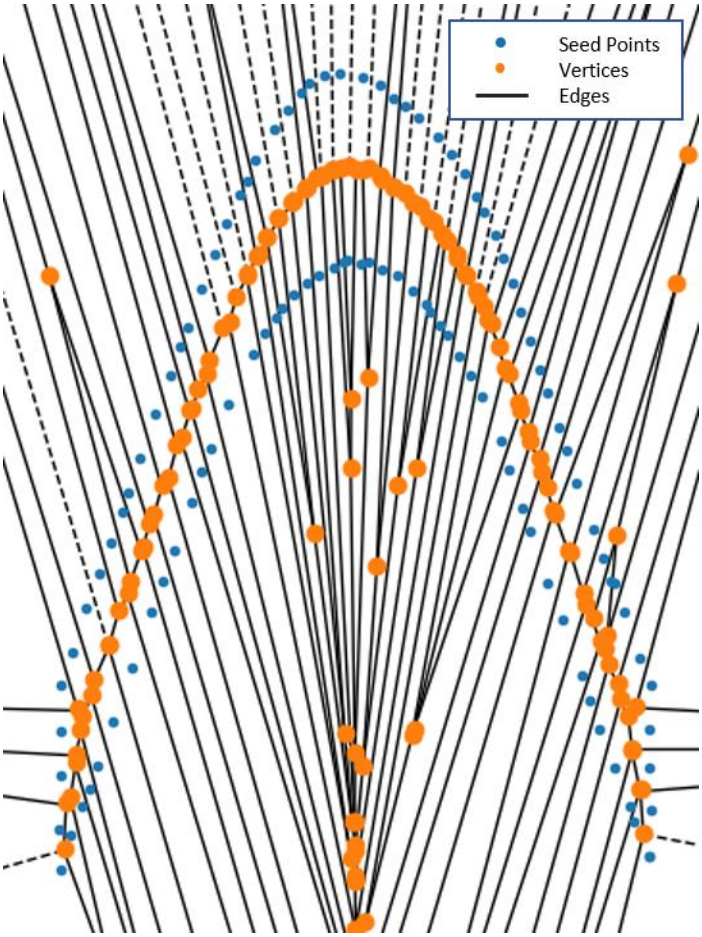


Figure 4.7: Voronoi Diagram for the Identification of Approximate Course Centerline

These edge artifacts can be removed through a number of potential methods. The authors considered a number of transformational or clustering approaches using the vertices of the edges that could be suitable for the application. However, if one notes a graph reflecting the connectivity of each of the edges, then a number of fast graph theoretic approaches can be deployed. To accomplish this, code was created to transform the list of edges from coordinate space to graph space such that connectivity information relating each edge to the overall set of edges could be determined. This produced a graph representing how each edge was bounded to neighboring edges.

Assuming these edge artifacts do not bridge across the interior of our pseudo-centerline, i.e. the artifacts represent a subgraph that is a simple path, then the centerline approximation is the shortest path from the leftmost to the rightmost edge vertex. This is quickly accomplished using Dijkstras Algorithm [146] by assuming that all of the edges in the graph have equal weight. Therefore, if the set of edges is small enough such that the process of mapping back and forth between graph space and coordinate space is efficient, then a complete centerline can be extracted.

*4.5.3 Creating Defect Measurements*

To further improve this centerline description, then a smoothing procedure by fitting a piecewise linear function to the centerline vertices achieves further improvement and importantly improves the smooth- ness of the centerline when taking the normal to the centerline for defect measurement [Figure 4.8].

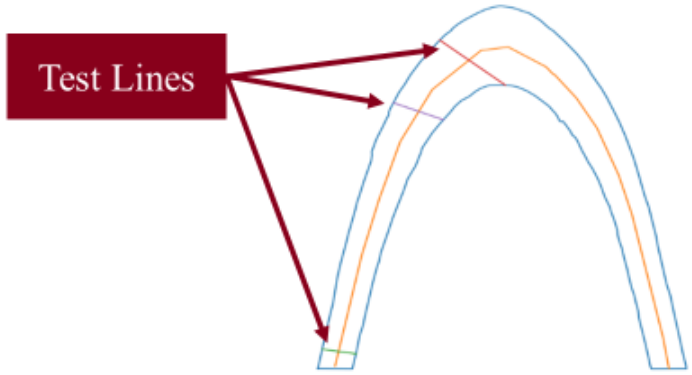


Figure 4.8: Test Lines for Defect Measurement Normal to the Course Centerline

To utilize the centerline information and the requisite geometry markers for each course, a line normal to the centerline is created and iterated 1000 times over the length of the centerline. At each point, the length of each defect that intersects with the normal line is measured. The measurement is normalized against the width of the course at the given

point, yielding the fraction of the course at that instant occupied by defects. Moving the normal line across each section of the course gives a defect production profile [Figure 4.9] measuring defects as a function of course length. While the application of this method is restricted to the two defect types of defects concerned in this document, there is little preventing an extension to many types of defects in AFP manufacturing.

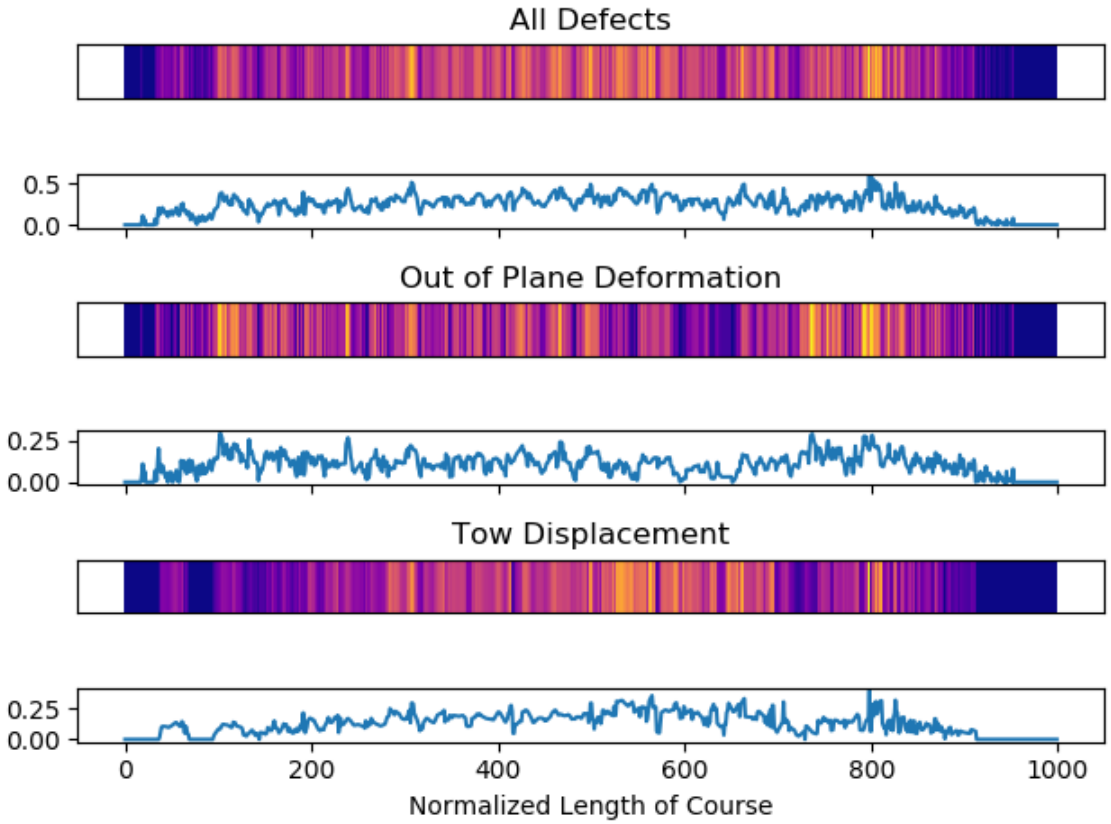


Figure 4.9: Course Quality as a Function of Course Length

## 4.6 METHODOLOGY FOR FEATURE RANKING AND PROCESS CHARACTERIZATION

### *4.6.1 Correlation Statistics*

An initial first estimate of the parameter influence on the response of the system in a data-centric way is to check the correlation statistics between each parameter and the production of the various defect classes. In this particular application, the classical correlation statistics of r and $r^2$ is used to examine the strength and direction of each parameter correlation.

For the r statistic, the linear strength of the relationship between two variables is indicated by the magnitude of the statistic, with $|r| = 0$ being completely uncorrelated, and $|r| = 1$ being perfectly correlated, i.e. having a relationship that is completely characterized by a linear fit. The direction of the relationship is indicated by the sign of the r metric, with a positive sign being correlated and a negative sign being anti-correlated. In other words, a positive correlation coefficient indicates that an increase in one variable coincides with the increase in another variable. Negative or Anti-correlation indicates that an increase in one variable coincides with a decrease in another variable. The coefficient of determination, or $r^2$ is simply the square of the correlation coefficient and is a raw strength measurement without directionality.

Note that an emphasis is placed on these metrics being an initial first examination of the strength of each parameters effect on the response. Correlation statistics make a number of assumptions, key among them are that (1) the two variables begin investigated are independent and (2) interactions between the additional variables in the system are negligible. In the case of layup speed and nip point temperature, this is clearly not an

applicable assumption. More sophisticated methods are needed to account for the interactions between variables to determine the strength of each parameters effect on layup quality in cases such as this.

*4.6.2 RReliefF Algorithm and Feature Ranking*

RReliefF [147] is an extension of the Relief Algorithm to continuous solution space $\ell$ with n-features. This family of algorithms provide a measurement of the variation in a response due to a specific feature. In general, RReliefF is attempting to determine for each feature the probability that an attribute A in a given instance is similar to A in a nearby instance. For a given set of predictions a weight W[A] is assigned for every feature such that

$$W[A] = \sum_{I1,I2} similarity(\tau, I1, I2) * similarity(A, I1, I2) \qquad 4.3$$

Where $I1, I2 \in \ell$. This similarity function is best represented as a generalized difference between two points in the set. RReliefF and its variants provide a quality ranking of each feature in the set ranging from -1 to 1 [148] with -1 being the worst weighting and 1 being the best. RReliefF offers a number of unique advantages: namely that there is no independence requirement between features, the construction of the similarity function can be used to remove the need for normalization, and the algorithm itself is computationally inexpensive compared to other filter-based feature ranking methods. The complete RReliefF Algorithm is presented in the appendix.

The RReliefF algorithm is applied to our dataset with each parameter included as a feature in the analysis with each defect type measurement as the $\tau$ target. For our finalized set of process parameters, the RReliefF code generated a series of feature rankings indicating the significance of each input parameter.

## 4.7 RESULTS

Examining the data can begin with the exploration of correlation coefficients and $r^2$ measures. As stated before, the conclusions drawn from these measures is somewhat limited, as it is well known that there is distinct interaction at the very least through the layup speed parameter and nip point temperature. This is demonstrated through the strong agreement through the empirical formulation for the relationship between heater power, speed, and nip point temperature.

However, for the furthering of this discussion, it becomes important to consider the indicated responses between defect production and the design/geometry dependent parameters (curvature) using r and $r^2$ as an initial indication about the direction as well as the strength of the response. It can clearly be seen from Figure 4.10a that the single strongest contribution to an increase in defect production comes from the curvature parameter.

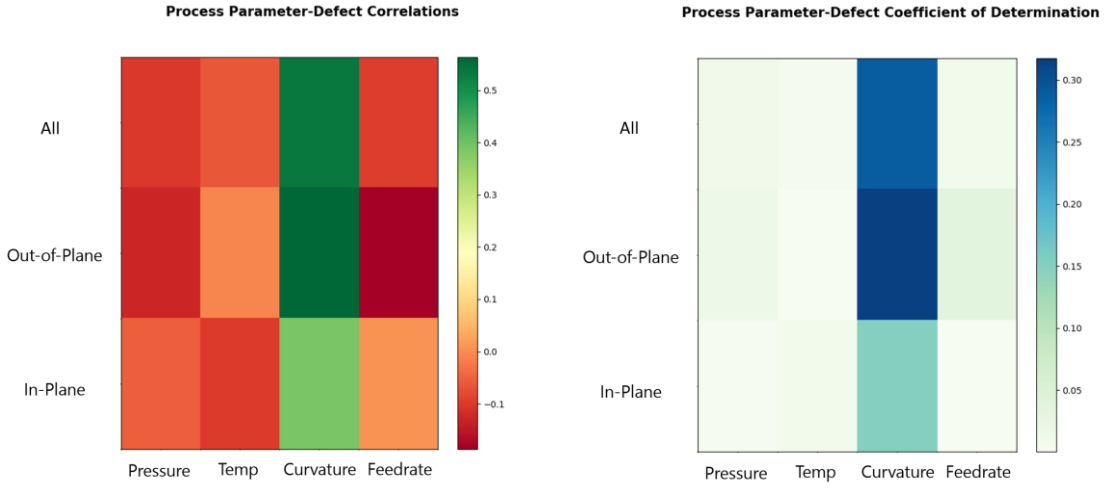


a. Correlation Coefficients Between Various Parameters

b. $r^2$ Metrics Between Various Parameters

Figure 4.10: Correlation Statistics from Constant Curvature Paths

The response is, in fact, so strong that it appears to wash out the effects from nearly every other process dependent parameter [Figure 4.10b]. The $r^2$ measure indicates that across the entire dataset, there is a far weaker relationship between the manufacturing parameters than with the geometric or design parameter.

However, interactions between various parameters can skew their correlation values. Therefore, it is important to move to more sophisticated analysis based on the RReliefF metric as mentioned in the previous section. Even when accounting for the interaction between the various parameters, RReliefF scores would indicated that geometry is still the most significant driver of defect production [Figure 4.11]. In the language of the RReliefF problem definition: curvature is the highest quality feature that best explains the data.

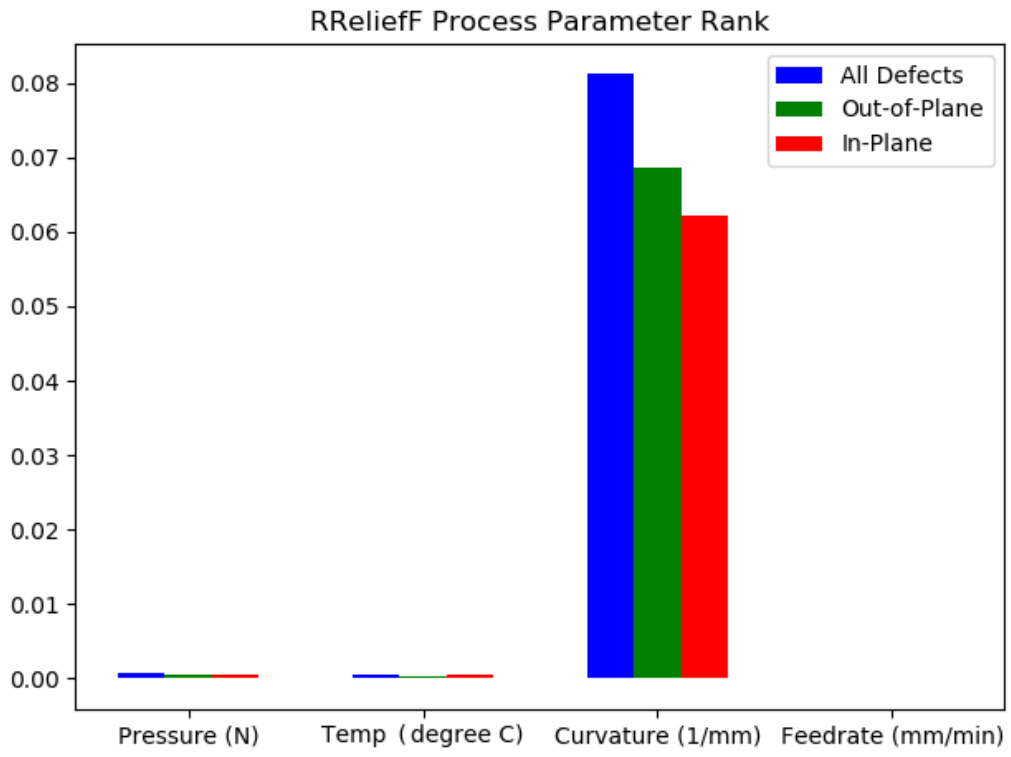


Figure 4.11: RReliefF Rankings for Constant Curvature Parameters

## 4.8 PREDICTION ERROR FOR VCP COMPUTED OVERLAPS

Another area where we can see the effectiveness of geometric arguments for the prediction of as-manufactured defects comes from the predicted layup defects resulting from a given toolpath and surface geometry as computed by VCP. To investigate this, a layup strategy for generating overlaps on complete coverage was produced for a doubly-curved tool.

### *4.8.1 Layup Strategy and Design*

Selecting the part to be produced for this experiment involved the reduction of multiple design variables into a design that addressed several considerations including a geometry that would naturally tend towards defects production, a layup strategy that is realistic to how such a part would be implemented in industry, and a shape that had relevance to aerospace components. The final design was a zero degree ply laid up on a doubly curved tool. The tool is approximately 2000mm in length. Seed point and layup strategy optimization were conducted in conformance with industry guidelines through the Computer-Aided Process Planning (CAPP) AFP tool developed in the neXt research team [149]. VCP is initially provided with the general laminate specifications to begin computing the fiber coverage. The laminate specifications indicated the extent of material coverage and primary fiber orientation for each ply. During the fiber coverage computation within each of the designated plies, the specific course paths were defined which were consistent with the fiber orientation and layup strategy. Layup strategies are key to planning fiber placement for complex surfaces, as they control individual fiber paths according to specific relationships between the surface geometry and previous fiber paths. A variety of layup strategies exist for different use cases, such as ensuring consistent fiber

angle (rosette), managing fiber curvature [150]. The course paths were the primary result of process planning, which are used along with machine processing parameters to create the final manufacturing program. However, the computed paths can be used to virtually reproduce the fiber placement and resulting geometry of the individual tows. e (natural), or ensuring consistent alignment between neighboring courses (parallel)

*4.8.2 Defect Predictions*

The zero-degree ply was processed through VCP to generate the defect predictions. A total of 8 tows were utilized for each course to match the manufacturing capabilities. The maximum course to course gap was set to zero millimeters and a maximum overlap of 6.35mm (one tow width). These settings ensured the presence of material overlap while preventing gaps. Those settings enabled the comparison of predictions and inspection for overlaps, while ensuring the presence of any gaps would occur as a result of manufacturing processes and would only be detected by the inspection. Following generation of the course paths and individual tow geometry, the defect analysis was performed for gaps, overlaps, and angle deviation.

No tow gaps were detected during the defect analysis. However, tow overlaps and angle deviation were detected extensively through the divergent regions of the tool surface. The overlaps Figure 4.12a depicted in red, exist between the neighboring courses, alternatingly depicted in white and gray. Fiber angle deviations Figure 4.12b are depicted on a continuous spectrum, where green represents little to no deviation, while yellow represents 3-4° of fiber angle deviation. The defects were then converted to the discretized pixel representation for further investigation.

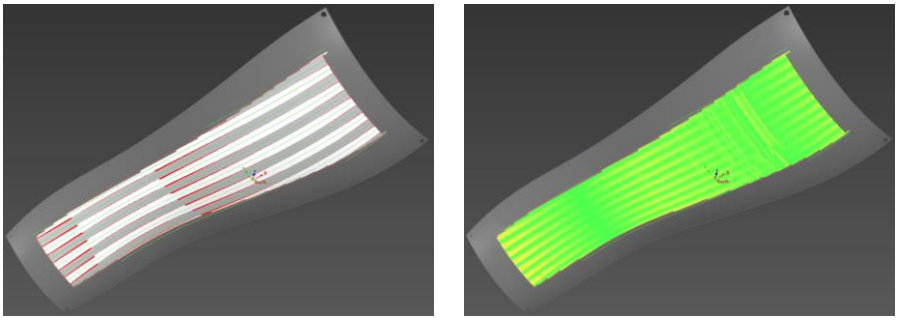

(a) (b)

Figure 4.12: VCP analysis of (a) overlaps and (b) angle deviations

*4.8.3 Comparison of Predicted and Detected Defects*

The comparison of the predicted and actual overlaps is presented in Figure 4.13. The predicted overlaps (red) correspond to the edge of neighboring courses, whereas the actual overlaps (blue) were measured over the entire ply and thus detected overlaps between tows within individual courses as well as the overlaps between courses. It is important to note that the prediction of gaps and overlaps were limited to simple geometric models in VCP, whereas prediction of tow-tow interactions may require more detailed models to account for tow deformation over the tool surface during placement.

Another possible reason for mismatch between the predicted and measured overlaps is the development of other types of defects in that region during manufacturing and their capture and labeling under another type of defect during inspection. For instance, the occurrence of a missing tow where a gap was predicted to occur can result in such discrepancy. The same applies to out-of-plane defects such as loose tow, surface separation, and bridging, where a "designed" overlap could possibly act as an instigator for such defects. As a result of this difference in capabilities between prediction and actual inspection, the actual overlap area was approximately 18.8% greater than the predicted area [Table 4.3].

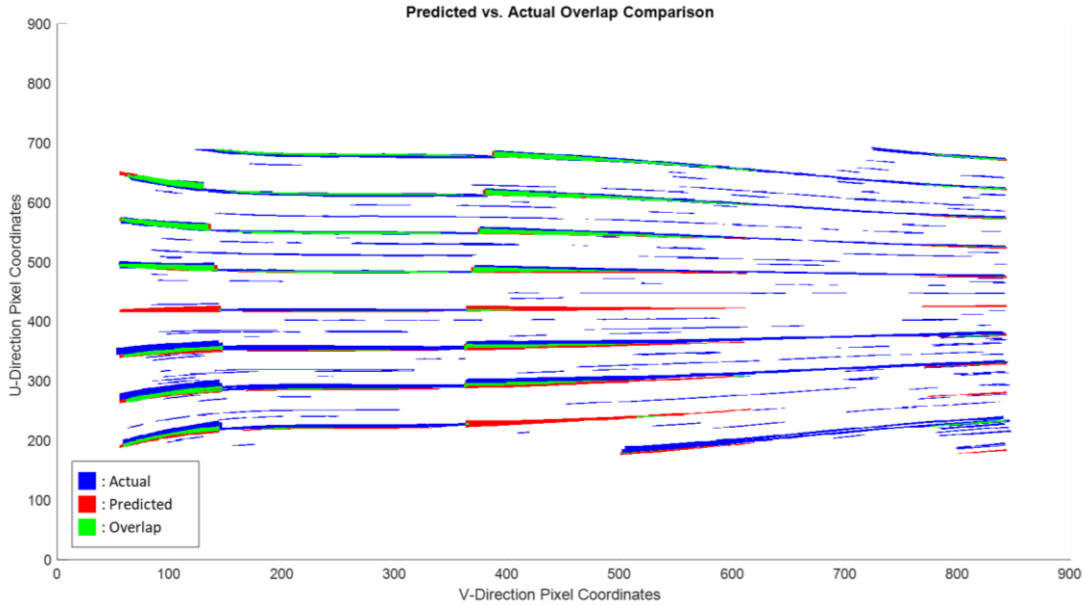


Figure 4.13: Predicted and actual comparisons between VCP and an Experimental Part

Table 4.3: VCP Predicted Overlap Error

| **Overlap Defect Area Comparisons** | | |
|---|---|---|
| Predicted area | 55001.6 | $mm^2$ |
| Actual area | 67717.9 | $mm^2$ |
| Error | 18.8% | |

Additionally, the results of the predicted and actual defects were overlayed onto the curvature of the surface [Figure 4.14]. The extent of the defects closely matches the curvature of the surface, where sets of defects are delineated at the changes of curvature. These results reflect on the modification of tow count and course direction in order to meet the gap and overlap settings that were utilized.

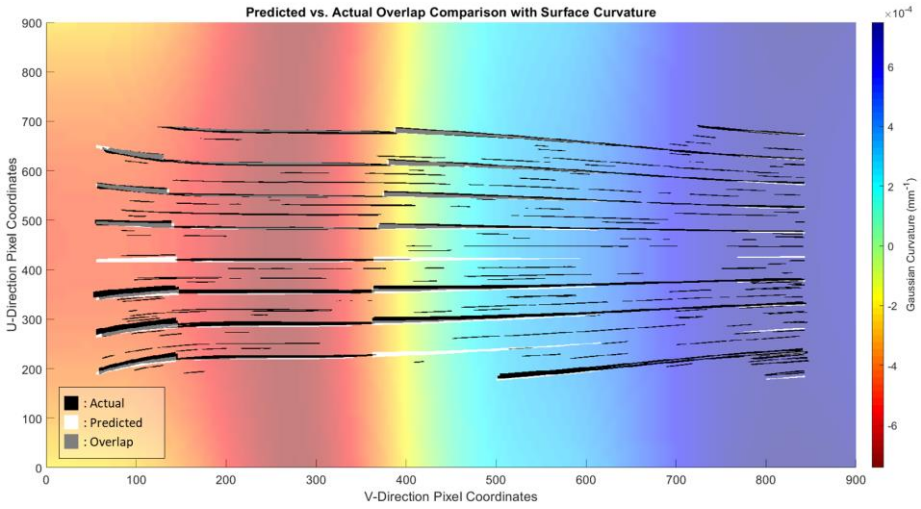


Figure 4.14: VCP and Predicted Overlaps Compared to Surface Curvature

## 4.9 CONCLUSION

By examining the response of defect production to assorted changes in design and process parameters, one can make a conclusion about the most significant factors driving the quality of a given AFP manufactured part. By considering both correlation coefficient and the RReliefF feature ranking algorithm, both direction and magnitude of defect drivers can be investigated. The results indicated that a significant amount of defect production is driven from the geometry of the part. An additional experiment was performed on a doubly-curved tool producing a 0 degree ply that shows reasonable agreement with experimental measurements for overlaps. Recall that VCP and CAPP are entirely geometry driven, with no consideration of any underlying physics. Therefore, it is reasonable to expect that geometric arguments for defect production can serve and an excellent selection for the mean function of the predictive GPR model. The final resulting model explains nominal behavior through the geometric arguments, with the stochastic component of the GPR model accounting for those variables such as material/surface interactions that are not well accounted for. It should be noted that in presentation of this chapter, it is assumed that the

results for high degrees of steering translate to other more conventional layup strategies such as incidental steering due to surface geometry.

# CHAPTER 5

# EXPERIMENTAL DESIGN

## 5.1 INTRODUCTION

The following chapter will provide an in-depth explanation of the experimental and data collection process necessary to build a dataset to both train and validate the hybridized quality prediction scheme. A single doubly-curved tool is use for AFP layup with a non-standard layup strategy, breaking away from the traditional quasi-isotropic paradigm. Additionally, two individual laminates were produced, further incorporating data from stain energy dissipation as more plies allow for more compliance of the underlying substrate.

Time limitations prevented a full characterization from multiple machines and multiple material systems. As such, this experiment will focus on those parameters that are directly relevant to process, while excluding those features mentioned in Section 3.2 pertaining directly to material and machine properties.

## 5.2 PARAMETER MEASUREMENTS AND DATA COLLECTION

To generate the necessary experimental defect mapping and parameters fields over the laminate, it is necessary to continuously collect data during the layup process and then to inspect after every ply. Some of this can be accomplished through the use of on-board data collection capabilities of the AFP machine. Other parameters need to be estimated from design of experiment and testing with individual components of the layup process.

Bellow is a table listing the measurements taken and the methodologies used to collect each parameter set [Table 5.1]. Each will be expanded upon in throughout this subsection.

Table 5.1: A Collection of Parameters Tracked During Layup and their Measurement Methods

| **Parameter** | **Collection Methodology** |
|---|---|
| **Tool Geometry** | CAD and Analytical Calculations |
| **Compaction Pressure** | Estimation from DOE |
| **Heat /Temperature** | Estimation from DOE |
| **Machine Motion** | Registered on AFP Motion Controller |
| **Tow Curvature** | Estimated through VCP |
| **Defect on Preceding Ply** | Captured During Inspection |

### *5.2.1 Tool Geometry*

Many of the important characteristics of tool geometry discussed in previous sections can be estimated directly from tool CAD and design files. Important metrics such as local curvature are trivial to estimate from tool geometry. Measurements are restricted to within the ply boundary to avoid singularities when computing various curvatures such as gaussian. Field estimates are created through the use of programmatic CAD tools such as PythonOCC.

### *5.2.2 Compaction Pressure*

Estimation of the compaction field over a ply is significantly more complicated. Several works on the effect of roller hardness and surface geometry on layup compaction pressure exist in the literature [151], [152]. In a variation on previous approaches, measurements of the roller used in the experiments were taken to determine the vertical

displacement of the roller and therefore the pressure patch formed under loading on a flat surface. This was used to set the roller stiffness parameters.

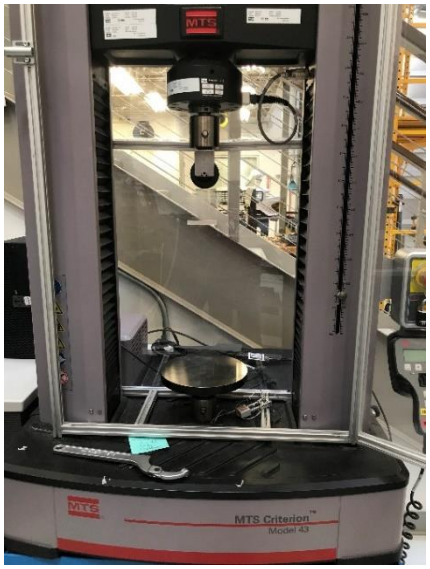


Figure 5.1: Testing Stand for Determining Roller Stiffness

A static compaction model used in literature [153] was examined and repurposed for use in ply level analysis. By considering the static pressure generated by the roller at a single point, informed by the experimental measurements, and iterating the compaction model over the course of an entire ply, one can generate a pressure distribution over the entire ply in a course-by course manner.

*5.2.3 Heat and Temperature*

To determine the distribution of heat, and therefore develop a metric closely related to the temperature of the substrate during layup, a series of calibration tests were conducted with the AFP machine heating element. Thermocouples were placed along the toolpath of the machine and collected temperature data during a series of dry runs across a course. By varying the layup speed and heater voltage, a parametric formula can be fit to determine the substrate temperature at any speed and voltage in a manner identical to what was

conducted in Section 4.4. In a similar manner to the compaction pressure, this temperature model was then applied course-by-course to determine the temperature distribution over an entire ply.

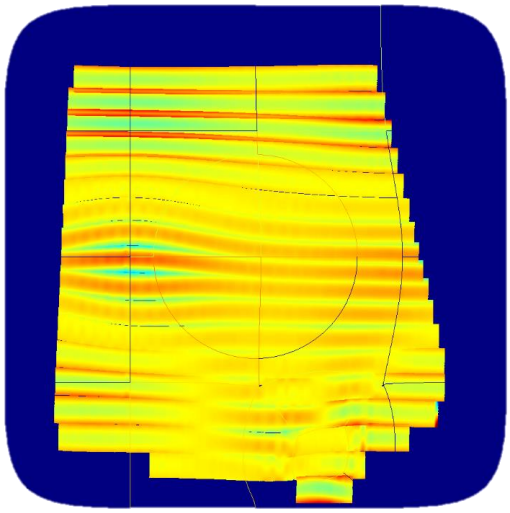

Figure 5.2: A Ply Level Analysis of Pressure Distribution

To construct an empirical measurement to map voltage and speed to temperature, material was placed at varying speeds and heater voltages over a series of thermocouples on a flat tool. By noting the results for every trial, a parametric representation can be formulated that maps well with the current data and lies within the confidence intervals for each variation in layup speed percentage. While this estimate may not be as effective as a full transient heat simulation, the representative power of this approach should be enough to establish the difference between temperature parameter variations across different sets of courses. In other words, the approach does not necessarily need exact parameter values, but values that are both consistent in measurement and differentiating between trials.

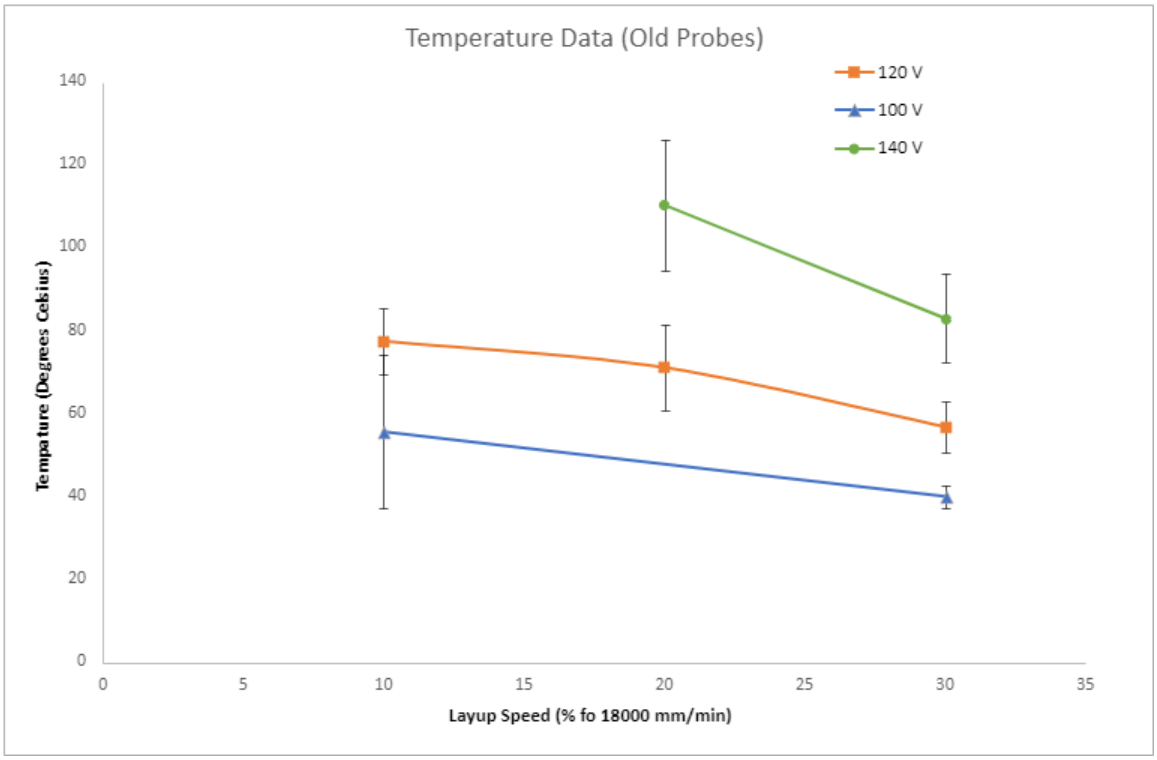


Figure 5.3: Empirical Temperature Measurements with Respect to Voltage and Layup Speed

From this data, one can assemble the following equation to express nip point temperature in terms of voltage and layup speed:

$$t = k(V)s + V\alpha(V) \tag{5.1}$$

Where

$$k(V) = -.000183V \tag{5.2}$$

$$\alpha(V) = .01095V \tag{5.3}$$

*5.2.4 Machine Motion*

The numerical control units on the AFP machine are capable of recording numerous parameters related to the control of the machine throughout the layup process. In case of

this particular investigation, many of the relevant parameters concerning machine motion and layup speed can be extracted through the query of this data in an OPC-DA server on the machine's Siemens PLC. From this, position, velocity, and acceleration data can easily be determined by considering motion data when the heater is also activated, indicating the machine is in the state of actively placing material.

### *5.2.5 Tow Curvature*

The final design parameter that has an extremely high degree of influence on the production of defects is the gaussian curvature of the individual tows as they cover the geometry of the tool surface. This is a feature that can be calculated both through the VCP design information and numerically through the raw toolpath data. It is the assumption of this model that the towpath described by VCP during the path planning process is close to the actual trajectory each tow takes on the physical part. Computing the curvature of each individual tow at a discrete set of points also generates a "tow curvature field" to be clustered and inserted into the hybridized model.

## 5.3 INSPECTION DATA

The determination of the physical response of the system, i.e. the overall quality of the layup, in experiment is the key by which our modeling approach distinguishes itself from many of the other attempts to predict layup quality in the literature. True measurement of defect production with accurate representation of defect features is difficult, but not impossible if one attempts to design an inspection system with the intent of maximizing the utilization of defect data.

To properly capture quality data on the manufactured part, an automated inspection system located at the McNair Center is used to create a precise map of the defects existing

in the part both pre-rework and post-rework. The IMT developed Advanced Composite Structures Inspection System (ACSIS) inspection platform consists of a Kuka KR120 robotic arm with 4 laser profilometers. The profilometers enable rapid height profiling of a structure with high resolution. These height maps are then collapsed into greyscale images for viewing or further processing. ACSIS is a ply-by-ply inspection system, meaning that to inspect a ply, the AFP machine must lay down a ply, the mandrel rotates to expose the ply to ACSIS, which then scans the entirety of the ply. Once the scan is complete, the mandrel rotates back over for the layup of a new ply. This is the same system as described in Section 4.3.2.

The ACSIS software suite encompasses the tools required to run the robotic arm and to stitch the images back together. In addition, machine learning and computer vision algorithms are also used within the ACSIS software to identify specific types of defects within the ply. The current ACSIS defect detection paradigm places a box each defect on the part. In prior work [143] the authors' developed an inspection tool that allows for the identification of defects down to individual pixels, allowing for precise representation of the defect. This precise characterization tool is used to extract and process defects from the scan images in this work. This pixel level representation is converted into a bounded polygon through the marching squares algorithm [154].

Building up on the ACSIS system discussed in previous sections, an approach for the precise characterization and digitization of defects in a layup were developed on two key principles: (1) identification of precise boundaries for each defect in a scan rather than simply detecting their presence, and (2) the location of defects in the part coordinates in such a manner that they can be linked in CAD to their exact location on the part.

Both of these goals require a high degree of automation such that data can be collected and rapidly processed. One cannot spend weeks manually marking the boundaries of each tiny gap in a ply. Similarly, the ability to trace a particular point or region of interest in an image back to its origin on the part is neigh impossible without input from the inspection system itself. It is proposed in this document that the solution to the first challenge of image processing can be solved through the application of machine learning. While the second challenge can be met with the incorporation of robot path planning data and a custom raytracing program. The following subsection is a summation of several years of work by the author and can be found in several publications [13], [20], [143], [144], [155], [156].

*5.3.1 Semantic Segmentation for Defect identification*

As discussed previously, the precise marking of each defect boundary through some software tool is incompatible with the ideas of short downtime and limited cognitive load for inspection. Therefore, an automated method for the size and shape characterization for AFP defects is required. ML is common tool in computer vision, but the traditional CNN architecture is simply to restrictive, only allowing for classification on a whole image or patch of an image.

While a patch-wise detection strategy with CNNs might have some success, context from outside of said image patch cannot be incorporated, and therefore learning from an entire scene cannot be accomplished. Just as importantly, we are only left with classification within a given box or region. One can know that a gap exists in the region, but also know nothing about its placement in that region, nor its size or shape. What is

needed is an ML system that is capable of learning may classes of defect and identifying them on a pixel-by-pixel basis.

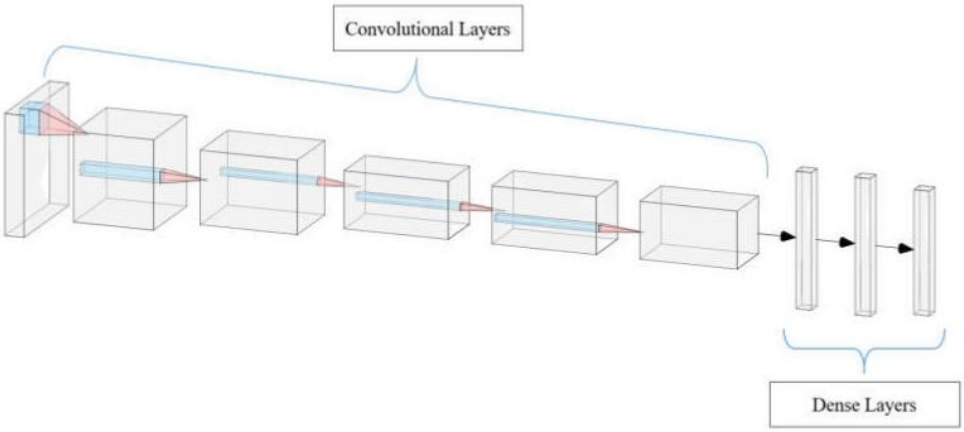


a. A Traditional CNN Architecture

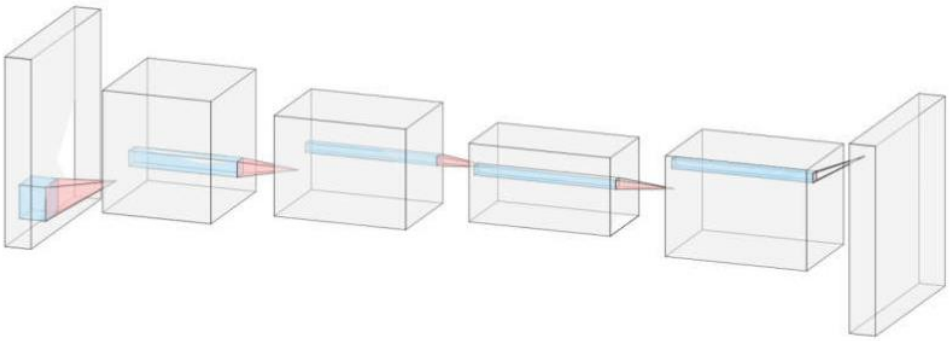

b. An FCN Architecture for Image Segmentation

Figure 5.4: A Comparison Between a Typical Image Classification CNN and an FCN

Long et. al. [81] proposed a neural network architecture that consisted entirely of convolutional layers, replacing the dense layers at the end of down-sampling in a traditional image classification CNN [30] with an up-sampling head consisting of convolutional layers. Up-sampling to the original image resolution then allows for pixel-level labels to be used to train the network to produce a classification for each pixel [Figure 5.4]. This

style of neural network, known as a Fully Convolutional Neural Network (FCN), has become popular for image segmentation tasks.

Table 5.2: Defects Identifiable with neXt Inspection Software

| Type | ID | R | G | B | Color |
|---|---|---|---|---|---|
| **Automatically Detected** | | | | | |
| No Defect | 0 | 0 | 0 | 0 | |
| Twist | 1 | 136 | 0 | 27 | |
| Fold | 2 | 247 | 249 | 165 | |
| Missing Tow | 3 | 0 | 168 | 243 | |
| Gap | 4 | 14 | 209 | 69 | |
| Overlap | 5 | 255 | 157 | 0 | |
| Wrinkle | 6 | 4 | 0 | 255 | |
| FOD | 7 | 255 | 0 | 255 | |
| Surface Separation | 8 | 153 | 153 | 102 | |
| Loose Tow End | 9 | 51 | 102 | 0 | |
| **Hand Labeled** | | | | | |
| Pucker | 10 | 13 | 255 | 0 | |
| Bridging | 11 | 140 | 255 | 251 | |
| Shredders | 12 | 142 | 137 | 143 | |
| Position Error | 13 | 204 | 153 | 0 | |
| Boundary Coverage | 14 | 221 | 162 | 234 | |
| Splice | 15 | 236 | 28 | 36 | |

This ML approach is adopted for the identification and characterization for AFP defects in ACSIS scan images. A dataset consisting of approximately 800 800x800 pixel ACSIS scan images and their ground truth counterparts were used to train an FCN to predict defects across 10 classes [Table 5.2].

The FCN architecture is based on a UNet design [157], with each downsampling or upsampling operation preceeded by a block of convolutional layers. Each block is also concatentated with the block of equal shape on the opposite side of the network. This allows latent encodings from earlier in the network to be passed forward and be continuously evalutated as training is occuring. To encourage tight clusters of pixels and prevent overfitting on over-represented classes, a Jaccard loss function [158] was used. The Jaccard loss function uses the Intersection Over Union (IoU) metric to train ML algorithms. By basing the network error score on ability to localize over specific class samples rather than raw sum-of-pixels metrics such as Cross Entropy, under-represented classes are weighted equally with more frequent samples. This is crucial in image segmentation where the majority of the pixel space is occupied by background.

*5.3.2 Manual Correction and Validation with User Interface (UI)*

While ML segmentation algorithms are useful for offloading much of the cognitive load for identifying and characterizing AFP defects, they are still prone to occasionally imperfect performance. In such a safety-critical application as quality assurance, it is necessary to give inspection operators tools to both review algorithm-identified defects and correct where necessary. To facilitate this, the next inspection software utilizes and corrective UI with the capability to add, delete, move, or modify algorithm-identified defects where necessary. One may note that Table 5.2 contains a section of defect for hand-

labelling. These are defects that require special context to distinguish from other, similar, defects. Therefore, the inspection operator can take more generally labelled defects and narrow in their classes based on other context not readily available in each image scene. A version of the UI can be seen in Figure 5.5.

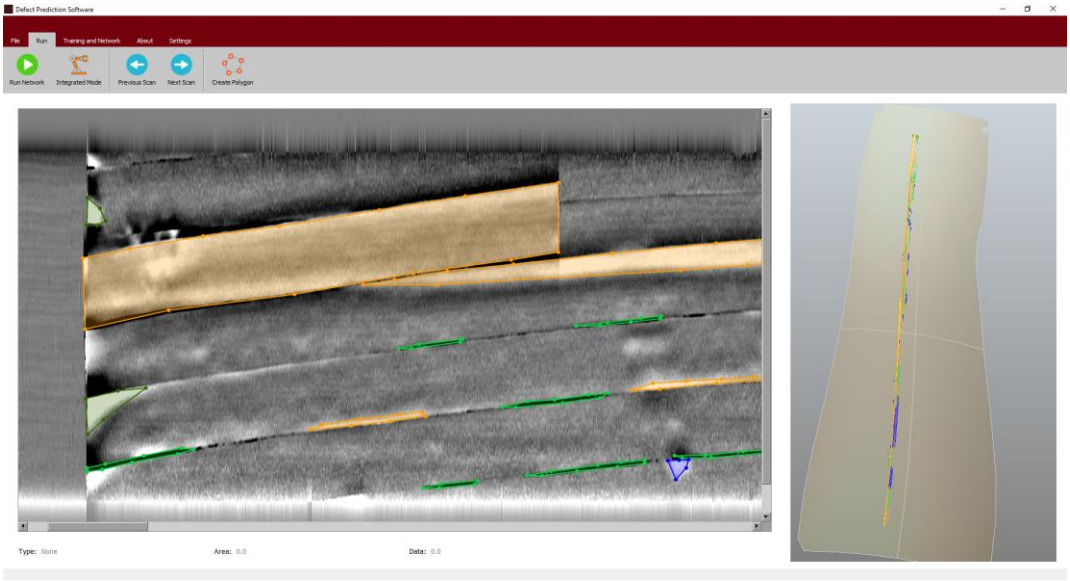


Figure 5.5: The Integrated neXt Inspection UI

*5.3.3 Defect Mapping in CAD*

The final component of the collection of defect data is the mapping of defect information back into a coordinate reference frame that is shared with the ply. To accomplish this, the robot toolpath for the ACSIS scans is linked with the inspection data to assign a position in 3D for every point of interest in the ACSIS scan images. This is accomplished by calculating the percentage length of a scan image that a point of interest is located. The author assumes that the profilometers on ACSIS are triggered at equal intervals, implying that each pixel in the horizontal direction is evenly distributed across the ACSIS toolpath.

With the spacing across the toolpath determined, compensation for there being far more horizontal pixels than there are points in the toolpath is necessary. One could take a number of approaches, including fitting a spline to the toolpath to parameterize it. Another approach that yields close results is to linearly interpolate between each point in the toolpath, assuming that the ACSIS head orientation also changes in a linear fashion for any two sets of vectors $R_0$ and $R_1$ separated by a parameterized path length $l$.

$$R_i = (l-1)R_0 + lR_1, l \in [0,1] \qquad 5.4$$

By understanding the head orientation, it is possible to determine the vector normal to the head, or the direction that a ray of light takes from the profilometer onto the part. When light cast along this vector is translated along the perpendicular vector k determined by the head orientation to the location of a pixel on the profilometer face, its intersection with the part directly corresponds to the location that pixel is recording in the scan image [Figure 5.6].

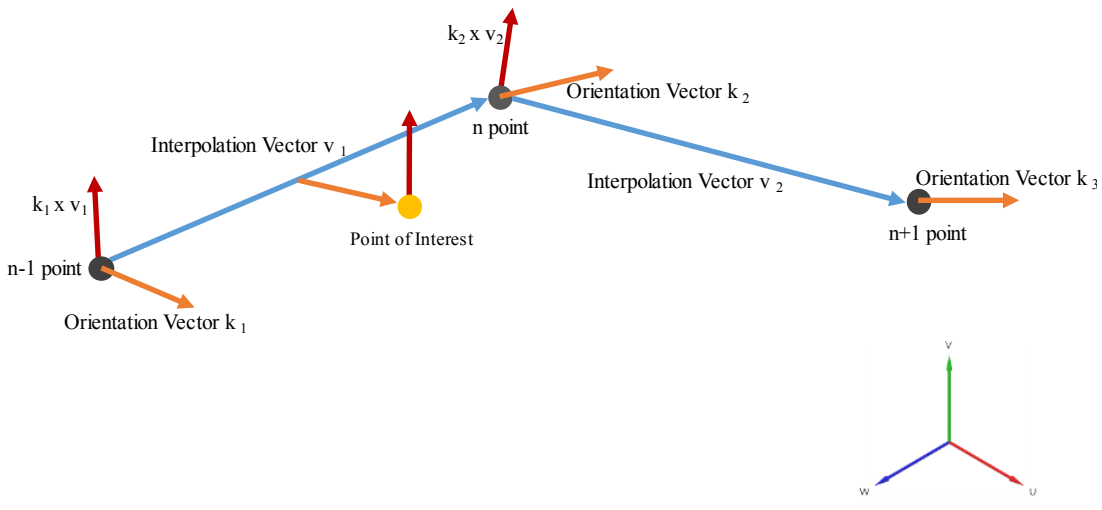


Figure 5.6: Calculating the Ray for Mapping a Point of Interest onto Part Surface

Assign a point of interest for every vertex in each polygon identified using the inspection software. By tracing the ray from the vertices in a single polygon back onto the tool surface, it becomes possible to link the vertex points together on the tool surface in the same order as they are organized in the respective image. Once mapped onto the tool surface, each point is transformed into the (u,v) parametric space of the tool surface and linked, yielding a closed path that is expressible as a collection of curves along the tool. This collection of curves, when linked, forms the outline of the polygon properly placed in its original location on the part. A defect polygons from a set of scans taken on a single ply can be seen in Figure 5.7.

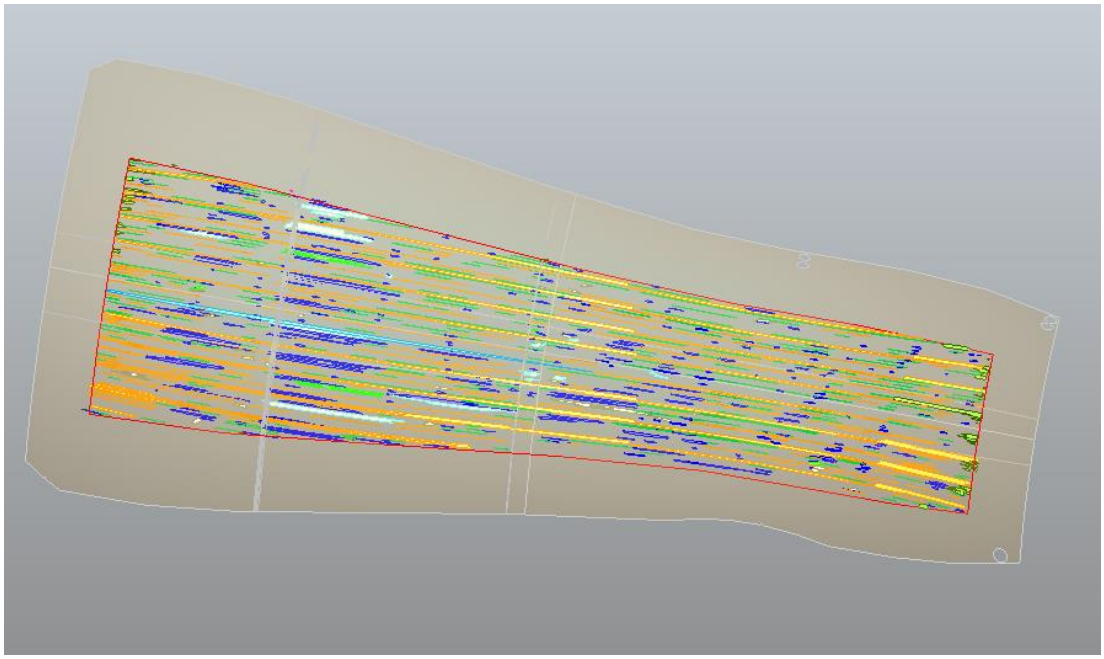

Figure 5.7: Inspection Data Mapped back onto Tool Surface Geometries

Unfortunately, a naïve mapping of the results of each scan image back onto the part does not yield a complete result ready for ingestion into the hybridize ML model. ACSIS scans consist of sets of 4 profilometer images for each scan path, with multiple overlapping paths required for complete coverage of a ply.

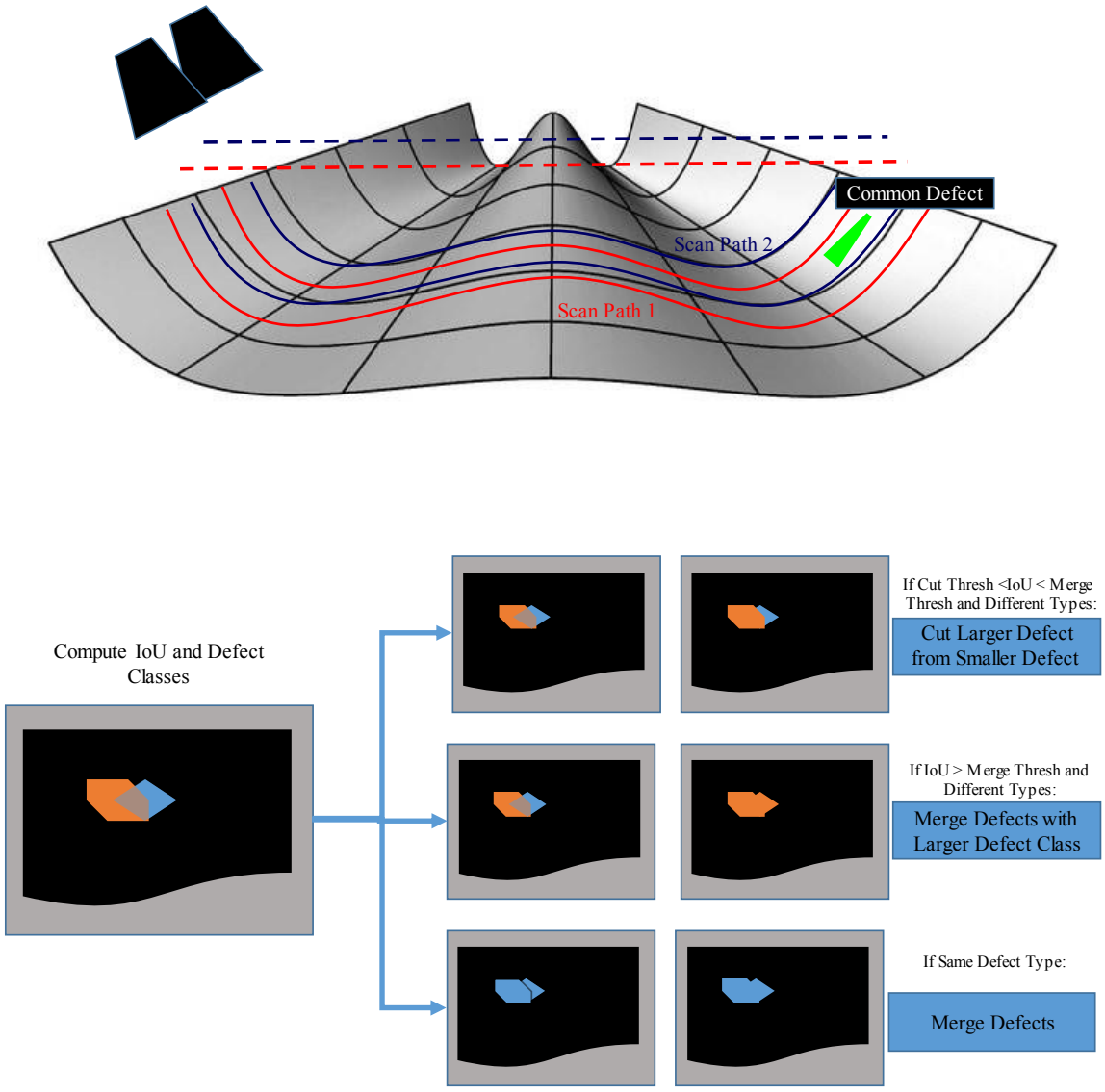


Figure 5.8: Defect Merging Rules for Overlapping Scan Areas

Therefore, it is necessary to map each scan image with a horizontal offset to account for each profilometer location and to identify overlapping defect that were covered in multiple scans and link them back together. To perform this defect stitching operation, a search and eliminate algorithm was developed to search through an unsorted list of defects, compute the IoU for each pair of defects, and merge if the IoU criteria met a threshold, cut

if IoU was significant but under the merge threshold, or merge if the defects were of the same type [Figure 5.8].

---

**Algorithm** 5-1**: Search and Merge Algorithm**

---

**Data:** A complete set of unmerged defect polygons in (u,v) space

**Result: A set of merged defects where no defect is overlapping**

$\boldsymbol{List_1 \rightarrow All\ Defects}$;

$\boldsymbol{List_2 \rightarrow List_1[0]}$

$\boldsymbol{Delete\ List_1[0]}$

**for defect in** $\boldsymbol{List_2}$ **do**

    **for merged_defect in** $\boldsymbol{List_1}$ **do**

        check merge condition

        **if** merged

            **append** $\boldsymbol{List_2}$ with **defect**

            **delete defect**

        **if** cut and merge

            **append** $\boldsymbol{List_2}$ with merged **defect** and **cut**

            **delete defect**

---

---

The search algorithm for determining the merging of defects begins with a complete list of each defect in the (u,v) space of the tool surface. A single defect is placed in a

separate list and checked for merge conditions against every defect in the original list. If a defect in the original list is checked against every defect in the merge list and does not meet merge conditions, then it is added into the post-merge list. A detailed explanation of the merge algorithm can be found bellow. For the purposes of this document, our cut threshold is set to a value of zero, whereas the merge threshold value of .5 is discovered through hand tuning to be an acceptable rate.

## 5.4 EXPERIMENTAL PARAMETERS

Now that the author has concluded a comprehensive discussion of measurement techniques and methodologies to determine the overall quality of a laminate, consider the overall form of the experiment and the assorted parameter variations to capture relevant behavior. This subsection begins with an overall discussion on how parameters are varied such that and general random sampling is achieved. Then details of the layup sequence for the two laminate produced are presented with insights as to how the design space was selected to provide a more comprehensive set of fiber angles than the standard quasi-isotropic strategy in typical studies of this nature.

### *5.4.1 Parameter Variations*

As discussed previously, metrics of layup speed, heater voltage, and compaction force are varied and tracked to account for the in-manufacturing parameters that can have a potential effect on the quality of layup. An initial bounds for each parameter was provided by the machine operator such that the operator was comfortable running at any parameter combination offered through the random sampling. A set of choices was provided for each parameter type and choices for each set of parameters was selected uniformly such as to

not bias the data in any particular way. The choices available for each parameter type is provided in Table 5.3.

Table 5.3: Parameter Choices to be Randomly Sampled

| Parameters | Parameter Choices | | | | |
|---|---|---|---|---|---|
| Speed | 10% | 20% | 30% | 40% | 50% |
| Heater Voltage | 90-150V | | | | |
| Compaction Force | 150-600N | | | | |

Courses were grouped into groups of 4, with all of the courses in the group being run at the same parameter set. This was not necessarily a strict rule, with the number of total courses in the ply dictating that the last group was not always consisting of exactly 4 courses. Nonetheless, this strategy of random selection and grouping gives an overall good characterization of the quality response space with a given set of parameters exposed to what was often quite a large amount of geometry variation over the tool surface. It should be also noted that at the machine operator's discretion, parameter sets were changed. All changes were tracked and reflected through in the raw data captured on the system. Thus is the nature of running experiments on a multi-million-dollar university machine.

*5.4.2 Ply Design and Stacking Sequence*

There were two individual laminates produced over the course of the experimental trials, with the first laminate consisting of 4 plies and the second consisting of 9 plies. Given the changes in surface tack properties between the base tool surface and subsequent plies, the data from the first plies in each layup were removed from the dataset. The complete stacking sequence for both plies is listed in Table 5.4.

Table 5.4: Stacking Sequence for Both Laminates Manufactured

| | Layup 1 | Layup 2 |
|---|---|---|
| Ply 0 | 0° | 0° |
| Ply 1 | 70° | -45° |
| Ply 2 | 0° | 70° |
| Ply 3 | 70° | 90° |
| Ply 4 | | 0° |
| Ply 5 | | 90° |
| Ply 6 | | -45° |
| Ply 7 | | 70° |
| Ply 8 | | 0° |

## 5.5 REVIEW OF WORK

In this section, the author has discussed in depth the experimental and data collection approach for capturing the necessary data to build a hybridized ML model. This includes details on the mechanisms to experimentally verify the layup quality of a given ply using automated inspection tools to reduce the manual data collection workload. Machine process data was collected through a combination of data returned through the AFP machine controller and empirical measurement through various sensors. An outline of the overall experiment was then presented, noting the stacking sequences for two laminates manufactured for data collection and validation. A proprietary material was used for the experiments, and therefore any in-depth discussion of materials and material properties has been omitted in this document.

# CHAPTER 6

# RESULTS AND ANALYSIS

## 6.1 INTRODUCTION

Previously in this document, the author has presented an overview of the problem of predicting the behavior of complex systems using purely data-driven and physics-driven approaches. Then, the concept of a hybrid physics-data model was introduced to the reader, with discussions of varying approaches to the problem and the advantages of such a hybridized approach to alternative methodologies. The author proposed a novel parameterization of the GPR algorithm as a vehicle to this hybridization approach with an emphasis on applications in AFP quality prediction utilizing fast geometric algorithms augmented with data. An experiment was proposed and conducted to collect data to feed into such a model. In an attempt to bring the discussion to its inevitable conclusion, the following chapter will present an attempt to predict the amount of overlaps in a given section of a ply utilizing all of the tools outlined and developed previously in this document.

As discussed in previous sections, the prediction target for this model will be the percentage of area occupied by a given defect type. In the primary case of this section, the author's concern will be overlaps due to the ready availability of overlap predictions from VCP created during the process planning phase. Initial results were also generated and will be displayed for wrinkles and puckers, but with the assumption that the degree of steering on the part is not high enough to generate significant wrinkling as informed by the models developed by Wehbe [129],and therefore will have a constant zero mean function.

## 6.2 DATASET

At final conclusion, a dataset of 240 individual cells from 9 plies placed on the tool were sampled to compile the dataset used to train the model. Note the extremely small number of plies actually produced to compile this dataset. To further reduce the number of features required for model convergence, the defect area in the preceding ply under a given element was excluded. It was concluded that this feature was more relevant to the formation of defects involving a lack of contact with the surface such as puckers, wrinkles, and bridges rather than the target defect of overlaps. It will be suggested in future work to find ways to tailor the feature selection to the individual defect types of interest.

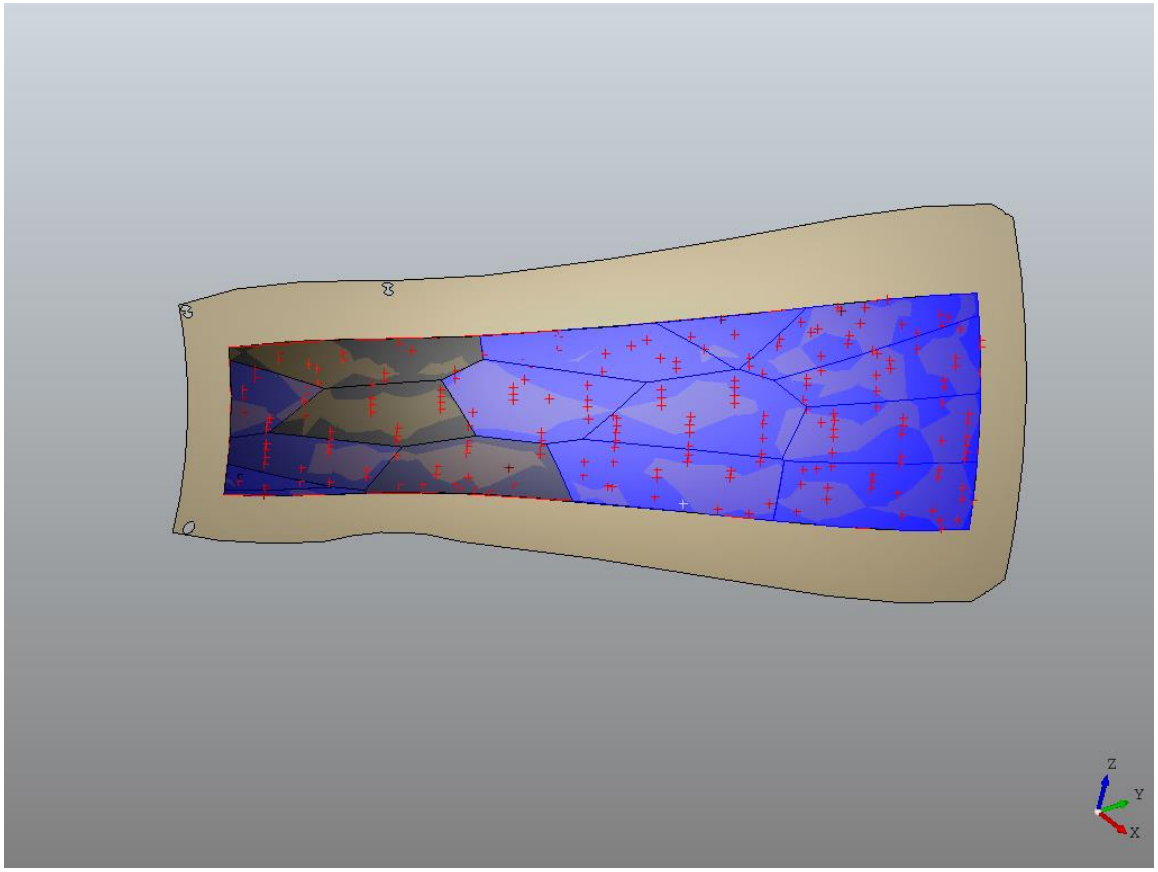


Figure 6.1: Clusters with Gaussian Curvature Displayed as Color Gradient

Each sample consisted of an input compiled from the average feature vectors in an element constructed from parameter clustering [Figure 6.1]. A response or ground truth value was derived from mapping overlaps onto the discretized element as demonstrated in Figure 6.2. One can also observe the defects from the ply underneath are also mapped to visualize defect stacking and propagation from one ply to another.

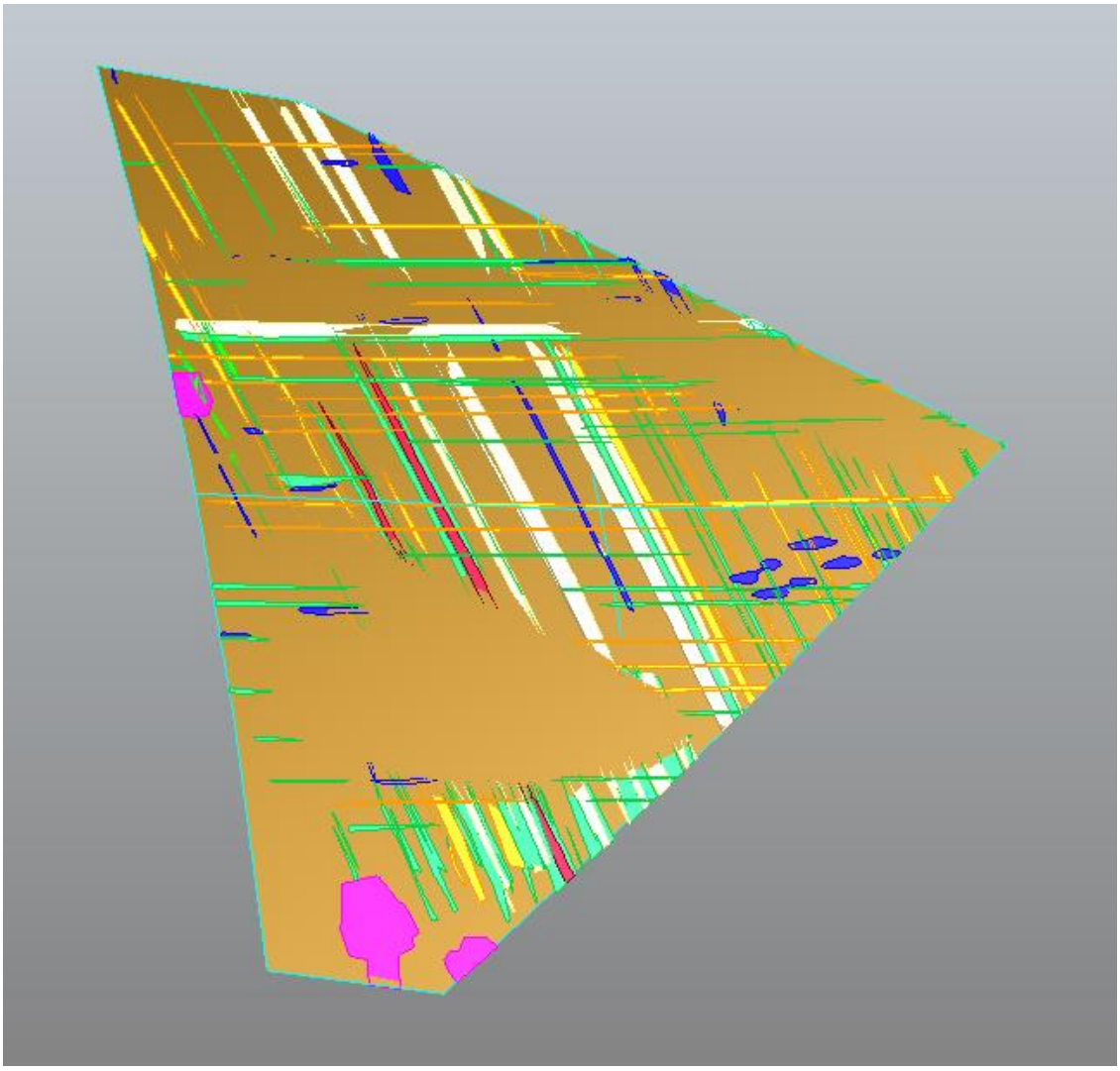

Figure 6.2: Defects Mapped onto a Single Discretized Element

A train-test split of 20% was made to give a large enough test sample size so as to be easily able to determine statistical significance. The split between training and testing

cases was determined randomly without bias toward any individual layup case. Constraints were enforced through the warping function approach outlined in Section 3.4.1.

## 6.3 OVERLAP PREDICTION PERFORMANCE

Three predictive models were compared for their accuracy in predicting the amount of overlap present in each sample. The three models consisted of raw VCP predictions using the geometry of the surface and the layup strategy, a standard neural network model, and the hybridized GPR model outlined in this document. The standard neural network was a simple 3-layer regression network with two 64 neuron hidden layers and a single output layer with a sigmoid activation function. Best performance was achieved with a single epoch of training over the data, with the output overfitting to the mean otherwise. Recall that the predicted quantity is the ratio of the surface area of the element to the surface area occupied by overlaps. Comparative results are noted in Table 6.1.

Table 6.1: Comparison of Predictive Accuracy Between VCP, Zero Mean GPR, and the Hybridized Model

| *Algorithm* | *Average Mean Squared Error* |
|---|---|
| *VCP* | 0.03450 |
| *Standard Neural Net* | 0.043942 |
| *Hybrid GPR* | 0.02712 |

Note that the Hybrid GPR model has better average predictive performance than both the VCP generate predictions and the neural network model. It can be concluded that much of the error in the VCP predictions comes from not being able to account for inter-course overlaps, stemming from the assumptions internal to VCP that tows do not wander

during layup. Similarly, the neural network does not properly account for geometry or layup strategy leaving a regression model that trends towards the upper extrema of the dataset. The Hybrid model appears to properly combine both of these information sources, calibrating the semi-accurate course-to-course predictions of VCP with the baseline potential for individual tow interactions to form defects.

### *6.3.1 Error Distributions*

Considering the average predictive behavior is an effective first step for a high level overview of model performance. However, the small percentages of areas occupied by overlaps leads one to question the magnitude and impact of the modeling approach. The reader can derive considerably more meaning in they consider how the errors are distributed. Figure 6.3 displays the usefulness of the hybrid and provides an explanation for the increase in performance. VCP has the potential to produce rare but extremely high error in overlap prediction. In the case of an underprediction, a result of this magnitude could lead to large areas of overlap to build upon and cause the part to violate dimensionality constraints. The hybrid model significantly reduces these extreme misses, and therefore can derive a strong use case in the evaluation of certain AFP manufacturing strategies with an eye towards defect reduction.

### *6.3.2 Mann-Whitney U Test and Showing Performance Improvement*

Let us take this level of analysis one step further and consider the possibility that prediction improvement in the hybridized model over VCP predictions can be explained by random stochastic system fluctuations. Given the magnitude of these error values is relatively close to one another in scale, further analysis must be conducted before definitively concluding that our hybridized approach is the superior one.

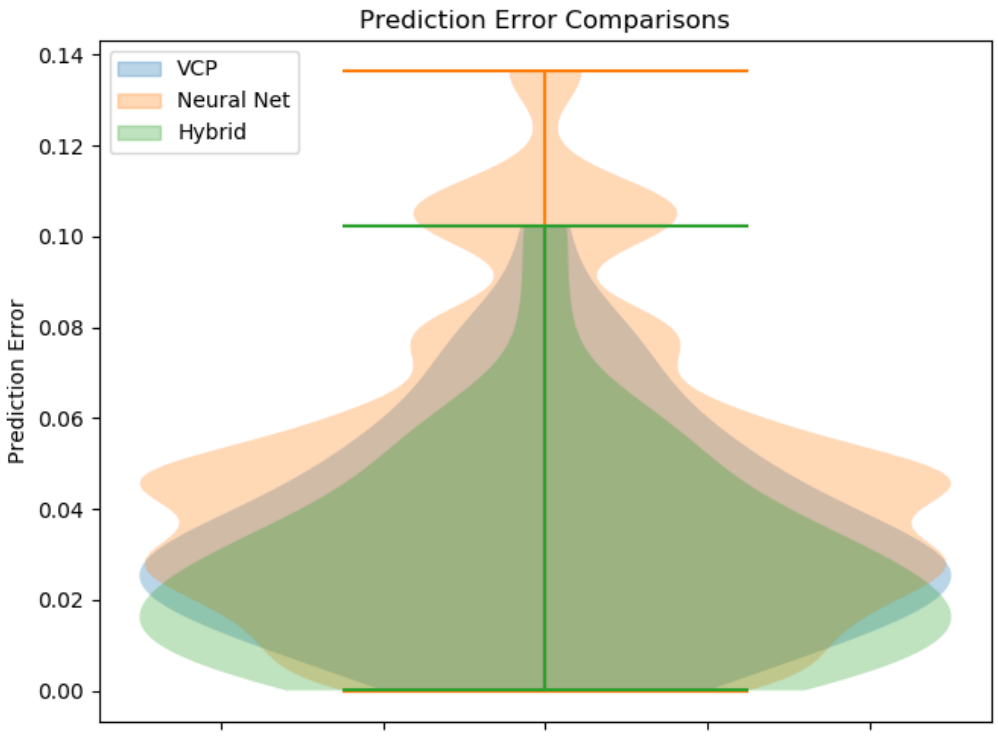


Figure 6.3: Test Error Distributions Between a Standard Neural Net, VCP, and the Hybrid Approach

A convenient statistical test to aide in answering this question is the Mann-Whitney U Test (MWUT) [159], [160]. In essence, the MWUT generalizes this by asking if two populations share a distribution. From this, a sub-alternative hypothesis can be constructed that concludes if the population mean is less than the mean of another population or a result of randomness; i.e. is the improvement in one prediction over another statistically significant. When applying this test criteria a p-value of $0.045 < .05$ is received. From this we can reject the null hypothesis that the improvement in prediction performance over VCP is strictly due to randomness.

## 6.4 PREDICTIONS FOR WRINKLES AND PUCKERS

Overlap predictions pose a nice mechanism for the presentation of the hybridized approach. The vast majority of defects predicted through VCP were overlaps, however there is still the potential to find use in the pure GPR model in the prediction of those defects that are primarily process driven. Bridging demonstrated a sparsity that made prediction difficult. However, wrinkles and puckers are highly process driven, and therefore some success can potentially be demonstrated in the prediction of the sum of the area occupied by wrinkles and puckers. Figure 6.4 shows the prediction error for the GPR model on the defect types.

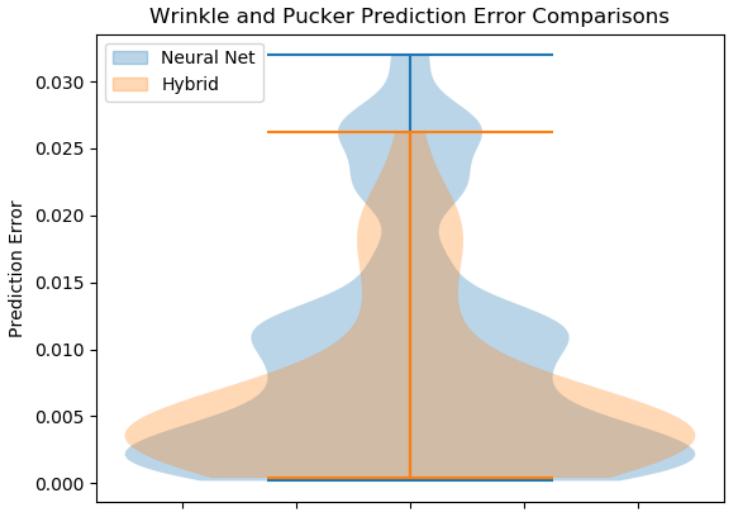


Figure 6.4: GPR and Neural Network Prediction Error for Combined Wrinkles and Puckers

One can also see that the prediction error is within rough 100% of the actual wrinkle and pucker values [Figure 6.5].

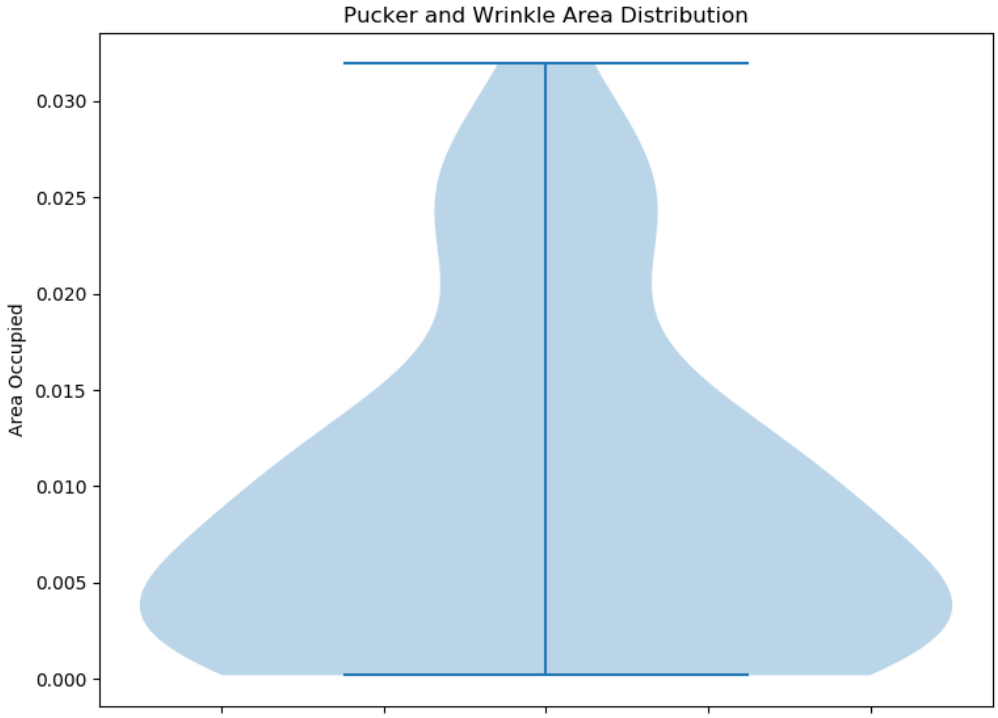


Figure 6.5: The Distribution of Wrinkle Defects in the Test Element Samples

## 6.5 NOTES ON IMPLEMENTATION

There are a few considerations for implementation that should be addressed for the keen practitioner looking to replicate this work. Firstly, one should be keen to invest a great deal of time in performing the hyperparameter tuning with Maximum Likelihood Estimation to properly set the prior covariance for the model. For variable mean functions, a drawback comes in the form of selecting a set of hyperparameter values that minimize the negative log likelihood across all points in the dataset. The variability in both the covariance values and the mean function prediction means that a limited number of free parameters shared amongst all covariance kernels may result in an over-constrained system, limiting the true ability to perform the minimization procedure. It was discovered

that this can be quite difficult for both traditional gradient descent algorithms and gradient-less approaches. The results outlined in this document are the function of both gradient-based optimization and some hand tunning on hyperparameter values to drive the negative log likelihood to an acceptable minimum. It may be wise for those continuing this work to consider a heteroskedastic approach that may liberate more free parameters such that the model is not overly constrained.

The GPR model itself was built in both TensorFlow (TF) using the TensorFlow Probabilities (TFP) [161], [162] package and a package meant specifically for building GPR models called GPFlow [163]. It is the author's opinion that better low-level control over the algorithm came from implementation in TFP, but rapid iteration of techniques was considerably better using GPFlow. GPFlow also has the capability of integrating with TF in a way that stackable approaches can be implemented with a relatively small effort. The final version of the GPR model was built entirely using GPFlow.

### *6.5.1 Run Time*

If one excludes the determination of hyperparameters to set the priors for the model and the initial mean function prediction through VCP, the GPR model discussed in this document generates the predictions on the overlaps test dataset in under a half a second when run on a 2013 Intel i7 CPU processor. As a note, VCP overlap and gap predictions generally takes one to several minutes to generate. When the complete hybirdized model is built on top of VCP, the additional time is essentially negligible.

# CHAPTER 7

# CONCLUSION

Throughout this document, the author has presented the justifications, underlying theory, peripheral considerations, and case study for the application of hybridized machine learning models to the prediction of AFP layup quality. It was the goal of this research to improve the time and accuracy of current quality estimations through the employment of using VCP to define nominal behavior and experimental data collected through an automated inspection system to define system response in a way that was more accurate than either of the two individual approaches. Hybridization was realized through the application of a GPR model with the mean function replaced by VCP defect predictions. Hypothesis testing was conducted to confirm an accuracy increase.

Furthermore, theoretical results were achieved by examining GPR in the explicit context of model hybridization. By assuming that the mean function is within some bound of the true function, one can obtain a very compact equation for the error bounds that can be expected for the hybridized GPR model. This is contrasted with a similar analysis, but with a constant mean function rather than the full hybridized approach. Wider applicability is shown for the hybrid model when compared to the constant mean function.

## 7.1 IMPACT OF WORK

It is hoped that the results of this work will further the adoption and democratization of AFP as a viable methodology for producing large structure across multiple industries. By better characterizing the potential for defect production when considering multiple

design, layup, and process parameters, one can hope to productionize and ready a given operation much more quickly. One can also note the potential of layering stochastic optimization on top of the modeling approach to directly optimize the entire manufacturing process. Reaching optimal states more quickly allows for manufacturing process to be employed more quickly with less manual resources required for complex testing.

It is also hoped that by achieving this result on a difficult to characterize process like AFP quality prediction, one could apply these approaches to other engineering problems. The theoretical results regarding error bounds in Section 3.5 should give practitioners much more confidence in how their models will perform over the complete expanse of the solution space. Controls and safety margins can easily be built from such analysis.

## 7.2 WORK IN THE GREATER CONTEXT OF AFP 4.0

The integration of inspection, process data collection, and process planning presented in this work is another step in the complete integration of each step of in the AFP toolchain. This mimic the movement across manufacturing generally referred to as Industry 4.0. The use of multi-source, multi-fidelity streams of data to improve the manufacturing process and increase automation is becoming a key theme in multiple industries, including aerospace, in the 21$^{st}$ century.

AFP 4.0 is an extension of this “Future Factories” concept to the AFP process specifically and the construction of large composite structures in general. This effort can be considered a piece of “Closing the AFP Loop”, where this data integration eventually leads to a completely circular AFP process cycle [Figure 7.1]. Rather than a linear chain of design informing manufacturing, which in turn informs product lifecycle and usage, a

circular AFP cycle implies that every step in the design and manufacturing of a structure with AFP can be both self-referential and pass data to every other step in the cycle. The author's work in this document enables a portion of this new AFP manufacturing paradigm by linking design, process parameters, inspection, and process planning together in a manner such that a well-designed optimization loop could potentially discover a pareto-front that informs design for manufacturing and how a structure can be best manufactured given a design.

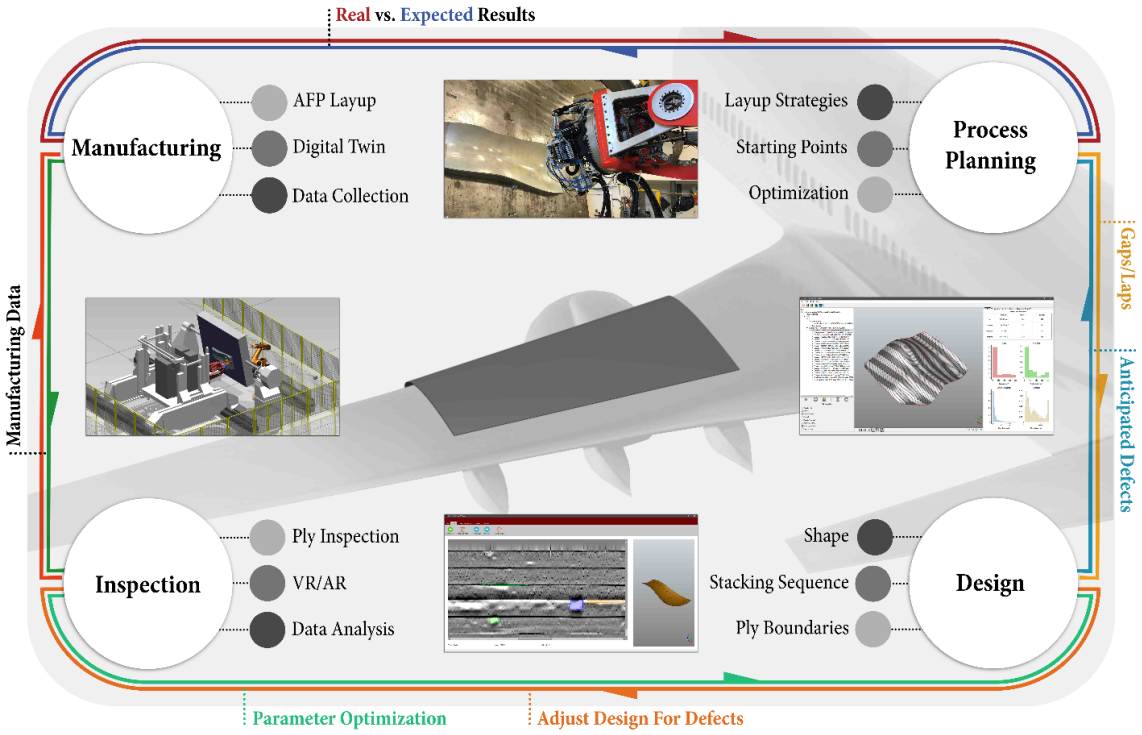


Figure 7.1: Closed AFP Cycle for AFP 4.0

## 7.3 FUTURE WORK

### *7.3.1 Identification of Optimal Processing Windows*

The advantage of using the GPR style modeling approach is that the mean function $\mu_n$ is analytically defined in the solution space. Therefore, it is possible to discover the global minima and maxima of the solution space with relatively straightforward gradient-

based solutions. Further, should the operator want to run at a specified manufacturing parameter, say speed, and identify other parameters that must adjust to counter the effects of increased speed, then this gradient following procedure becomes a standard constrained optimization problem. In other words, given a set of manufacturing parameters y, testing points $\boldsymbol{x}$, and model hyper parameters θ, the optimal set of manufacturing parameters y* can be defined as

$$y^* = argmax_y E[f(y)|f(\boldsymbol{x}), \theta] \quad 7.1$$

This defines a complete methodology to utilize the GPR hybrid model to quickly identify optimal processing windows under constrained or unconstrained process parameters with minimal experimental data. Given that the modeling approach outlined in this document is GPR, Bayesian Optimization (BO) represents an excellent candidate stochastic optimization algorithm [164].

Should the distribution prove not to be purely Gaussian, the extensions mentioned in the previous answers can easily be adapted to BO schemes as shown in several literature examples [165], [166] [83], [84]. It should be noted that both of these solutions have analytically discoverable process extensions that make their application to BO relatively straightforward. In effect, to utilize many of the acquisition functions, a mean and variance need to be determined.

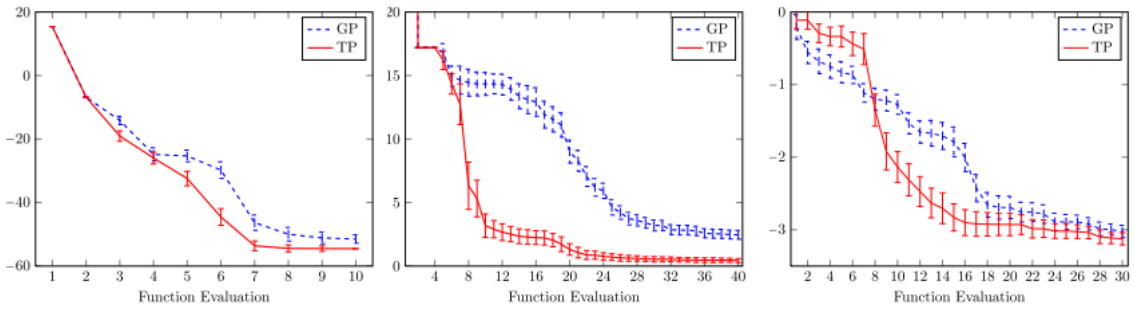


Figure 7.2: Bayesian Optimization Benchmarks Comparing the Number of Required Evaluations of a Traditional GPR Prior with a Student's-T Prior

In the case of a BO scheme based on Student's-t distribution, fat-tailed behavior can be explicitly modeled and has demonstrated strong performance on several benchmarks [Figure 7.2]. Further, the covariance can be analytically expressed, keeping much of the interpretability that is often encouraged through the use of the traditional Gaussian Process priors. For Deep Gaussian Processes, a composition of Gaussian Processes are assembled such that the representative power of the ensemble is greater than any one of the individual processes. This makes Deep Gaussian BO ideal for applications in fluid flow, heat transfer, and other non-stationary problems. This approach also appears to preserve some of the data-conserving properties of traditional Gaussian Processes.

Should the prior come from a distribution that can be shown to not have a clean analytic solution, then Markov Chain Monte Carlo method can be used to sample and numerically determine the prior. Unfortunately, this causes the data requirement to properly perform the BO to increase and therefore should be avoided if possible.

If defining a statistical process is impossible, there even exist potential applications from neural networks to the problem [167]. This process also leads to greater data requirements in order to properly construct these machine learning models, which the author is hoping to avoid through the creation of explicit statistical process modeling.

*7.3.2 An Alternative Experimental Approach*

It is the goal of these experiments to collect data and then demonstrate a working hybridized model for the prediction of defects in the AFP manufacturing process. Recall the set of features considered as input into the model as discussed in Section 3.2. Each feature needs to be identified and tracked in a spatio-temporal manner such that the individual feature points on the surface can be readily determined. To accomplish this, a manufacturing dataset equipped with material properties, machine parameters correlated to points on the layup, as well as inspection data must be built. Figure 7.3 shows how the testing procedure might work, with a testing loop on a two separate geometries. The dual geometry approach is intended to act as a potential avenue towards expanding the hybridized model to multiple machines. It is suggested the different machines may have small random fluctuations in defect production. By testing on a consistent flat panel, then a common part can be built between multiple machines. Over a large enough testing campaign, a slight augmentation to the mean function can be built such that

$$\mu = \mu_0 + \epsilon_f, \epsilon_f \sim D \tag{7.2}$$

Where $\epsilon_f$ is an error term based on the baseline defect production of the flat test part. This term can be determined through the assumption of a distribution D over the term. Therefore, the end result is a hierarchical Bayesian model with the embedded hybrid physics-data model.

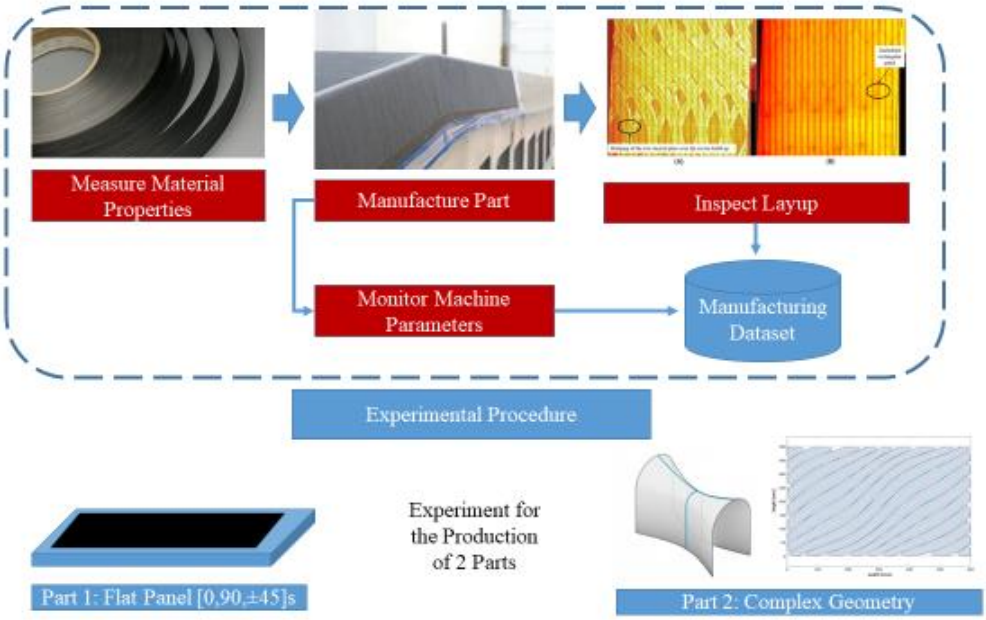


Figure 7.3: An Overview of the Experimental Approach

It is the goal of the experiment to validate over a wide distribution of each feature being keen not to bias the model heavily towards one side of the feature distribution. Therefore all of the potential features will be sampled from a uniform distribution. For the laminate design, each ply with be sampled uniformly from a selection of standard plies that would traditionally construct a quasi-isotropic part: [0,±45, 90]. A total of 15 plies will be used for the experiment, with a final stacking sequence of [0, -45, 0, 0, 0, 45, -45, 0, 90, -45, 90, 90, 90, 0, 0]. An initial 0° ply will be inserted at the beginning to provide a substrate for the first ply to adhere to. A 40% course width shift will be applied to each ply of the same fiber angle to prevent a build-up of defects through the thickness. Each ply will be fully repaired after layup and inspection.

Manufacturing parameters will also be selected uniformly per course. Each course will consist of a set speed (s), compaction (c), and heater power (p). The ranges over which the parameter values will be selected for each course can be seen in Equation 7.3. Note that

the speed setting is a percentage of the maximum layup speed. This is variable depending on the surface, so while each course will have a discrete speed setting, the overall speed of the layup will continuously vary across the length of the course.

$$c \in [60,150]lbs, s \in [10,100]\%, p \in [2,4]kW \quad 7.3$$

*7.3.3 Hierarchical Modeling for Multi-Machine and Multi-Material Systems*

It is difficult to directly transfer the parameters learned in a statistical model from one population set to the other. Neural networks can share weights with previously trained models to extend to new datasets through the application of transfer learning. However, GPRs nature as a non-parametric approach does not lend itself well to such an approach. Modeling approaches then would appear to consist of binning all populations together and learning a global model or placing each population in silos and learning individual models for each underlying population.

Multi-level Bayesian models allow us to overcome this by assuming that a given set of parameter in the model are shared between all subpopulations. A distribution is then placed over these parameters such that their distribution across the individual populations is reflected. A simple extension to Bayes' Rule can then be demonstrated such that the prediction for each subpopulation is made which weighting by the probability of the shared parameters are true values. This allows information from the binned population data to filter down into the predictions for each subpopulation.

This may be an appropriate way of addressing both the small stochastic variations between different machines and the large first-principles driven variation in differing materials systems. In both cases, information from previous trials with different machines and different material systems may be propagated forward into the development of new

models without having to create a general model accounting for every possible material system and every possible machine. This reduces the potential for dramatically increasing the number of features for a given GPR model. This prevents the development of a high modality dataset which, as discussed previously, is difficult for GPR approaches to account for.

It can also be shown that such a hierarchical approach to modeling the population distribution does not interfere with any stochastic optimization algorithms layered on top of the predictive model. This includes the Bayesian optimization approaches outlined in the section previous. The prior expressed is certainly significantly more complicated, and the integration of the model with a prior defined by stochastically distributed hyperparameters may need to be integrated using advanced sampling techniques such as Gibbs Sampling [168].

### *7.3.4 Mean Function Informed Covariance Predictions*

When expressing the degree of uncertainty in the model predictions, the covariances are entirely computed from past data. However, there may be an opportunity to better characterize the prediction uncertainty by also denoting how accurate the mean function is as a predictor by itself.

Consider a circumstance where a decision is required based on the uncertainty of the prediction. Suppose a hybridized model used a mean function with a perfect predictive power. Note that if this is the case, then the final predictive mean will default to the hybridized mean function. However, this perfect predictive accuracy is not reflected in the covariances of model, which would be computed as a function of the distance between the new test point and previous points in the dataset regardless of the strength of the mean

function. This could lead to conservative decisions, where final selected solutions are designed to stay close to previously evaluated points in the dataset rather than trusting the relative accuracy of the mean function.

Expressing this in a more formal manner, we would like to have the covariance prediction moderated by the mean function such that

$$\Sigma_n \left( x_k, \left( f(x_{1:n}) - \mu_0(x_{1:n}) \right) \right) \tag{7.4}$$

$$\Sigma_n = 0, where\ r^2(f(x_{1:n}), \mu_0(x_{1:n})) = 1 \tag{7.5}$$

$$\Sigma_n = \Sigma_n(x_k), where\ r^2(f(x_{1:n}), \mu_0(x_{1:n})) = 0 \tag{7.6}$$

In other words, where the mean function and the dataset are completely correlated, the covariances should be zero. Whereas if the mean function and the dataset are completely uncorrelated, then the covariances should revert back to the original covariance formulation expressed from just the data in the dataset.

### *7.3.5 Relaxing Element Independence Assumption*

As noted previously, when developing this model it was shown that by controlling the sizing of the element produced from the clustering algorithm one could create independence between elements; implying that conditions in one element could not influence the production of defects in another. This does not always hold and may be a contributing factor in the breakdown of the model at certain points. It may be beneficial to relax this assumption at some point and provide estimates including the defects in immediately adjacent cells.

There are some potential mechanisms to accomplish this including changing the underlying prior that the process is built upon. In other words, removing the gaussian from

GPR. Student's T and Cauchy processes have been well characterized in literature. In the case of the Student's T process, the author knows of a number of approaches that create regression algorithms from such a distribution. However, Student's T process, while more resistant to outlier behavior, still have a number of independence assumptions included in Gaussians that we are attempting to avoid. Cauchy distributions, without an expressible mean, are significantly more difficult and would likely require some complex new mathematics.

Capturing the "defect flux" [Figure 7.4] between cells might be another acceptable approach, where the defect production of adjacent cells is fed in as an additional feature. This strategy has a number of drawbacks, including increasing the number of features in a modeling strategy that fails on high-modality data. This also introduces features into the model that may not interreact in a smooth, closed-form manner with the current GPR formulation.

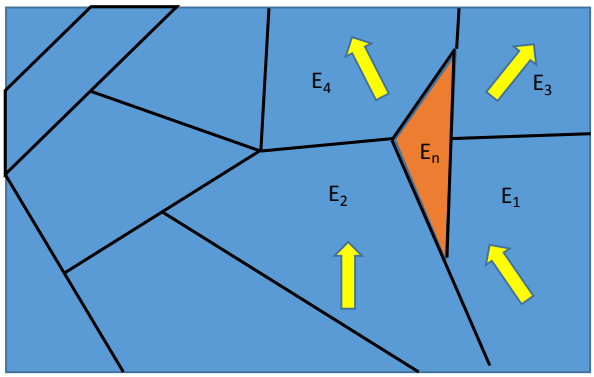


$$P(d, E_n) = P(d, E_n | E_1, E_2, E_3, E_4)$$

Figure 7.4: An Illustration of Defect Flux from Preceding and Following Elements

*7.3.6 A Comprehensive Planning Tool*

With the realization of an effective process to predict the behavior of the AFP layup system, one can consider a number of ways to incorporate the tool into integrated process

planning software. Traditional process planning software, such as VCP or Ingersoll ICPS cannot take into account process parameters in the ability to predict layup quality. A new software tool is needed to properly interact with these new features and give operators and machine programmers the ability to alter process parameter selection strategies to best fit the needs of the given project.

Such a tool would also need clean integration with inspection systems and have the ability to review and process data from multiple data sources on the machine. Databasing and long-term storage of each training sample, such that long term model accuracy could be increase over time, would also be a convenient function to accompany this software. One could also see how such a tool would likely need novel data visualization tools to review both inspection data and data collected through the machine and sensors. Scheduling and operations data likely could also play a role, with long term trends in quality across materials systems and machines being tracked in addition to production times by part.

In many ways, this reflects the long-term goals of the neXt Research team. Comprehensive tools build across the AFP toolchain can be integrated into one seamless system. The efforts by Halbritter with CAPP serve as an excellent roadmap for how such model and data integration could take place.

### *7.3.7 Prediction of Other Defects*

It is the author's opinion that the single most difficult cases for the application of the modeling approach outlined in this document is in gaps and overlaps from the perspective of learning relevant information from data. The next logical step is the application of this model paradigm to other, potentially even more process relevant, AFP

defects. Wrinkles, puckers, and bridging are areas that are ripe for continued development. All of these defect types are highly process dependent, indicating that large predictive performance gains can be achieved.

The difficulty in developing a hybrid model for these defect lies in the creation of a fast, semi-accurate analytical model to become the physics backbone of the hybrid approach. Bridging in particular has influence from both material tack, tow tension, and the geometry of the layup surface. If a rough calculation to indicate the probability of bridging from these factors can be constructed, the application of the hybrid model becomes trivial.

### *7.3.8 Expanding Analysis of Hybridized Error Bounds*

One could easily extend the analysis of error bounds from the hybridized scheme to other types of mean function error descriptions beyond symmetric error bounds. As mentioned previously, the expression is equally trivial to derive for biased error. Similarly, a probabilistic error description can also be easily supplemented. Gaussian error is also similarly simple to perform analysis with. What becomes interesting is where non-standard probability distributions are used for this estimation, such as truncated or bounded distributions. This would further improve expressiveness of the model error, with constrained error, average error, and the highest probability error values being estimated and further improving model understanding a visibility

# REFERENCES


[1] D. Bharath, B. Sandhya Rani, V. Saritha, P. Irshad Khan, and S. Kumar Chokka, "Tensile and erosion behaviour of medium calcined alumina microparticles on GFRP composites fabricated with vacuum bagging process," *Mater. Today Proc.*, no. xxxx, pp. 8–11, 2020.

[2] L. Nele, A. Caggiano, and R. Teti, "Autoclave Cycle Optimization for High Performance Composite Parts Manufacturing," *Procedia CIRP*, vol. 57, pp. 241–246, 2016.

[3] K. Yassin and M. Hojjati, "Processing of thermoplastic matrix composites through automated fiber placement and tape laying methods: A review," *J. Thermoplast. Compos. Mater.*, vol. 31, no. 12, pp. 1676–1725, 2018.

[4] G. Marsh, "Automating aerospace composites production with fibre placement," *Reinf. Plast.*, vol. 55, no. 3, pp. 32–37, 2011.

[5] K. C. Wu, B. K. Stewart, and R. A. Martin, "ISAAC advanced composites research testbed," in *The Second International Symposium on Automated Composites Manufacturing*, 2015.

[6] T. R. Brooks, J. R. R. A. Martins, and G. J. Kennedy, "High-fidelity aerostructural optimization of tow-steered composite wings," *J. Fluids Struct.*, vol. 88, pp. 122–147, 2019.

[7] A. Khani, M. M. Abdalla, Z. Gürdal, J. Sinke, A. Buitenhuis, and M. J. L. Van Tooren, "Design, manufacturing and testing of a fibre steered panel with a large cut-out," *Compos. Struct.*, vol. 180, pp. 821–830, 2017.

[8] F. J. van Zanten, C. Pupo, D. Barazanchy, and M. van Tooren, "Optimization of 3d curved fiber steered shells," in *AIAA Scitech 2019 Forum*, 2019.

[9] A. Marouene, P. Legay, and R. Boukhili, "Experimental and Numerical Investigation on the Open-Hole Compressive Strength of AFP Composites Containing Gaps and Overlaps," in *Journal of Composite Materials*, 2017, vol. 51, no. 26, pp. 3631–3646.

[10] F. Heinecke, W. van den Brink, and T. Wille, "Assessing the Structural Response of Automated Fibre Placement Composite Structures With Gaps and Overlaps By Means of Numerical Approaches," in *20th International Conference on Composite Materials*, 2015.

[11] C. Sacco, A. B. Radwan, R. Harik, and M. Van Tooren, "Automated Fiber Placement Defects: Automated Inspection and Characterization," *SAMPE 2018 Conf. Proceeding*, 2018.

[12] C. Sacco, A. B. Radwan, A. Anderson, R. Harik, and S. Carolina, "NDE Inspection of AFP Manufactured Cylinders Using and Intelligent Segmentation Algorithm," in *SAMPE 2020 Virtual Conference*, 2020.

[13] C. Sacco, A. Baz Radwan, T. Beatty, and R. Harik, "Machine learning based AFP inspection: A tool for characterization and integration," in *International SAMPE*

*Technical Conference*, 2019, vol. 2019–May.
[14] R. Harik, C. Saidy, S. J. Williams, Z. Gurdal, and B. Grimsley, "Automated fiber placement defect identity cards: cause, anticipation, existence, significance, and progression," in *SAMPE Conference Proceedings*, 2018.
[15] J. Moore, A. Colvin, S. Ghose, and B. Johnson, "Design for manufacturing: Laminate focused design and analysis tools for automated composites manufacturing," in *International SAMPE Technical Conference*, 2019.
[16] A. Kampker, H. Heimes, U. Bührer, C. Lienemann, and S. Krotil, "Enabling Data Analytics in Large Scale Manufacturing," *Procedia Manuf.*, vol. 24, pp. 120–127, 2018.
[17] C. Sacco, A. B. Radwan, T. Beatty, and R. Harik, "Machine Learning Based AFP Inspection : A Tool for Characterization and Integration," *SAMPE Conf. Proc.*, 2019.
[18] P. D. Juarez and E. D. Gregory, "In situ thermal inspection of automated fiber placement manufacturing," in *AIP Conference Proceedings*, 2019.
[19] E. D. Gregory and P. D. Juarez, "In-situ thermography of automated fiber placement parts," in *AIP Conference Proceedings*, 2018.
[20] C. Sacco *et al.*, "A Quantitative Evaluation of AFP Steered Courses Through Inspection," in *SAMPE 2020 Virtual Conference*, 2020.
[21] J. Schmidhuber, "Deep Learning in neural networks: An overview," *Neural Networks*. 2015.
[22] A. K. Jain, J. Mao, and K. M. Mohiuddin, "Artificial neural networks: A tutorial," *Computer*. 1996.
[23] C. Cortes and V. Vapnik, "Support-Vector Networks," *Mach. Learn.*, vol. 20, no. 3, pp. 273–297, 1995.
[24] K. Hornik, M. Stinchcombe, and H. White, "Multilayer feedforward networks are universal approximators," *Neural Networks*, vol. 2, no. 5, pp. 359–366, 1989.
[25] G. Bin Huang, Q. Y. Zhu, and C. K. Siew, "Extreme learning machine: Theory and applications," *Neurocomputing*, vol. 70, no. 1–3, pp. 489–501, 2006.
[26] M. L. Zhang and Z. H. Zhou, "ML-KNN: A lazy learning approach to multi-label learning," *Pattern Recognit.*, vol. 40, no. 7, pp. 2038–2048, 2007.
[27] J. Duchi, E. Hazan, and Y. Singer, "Adaptive Subgradient Methods for Online Learning and Stochastic Optimization," *JMLR*, 2011.
[28] A. for Computing Machinery *et al.*, "ADADELTA: An Adaptive Learning Rate Method," in *Proceedings of ACL-IJNLP 2015*, 2015.
[29] S. J. Reddi, S. Kale, and S. Kumar, "On the Convergence of Adam and Beyond," in *ICLR 2018*, 2018.
[30] A. Krizhevsky, I. Sutskever, and G. E. Hinton, "ImageNet Classification with Deep Convolutional Neural Networks," *Adv. Neural Inf. Process. Syst.*, pp. 1–9, 2012.
[31] I. Goodfellow *et al.*, "Generative Adversarial Nets," *Adv. Neural Inf. Process. Syst. 27*, pp. 2672–2680, 2014.
[32] D. Wang and J. Gu, "VASC: Dimension Reduction and Visualization of Single-cell RNA-seq Data by Deep Variational Autoencoder," *Genomics. Proteomics Bioinformatics*, no. xxxx, 2018.
[33] T. Kohonen, "The self-organizing map," *Neurocomputing*, vol. 21, no. 1–3, pp. 1–6, 1998.

[34] Y. Meng, J. Liang, F. Cao, and Y. He, “A new distance with derivative information for functional k-means clustering algorithm,” *Inf. Sci. (Ny).*, vol. 463–464, pp. 166–185, 2018.
[35] L. P. Kaelbling, M. L. Littman, and A. W. Moore, “Reinforcement learning: A survey,” *J. Artif. Intell. Res.*, 1996.
[36] X. Ou, Q. Chang, and N. Chakraborty, “Simulation study on reward function of reinforcement learning in gantry work cell scheduling,” *J. Manuf. Syst.*, vol. 50, no. November 2018, pp. 1–8, 2019.
[37] M. Riedmiller *et al.*, “Learning by Playing - Solving Sparse Reward Tasks from Scratch,” no. 2017, 2018.
[38] Y. Zhan, H. B. Ammar, and M. E. Taylor, “Theoretically-grounded policy advice from multiple teachers in reinforcement learning settings with applications to negative transfer,” *IJCAI Int. Jt. Conf. Artif. Intell.*, vol. 2016–Janua, no. 7540, pp. 2315–2321, 2016.
[39] K. Xia, C. Sacco, M. Kirkpatrick, R. Harik, and A. Bayoumi, “Virtual comissioning of manufacturing system intelligent control,” *SAMPE Conf. Proc.*, 2019.
[40] M. A. Franco and J. Bacardit, “Large-scale experimental evaluation of GPU strategies for evolutionary machine learning,” *Inf. Sci. (Ny).*, vol. 330, pp. 385–402, 2016.
[41] B. Krawczyk, “GPU-accelerated extreme learning machines for imbalanced data streams with Concept Drift,” *Procedia Comput. Sci.*, vol. 80, pp. 1692–1701, 2016.
[42] Y. Ma, N. Suda, Y. Cao, S. Vrudhula, and J. sun Seo, “ALAMO: FPGA acceleration of deep learning algorithms with a modularized RTL compiler,” *Integration*, vol. 62, no. August 2017, pp. 14–23, 2018.
[43] S. Liang, S. Yin, L. Liu, W. Luk, and S. Wei, “FP-BNN: Binarized neural network on FPGA,” *Neurocomputing*, vol. 275, pp. 1072–1086, 2018.
[44] T. Posewsky and D. Ziener, “Throughput optimizations for FPGA-based deep neural network inference,” *Microprocess. Microsyst.*, vol. 60, no. June 2017, pp. 151–161, 2018.
[45] C. K. H. Lee, “A review of applications of genetic algorithms in operations management,” *Eng. Appl. Artif. Intell.*, vol. 76, no. May, pp. 1–12, 2018.
[46] Z. Tian, Y. Yan, Y. Hong, F. Guo, J. Ye, and J. Li, “Improved genetic algorithm for optimization design of a three-dimensional braided composite joint,” *Compos. Struct.*, vol. 206, no. May, pp. 668–680, 2018.
[47] V. Venugopal and T. T. Narendran, “A genetic algorithm approach to the machine-component grouping problem with multiple objectives,” *Comput. Ind. Eng.*, vol. 22, no. 4, pp. 469–480, 1992.
[48] F. Safiyullah, S. A. Sulaiman, M. Y. Naz, M. S. Jasmani, and S. M. A. Ghazali, “Prediction on performance degradation and maintenance of centrifugal gas compressors using genetic programming,” *Energy*, vol. 158, pp. 485–494, 2018.
[49] P. J. Angeline, “Genetic programming: On the programming of computers by means of natural selection,” *Biosystems*, 2003.
[50] R. Poli and J. Koza, “Genetic programming,” in *Search Methodologies: Introductory Tutorials in Optimization and Decision Support Techniques, Second Edition*, 2014.
[51] J. R. Koza, “Survey of genetic algorithms and genetic programming,” 2002.

[52] B. Chopard and M. Tomassini, “Particle swarm optimization,” in *Natural Computing Series*, 2018.
[53] Eberhart and Yuhui Shi, “Particle swarm optimization: developments, applications and resources,” 2002.
[54] Y. Shi and R. C. Eberhart, “Empirical study of particle swarm optimization,” in *Proceedings of the 1999 Congress on Evolutionary Computation, CEC 1999*, 1999.
[55] R. Poli, J. Kennedy, and T. Blackwell, “Particle swarm optimization. An overview,” *Swarm Intell.*, 2007.
[56] M. A. de Oliveira, N. V. S. Araujo, D. J. Inman, and J. V. Filho, “Kappa-PSO-FAN based method for damage identification on composite structural health monitoring,” *Expert Syst. Appl.*, vol. 95, pp. 1–13, 2018.
[57] S. G. Pickering, K. Chatterjee, D. P. Almond, and S. Tuli, “LED optical excitation for the long pulse and lock-in thermographic techniques,” *NDT E Int.*, vol. 58, pp. 72–77, 2013.
[58] I. Jorge Aldave *et al.*, “Review of thermal imaging systems in composite defect detection,” *Infrared Phys. Technol.*, vol. 61, pp. 167–175, 2013.
[59] V. Kalyanavalli, T. K. A. Ramadhas, and D. Sastikumar, “Long pulse thermography investigations of basalt fiber reinforced composite,” *NDT E Int.*, vol. 100, no. December 2017, pp. 84–91, 2018.
[60] M. A. Caminero, I. García-Moreno, G. P. Rodríguez, and J. M. Chacón, “Internal damage evaluation of composite structures using phased array ultrasonic technique: Impact damage assessment in CFRP and 3D printed reinforced composites,” *Compos. Part B Eng.*, 2018.
[61] E. Sert, D. Tas, and A. Alkan, “Three stepped calibration of structured light system with adaptive thresholding for 3D measurements,” *Optik (Stuttg).*, vol. 126, pp. 5176–5181, 2015.
[62] S. Moustakidis, A. Anagnostis, P. Karlsson, and K. Hrissagis, “Non-destructive inspection of aircraft composite materials using triple IR imaging,” *IFAC-PapersOnLine*, vol. 49, no. 28, pp. 291–296, 2016.
[63] A. P. Chrysafi, N. Athanasopoulos, and N. J. Siakavellas, “Damage detection on composite materials with active thermography and digital image processing,” *Int. J. Therm. Sci.*, vol. 116, pp. 242–253, 2017.
[64] J. Y. Wu, S. Sfarra, and Y. Yao, “Sparse Principal Component Thermography for Subsurface Defect Detection in Composite Products,” *IEEE Trans. Ind. Informatics*, vol. 51, no. 24, pp. 855–860, 2018.
[65] E. Hu and F. Haifeng, “Surface profile inspection of a moving object by using dual-frequency Fourier transform profilometry,” *Optik (Stuttg).*, vol. 122, no. 14, pp. 1245–1248, 2011.
[66] A. Wronkowicz, K. Dragan, and K. Lis, “Assessment of uncertainty in damage evaluation by ultrasonic testing of composite structures,” *Compos. Struct.*, vol. 203, no. July, pp. 71–84, 2018.
[67] M. Jolly *et al.*, “Review of Non-destructive Testing (NDT) Techniques and their Applicability to Thick Walled Composites,” *Procedia CIRP*, vol. 38, pp. 129–136, 2015.
[68] M. Meng, Y. J. Chua, E. Wouterson, and C. P. K. Ong, “Ultrasonic signal classification and imaging system for composite materials via deep convolutional

neural networks," *Neurocomputing*, vol. 257, pp. 128–135, 2017.
[69] R. R. Hughes, B. W. Drinkwater, and R. A. Smith, "Characterisation of carbon fibre-reinforced polymer composites through radon-transform analysis of complex eddy-current data," *Compos. Part B Eng.*, vol. 148, no. May, pp. 252–259, 2018.
[70] H. Heuer *et al.*, "Review on quality assurance along the CFRP value chain - Non-destructive testing of fabrics, preforms and CFRP by HF radio wave techniques," *Compos. Part B Eng.*, vol. 77, pp. 494–501, 2015.
[71] M. Sharp, R. Ak, and T. Hedberg, "A survey of the advancing use and development of machine learning in smart manufacturing," *J. Manuf. Syst.*, 2018.
[72] M. Kuhl, T. Wiener, and M. Krauß, "Multisensorial self-learning systems for quality monitoring of carbon fiber composites in aircraft production," *Procedia CIRP*, vol. 12, pp. 103–108, 2013.
[73] M. Cacciola, S. Calcagno, F. C. Morabito, and M. Versaci, "Computational intelligence aspects for defect classification in aeronautic composites by using ultrasonic pulses," *IEEE Trans. Ultrason. Ferroelectr. Freq. Control*, vol. 55, no. 4, pp. 870–878, 2008.
[74] J. Brüning, B. Denkena, M. A. Dittrich, and T. Hocke, "Machine Learning Approach for Optimization of Automated Fiber Placement Processes," *Procedia CIRP*, vol. 66, pp. 74–78, 2017.
[75] H. D. Benítez, H. Loaiza, E. Caicedo, C. Ibarra-Castanedo, A. H. Bendada, and X. Maldague, "Defect characterization in infrared non-destructive testing with learning machines," *NDT E Int.*, vol. 42, no. 7, pp. 630–643, 2009.
[76] G. D'Angelo and S. Rampone, "Feature extraction and soft computing methods for aerospace structure defect classification," *Meas. J. Int. Meas. Confed.*, vol. 85, pp. 192–209, 2016.
[77] R. Marani, D. Palumbo, V. Renò, U. Galietti, E. Stella, and T. D'Orazio, "Modeling and classification of defects in CFRP laminates by thermal non-destructive testing," *Compos. Part B Eng.*, vol. 135, no. June 2017, pp. 129–141, 2018.
[78] P. Nazarko and L. Ziemiański, "Anomaly detection in composite elements using Lamb waves and soft computing methods," *Procedia Struct. Integr.*, vol. 5, pp. 131–138, 2017.
[79] R. J. O'Brien, J. M. Fontana, N. Ponso, and L. Molisani, "A pattern recognition system based on acoustic signals for fault detection on composite materials," *Eur. J. Mech. A/Solids*, vol. 64, pp. 1–10, 2017.
[80] D. Sammons, W. P. Winfree, E. Burke, and S. Ji, "Segmenting delaminations in carbon fiber reinforced polymer composite CT using convolutional neural networks," *AIP Conf. Proc.*, vol. 1706, 2016.
[81] J. Long, E. Shelhamer, and T. Darrell, "Fully convolutional networks for semantic segmentation," *Proc. IEEE Comput. Soc. Conf. Comput. Vis. Pattern Recognit.*, vol. 07–12–June, pp. 3431–3440, 2015.
[82] S. Wu, S. Zhong, and Y. Liu, "Deep residual learning for image steganalysis," *Multimed. Tools Appl.*, pp. 1–17, 2017.
[83] J. Luo, Z. Liang, C. Zhang, and B. Wang, "Optimum tooling design for resin transfer molding with virtual manufacturing and artificial intelligence," *Compos. - Part A Appl. Sci. Manuf.*, vol. 32, no. 6, pp. 877–888, 2001.
[84] I. de Jesus Gonzalez Ojeda, O. Patrouix, and Y. Aoustin, "Pressure based approach

for Automated Fiber Placement (AFP) with sensor based feedback loop and flexible component in the effector," *IFAC-PapersOnLine*, vol. 50, no. 1, pp. 794–799, 2017.
[85] S. R. Karnik, V. N. Gaitonde, J. C. Rubio, A. E. Correia, A. M. Abrão, and J. P. Davim, "Delamination analysis in high speed drilling of carbon fiber reinforced plastics (CFRP) using artificial neural network model," *Mater. Des.*, vol. 29, no. 9, pp. 1768–1776, 2008.
[86] A. Krishnamoorthy, S. Rajendra Boopathy, and K. Palanikumar, "Delamination prediction in drilling of CFRP composites using artificial neural network," *J. Eng. Sci. Technol.*, vol. 6, no. 2, pp. 191–203, 2011.
[87] P. Patel, S. Sheth, and T. Patel, "Experimental Analysis and ANN Modelling of HAZ in Laser Cutting of Glass Fibre Reinforced Plastic Composites," *Procedia Technol.*, vol. 23, pp. 406–413, 2016.
[88] A. G. Stamopoulos, K. I. Tserpes, and A. J. Dentsoras, "Quality assessment of porous CFRP specimens using X-ray Computed Tomography data and Artificial Neural Networks," *Compos. Struct.*, vol. 192, no. February, pp. 327–335, 2018.
[89] A. T. Seyhan, G. Tayfur, M. Karakurt, and M. Tanoğlu, "Artificial neural network (ANN) prediction of compressive strength of VARTM processed polymer composites," *Comput. Mater. Sci.*, vol. 34, no. 1, pp. 99–105, 2005.
[90] J. Spoerre, C. Zhang, B. Wang, and R. Parnas, "Integrated Product and Process Design for Resin Transfer Molded Parts," *Journal of Composite Materials*, vol. 32, no. 13. pp. 1244–1272, 1998.
[91] G. Golkarnarenji, M. Naebe, K. Badii, A. S. Milani, R. N. Jazar, and H. Khayyam, "Production of low cost carbon-fiber through energy optimization of stabilization process," *Materials (Basel).*, vol. 11, no. 3, pp. 1–13, 2018.
[92] J. A. D. Wilcox and D. T. Wright, "Towards pultrusion process optimisation using artificial neural networks," *J. Mater. Process. Technol.*, vol. 83, no. 1–3, pp. 131–141, 1998.
[93] J. Pfrommer, C. Zimmerling, J. Liu, L. Kärger, F. Henning, and J. Beyerer, "Optimisation of manufacturing process parameters using deep neural networks as surrogate models," *Procedia CIRP*, vol. 00, pp. 426–431, 2018.
[94] L. E. Lwakatare, A. Raj, I. Crnkovic, J. Bosch, and H. H. Olsson, "Large-scale machine learning systems in real-world industrial settings: A review of challenges and solutions," *Inf. Softw. Technol.*, vol. 127, no. May, 2020.
[95] D. Sculley *et al.*, "Hidden technical debt in machine learning systems," *Adv. Neural Inf. Process. Syst.*, vol. 2015–Janua, pp. 2503–2511, 2015.
[96] S. Lawrence, C. L. Giles, and A. C. Tsoi, "What Size Neural Network Gives Optimal Generalization? Convergence Properties ofBackpropagation," 1996.
[97] P. Jin, L. Lu, Y. Tang, and G. E. Karniadakis, "Quantifying the generalization error in deep learning in terms of data distribution and neural network smoothness," *Neural Networks*, vol. 130, pp. 85–99, 2020.
[98] L. Sun, H. Gao, S. Pan, and J. X. Wang, "Surrogate modeling for fluid flows based on physics-constrained deep learning without simulation data," *Comput. Methods Appl. Mech. Eng.*, vol. 361, p. 112732, 2020.
[99] Y. Zhu, N. Zabaras, P. S. Koutsourelakis, and P. Perdikaris, "Physics-constrained deep learning for high-dimensional surrogate modeling and uncertainty quantification without labeled data," *J. Comput. Phys.*, vol. 394, pp. 56–81, 2019.

[100] H. Wei, H. Bao, and X. Ruan, "Machine learning prediction of thermal transport in porous media with physics-based descriptors," *Int. J. Heat Mass Transf.*, vol. 160, p. 120176, 2020.
[101] T. Wu and J. Wang, "Global discovery of stable and non-toxic hybrid organic-inorganic perovskites for photovoltaic systems by combining machine learning method with first principle calculations," *Nano Energy*, vol. 66, no. August, p. 104070, 2019.
[102] J. Wu, H. Xiao, and E. Paterson, "Physics-informed machine learning approach for augmenting turbulence models: A comprehensive framework," *Phys. Rev. FLUIDS*, vol. 3, pp. 1–28, 2018.
[103] T. Bikmukhametov and J. Jäschke, "Combining machine learning and process engineering physics towards enhanced accuracy and explainability of data-driven models," *Comput. Chem. Eng.*, vol. 138, 2020.
[104] N. Hvala and J. Kocijan, "Design of a hybrid mechanistic/Gaussian process model to predict full-scale wastewater treatment plant effluent," *Comput. Chem. Eng.*, vol. 140, 2020.
[105] R. G. Nascimento, K. Fricke, and F. A. C. Viana, "A tutorial on solving ordinary differential equations using Python and hybrid physics-informed neural network," *Eng. Appl. Artif. Intell.*, vol. 96, no. October, p. 103996, 2020.
[106] C. Rao, H. Sun, and Y. Liu, "Physics-informed deep learning for incompressible laminar flows," *Theor. Appl. Mech. Lett.*, vol. 10, no. 3, pp. 207–212, 2020.
[107] R. Swischuk, L. Mainini, B. Peherstorfer, and K. Willcox, "Projection-based model reduction: Formulations for physics-based machine learning," *Comput. Fluids*, pp. 1–14, 2018.
[108] A. M. Lattimer, "Model Reduction of Nonlinear Fire Dynamics Models," 2016.
[109] C. Rao, H. Sun, and Y. Liu, "Physics-informed deep learning for incompressible laminar flows," *Theor. Appl. Mech. Lett.*, vol. 10, no. 3, pp. 207–212, 2020.
[110] S. Karimpouli and P. Tahmasebi, "Physics informed machine learning: Seismic wave equation," *Geosci. Front.*, 2020.
[111] R. Subramanian, R. R. Moar, and S. Singh, "White-box Machine learning approaches to identify governing equations for overall dynamics of manufacturing systems: A case study on distillation column," *Mach. Learn. with Appl.*, vol. 3, no. November 2020, p. 100014, 2021.
[112] S. L. Brunton, J. L. Proctor, J. N. Kutz, and W. Bialek, "Discovering governing equations from data by sparse identification of nonlinear dynamical systems," *Proc. Natl. Acad. Sci. U. S. A.*, vol. 113, no. 15, pp. 3932–3937, 2016.
[113] M. K. Kazi, F. Eljack, and E. Mahdi, "Data-driven modeling to predict the load vs. displacement curves of targeted composite materials for industry 4.0 and smart manufacturing," *Compos. Struct.*, vol. 258, no. August 2020, p. 113207, 2021.
[114] A. De Luca and F. Caputo, "A review on analytical failure criteria for composite materials," *AIMS Mater. Sci.*, vol. 4, no. 5, pp. 1165–1185, 2017.
[115] T. W. F. Exercise, *Failure Criteria in Fibre Reinforced Polymer Composites: TheWorld-Wide Failure Exercise*. 2004.
[116] M. J. Hinton, A. S. Kaddour, and P. D. Soden, "The world-wide failure exercise. Its origin, concept and content," in *Failure Criteria in Fibre-Reinforced-Polymer Composites*, 2004.

[117] H. Bao and G. Liu, “Progressive failure analysis on scaled open-hole tensile composite laminates,” *Compos. Struct.*, vol. 150, pp. 173–180, 2016.
[118] P. L. Chevalier, C. Kassapoglou, and Z. Gürdal, “Fatigue behavior of composite laminates with automated fiber placement induced defects- a review,” *Int. J. Fatigue*, vol. 140, no. April, p. 105775, 2020.
[119] A. Karpatne *et al.*, “Theory-guided data science: A new paradigm for scientific discovery from data,” *IEEE Trans. Knowl. Data Eng.*, vol. 29, no. 10, pp. 2318–2331, 2017.
[120] O. R. Abuodeh, J. A. Abdalla, and R. A. Hawileh, “Prediction of shear strength and behavior of RC beams strengthened with externally bonded FRP sheets using machine learning techniques,” *Compos. Struct.*, vol. 234, no. August 2019, p. 111698, 2020.
[121] G. X. Gu, C. T. Chen, and M. J. Buehler, “De novo composite design based on machine learning algorithm,” *Extrem. Mech. Lett.*, vol. 18, pp. 19–28, 2018.
[122] N. Zobeiry, J. Reiner, and R. Vaziri, “Theory-guided machine learning for damage characterization of composites,” *Compos. Struct.*, vol. 246, no. April, p. 112407, 2020.
[123] H. Wei, S. Zhao, Q. Rong, and H. Bao, “Predicting the effective thermal conductivities of composite materials and porous media by machine learning methods,” *Int. J. Heat Mass Transf.*, vol. 127, pp. 908–916, 2018.
[124] Q. Sun, Y. Liu, T. Chua, and B. Schiele, “Meta-Transfer Learning for Few-Shot Learning,” in *Proceedings of the IEEE/CVF Conference on Computer Vision and Pattern Recognition (CVPR)*, 2019, pp. 403–412.
[125] A. Behjat, C. Zeng, R. Rai, I. Matei, D. Doermann, and S. Chowdhury, “A physics-aware learning architecture with input transfer networks for predictive modeling,” *Appl. Soft Comput. J.*, vol. 96, p. 106665, 2020.
[126] R. Lichtinger, J. Lacalle, R. Hinterhölzl, U. Beier, and K. Drechsler, “Simulation and experimental validation of gaps and bridging in the automated fiber placement process,” *Sci. Eng. Compos. Mater.*, vol. 22, no. 2, pp. 131–148, 2015.
[127] R. Wehbe, “Modeling of Tow Wrinkling in Automated Fiber Placement based on Geometrical Considerations,” University of South Carolina, 2017.
[128] R. Wehbe, B. Tatting, R. Harik, Z. Gurdal, A. Halbritter, and A. Wanthal, “Tow-Path Based Modeling of Wrinkling During the Automated Fiber Placement Process,” *Compos. Adv. Mater. Expo 2017 (CAMX 2017)*, no. September 11-14, Florida, United States, 2017.
[129] R. Wehbe, B. Tatting, S. Rajan, R. Harik, M. Sutton, and Z. Gürdal, “Geometrical modeling of tow wrinkles in automated fiber placement,” *Compos. Struct.*, vol. 246, no. January, p. 112394, 2020.
[130] N. Bakhshi and M. Hojjati, “An experimental and simulative study on the defects appeared during tow steering in automated fiber placement,” *Compos. Part A Appl. Sci. Manuf.*, vol. 113, no. March, pp. 122–131, 2018.
[131] S. Rajan, M. A. Sutton, S. Sockalingam, W. McMakin, Z. Gurdal, and A. Kidane, “Simulations and experiments for automated fiber placement of prepreg slit tape: Wrinkle formation and fundamental observations,” *Compos. Part B Eng.*, vol. 201, no. August, p. 108287, 2020.
[132] V. Hutten *et al.*, “A Validation Study of a Physics-Based Tack Model for an

Automated Fiber Placement Process Simulation," in : *SAMPE Conference and Exhibition : conference, May 20-23, 2019, exhibition, May 21-22, 2019, Charlotte Convention Center, Charlotte, North Carolina : SAMPE North America*, 2018.
[133] C. Wohl *et al.*, "Tack measurements of prepreg tape at variable temperature and humidity," *CAMX 2017 - Compos. Adv. Mater. Expo*, vol. 2017–Decem, 2017.
[134] S. Rajan *et al.*, "Characterization of Mode I and Mode II traction–separation laws for cohesive separation of uncured thermoset tows," *Int. J. Fract.*, vol. 221, no. 1, pp. 25–38, 2020.
[135] R. Wehbe, B. Tatting, Z. Gürdal, and R. Harik, "Fiber Tow Deformations During Layup of Steered Paths Using Automated Fiber Placement Process," *SAMPE 2019 Conf. Exhib. Charlotte, North Carolina, US, 20 – 23 May 2019*, 2019.
[136] R. Wehbe, "Tow-Path Characterization for Automated Fiber Placement," Univeristy of South Carolina, 2017.
[137] R. Wehbe, B. Tatting, S. Rajan, R. Harik, M. Sutton, and Z. Gürdal, "Geometrical modeling of tow wrinkles in automated fiber placement," *Compos. Struct.*, vol. 246, no. January, p. 112394, 2020.
[138] J. Friedrich, J. Torzewski, and A. Verl, "Online Learning of Stability Lobe Diagrams in Milling," *Procedia CIRP*, vol. 67, pp. 278–283, 2018.
[139] A. Noevere, C. Collier, and R. Harik, "Integrated design and manufacturing analysis for Automated Fiber Placement structures," *SAMPE 2019 Conf. Exhib. Charlotte, North Carolina, US, 20 – 23 May 2019*, 2019.
[140] A. Beakou, M. Cano, J. B. Le Cam, and V. Verney, "Modelling slit tape buckling during automated prepreg manufacturing: A local approach," *Compos. Struct.*, vol. 93, no. 10, pp. 2628–2635, 2011.
[141] N. Bakhshi and M. Hojjati, "Time-dependent wrinkle formation during tow steering in automated fiber placement," *Compos. Part B Eng.*, vol. 165, pp. 586–593, May 2019.
[142] L. Swiler, M. Gulian, A. Frankel, C. Safta, and J. Jakeman, "A Survey of Constrained Gaussian Process Regression: Approaches and Implementation Challenges," *arXiv*, pp. 1–40, 2020.
[143] C. Sacco, A. B. Radwan, A. Anderson, R. Harik, and E. Gregory, "Machine Learning in Composites Manufacturing: A Case Study of Automated Fiber Placement Inspection," *Compos. Struct.*, vol. 250, no. May, p. 112514, 2020.
[144] R. Wehbe, C. Sacco, A. B. Radwan, M. Albazzan, and R. Harik, "Influence of process parameters in AFP fiber steering on cylinders : Constant curvature paths," *Compos. Part C Open Access*, vol. 2, no. September, 2020.
[145] M. Erwig, "The graph Voronoi diagram with applications," *Networks*, 2000.
[146] "Dijkstra's Algorithm," in *Encyclopedia of Operations Research and Management Science*, 2013.
[147] M. Robnik-Sikonja and I. Kononenko, "Theoretical and Empirical Analysis of ReliefF and RReliefF," *Mach. Lang.*, vol. 53, pp. 23–69, 2003.
[148] R. J. Urbanowicz, M. Meeker, W. La Cava, R. S. Olson, and J. H. Moore, "Relief-based feature selection: Introduction and review," *J. Biomed. Inform.*, vol. 85, no. January, pp. 189–203, 2018.
[149] A. T. Noevere and C. S. Collier, "Mapping AFP manufacturing data from VCP to hypersizer for stress analysis and optimization," in *AIAA/ASCE/AHS/ASC*

*Structures, Structural Dynamics, and Materials Conference, 2018*, 2018.
[150] A. Brasington, C. Sacco, J. Halbritter, and C. Sacco, "Automated Fiber Placement: A Review of History, Current Technologies, and Future Paths Forward," *Compos. Part C Open Access*, p. 100182, 2021.
[151] J. Jiang, Y. He, H. Wang, and Y. Ke, "Modeling and experimental validation of compaction pressure distribution for automated fiber placement," *Compos. Struct.*, vol. 256, no. October 2020, p. 113101, 2021.
[152] R. Engelhardt, R. Irmanputra, K. Brath, N. Aufenanger, and K. Drechsler, "Thermoset Prepreg Compaction during Automated Fiber Placement and Vacuum Debulking," *Procedia CIRP*, vol. 85, pp. 153–158, Jan. 2019.
[153] J. Cheng, D. Zhao, K. Liu, Y. Wang, and H. Chen, "Modeling and impact analysis on contact characteristic of the compaction roller for composite automated placement," *J. Reinf. Plast. Compos.*, vol. 37, no. 23, pp. 1418–1432, 2018.
[154] C. Maple, "Geometric design and space planning using the marching squares and marching cube algorithms," in *Proceedings - 2003 International Conference on Geometric Modeling and Graphics, GMAG 2003*, 2003.
[155] C. Sacco, A. B. Radwan, R. Harik, and M. Van Tooren, "Automated fiber placement defects: Automated inspection and characterization," in *International SAMPE Technical Conference*, 2018, vol. 2018–May.
[156] C. Sacco *et al.*, "On the effect of manual rework in AFP quality control for a doubly-curved part," *Compos. Part B Eng.*, 2021.
[157] Z. Zhang, Q. Liu, and Y. Wang, "Road Extraction by Deep Residual U-Net," *IEEE Geosci. Remote Sens. Lett.*, 2018.
[158] D. Duque-Arias *et al.*, "On power jaccard losses for semantic segmentation," in *VISIGRAPP 2021 - Proceedings of the 16th International Joint Conference on Computer Vision, Imaging and Computer Graphics Theory and Applications*, 2021.
[159] Laerd Statistics, "Mann-Whitney U test using SPSS Statistics.," *Stat. tutorials Softw. Guid.*, 2015.
[160] E. U. Oti, M. O. Olusola, and P. A. Esemokumo, "Statistical Analysis of the Median Test and the Mann-Whitney U Test," *Int. J. Adv. Acad. Res.*, 2021.
[161] A. Fanfarillo, "Quantifying uncertainty in source term estimation with tensorflow probability," in *Proceedings of UrgentHPC 2019: 1st International Workshop on HPC for Urgent Decision Making - Held in conjunction with SC 2019: The International Conference for High Performance Computing, Networking, Storage and Analysis*, 2019.
[162] B. Pang, E. Nijkamp, and Y. N. Wu, "Deep Learning With TensorFlow: A Review," *Journal of Educational and Behavioral Statistics*. 2020.
[163] A. G. D. G. Matthews *et al.*, "GPflow: A Gaussian Process Library using TensorFlow," *J. Mach. Learn. Res.*, 2017.
[164] P. I. Frazier, "A Tutorial on Bayesian Optimization," no. Section 5, pp. 1–22, 2018.
[165] A. Hebbal, L. Brevault, M. Balesdent, E.-G. Talbi, and N. Melab, "Bayesian Optimization using Deep Gaussian Processes," 2019.
[166] A. Shah, A. G. Wilson, and Z. Ghahramani, "Bayesian Optimization using Student-t Processes," no. 2, pp. 1–5, 2014.
[167] J. T. Springenberg, A. Klein, S. Falkner, and F. Hutter, "Bayesian optimization with Robust Bayesian neural networks," *Adv. Neural Inf. Process. Syst.*, no. Section 4,

pp. 4141–4149, 2016.
[168] P. Resnik, P. Resnik, E. Hardisty, and E. Hardisty, “Gibbs Sampling for the Uninitiated,” *Umiacs.Umd.Edu*, 2009.

# APPENDIX A

## A.1 PARAMETERS FOR CURVATURE EXPERIMENTS

Table A.1: The Full Testing Set for Constant Curvature Courses

| Course # | Radius (mm) | S (%) | P (N) | T (V) |
|---|---|---|---|---|
| 130 | 1270 | 30 | 600 | 150 |
| 131 | 1270 | 50 | 445 | 170 |
| 132 | 1270 | 100 | 445 | 150 |
| 133 | 1270 | 50 | 445 | 170 |
| 134 | 1270 | 100 | 300 | 170 |
| 135 | 1270 | 100 | 600 | 170 |
| 136 | 1270 | 200 | 600 | 170 |
| 137 | 1270 | 20 | 750 | 170 |
| 138 | 1270 | 20 | 445 | 170 |
| 139 | 635 | 30 | 600 | 170 |
| 140 | 635 | 20 | 600 | 170 |
| 141 | 635 | 10 | 600 | 150 |
| 142 | 635 | 10 | 600 | 150 |
| 143 | 635 | 10 | 750 | 170 |
| 144 | 635 | 20 | 750 | 170 |
| 145 | 635 | 100 | 750 | 190 |

| | | | | |
|---|---|---|---|---|
| 146 | 635 | 30 | 750 | 180 |
| 147 | 635 | 100 | 750 | 190 |
| 149 | 318 | 10 | 445 | 170 |
| 150 | 318 | 10 | 300 | 170 |
| 151 | 318 | 10 | 178 | 170 |
| 152 | 318 | 50 | 445 | 180 |
| 153 | 318 | 50 | 445 | 150 |
| 154 | 318 | 100 | 445 | 180 |
| 155 | 318 | 6 | 445 | 150 |

## A.2 RRELIEFF VALUES FOR STEERING EXPERIMENTS

Table A.2: RReliefF Quality Metris for Radius ∞

| *Parameter* | *Total Defects* | *Out-of-Plane* | *In-Plane* |
|---|---|---|---|
| *Pressure* | $3.06*10^{-4}$ | $5.20*10^{-4}$ | $7.44*10^{-4}$ |
| *Temperature* | $1.26*10^{-3}$ | $9.99*10^{-4}$ | $1.21*10^{-3}$ |
| *Feedrate* | $-9.89*10^{-5}$ | $-6.24*10^{-5}$ | $1.19*10^{-4}$ |

Table A.3: RReliefF Quality Metrics for Radius 1270mm

| *Parameter* | *Total Defects* | *Out-of-Plane* | *In-Plane* |
|---|---|---|---|
| *Pressure* | $5.57*10^{-3}$ | $4.99*10^{-3}$ | $3.84*10^{-3}$ |
| *Temperature* | $1.48*10^{-2}$ | $6.38*10^{-3}$ | $2.25*10^{-2}$ |
| *Feedrate* | $1.84*10^{-4}$ | $1.36*10^{-4}$ | $1.76*10^{-4}$ |

Table A.4: RReliefF Quality Metrics for Radius 635mm

| *Parameter* | *Total Defects* | *Out-of-Plane* | *In-Plane* |
|---|---|---|---|
| *Pressure* | $-2.48*10^{-5}$ | $-5.49*10^{-5}$ | $1.24*10^{-4}$ |
| *Temperature* | $1.91*10^{-4}$ | $1.14*10^{-4}$ | $3.50*10^{-4}$ |
| *Feedrate* | $-1.71*10^{-4}$ | $-9.67*10^{-5}$ | $-4.73*10^{-5}$ |

Table A.5: RReliefF Quality Metrics for Radius 318mm

| *Parameter* | *Total Defects* | *Out-of-Plane* | *In-Plane* |
|---|---|---|---|
| *Pressure* | 0 | 0 | 0 |
| *Temperature* | $1.33*10^{-3}$ | $4.28*10^{-4}$ | $4.00*10^{-4}$ |
| *Feedrate* | $-9.15*10^{-5}$ | $-3.75*10^{-7}$ | $-9.12*10^{-5}$ |

## A.3 DETAILS OF RRELIEFF ALGORITHM

**Algorithm A.1: RReliefF for Regression Feature Ranking**

**Data:** A vector of features *R* and response values *τ(x)*

**Result:** Vector W of estimations of the qualities of each feature A

$\boldsymbol{N_{dC}, N_{dA}[A], N_{dC\&dA}[A], W[A] \rightarrow 0}$;

**for** i = 1 to m **do**

get random instance $R_i$

select k instances $I_j$ nearest to $R_i$

**for** j = 1 to k **do**

$\boldsymbol{N_{dC} \rightarrow N_{dC} + diff(\tau, R_i, I_j)d(i,j)}$

**for** A = 1 to a **do**

$\boldsymbol{N_{dA}[A] \rightarrow N_{dA}[A] + diff(A, R_i, I_j)d(i,j)}$

$\boldsymbol{N_{dC\&dA}[A] \rightarrow N_{dC\&dA}[A] + diff(\tau, R_i, I_j)diff(A, R_i, I_j)d(i,j)}$

**for** A= 1 to a **do**

$\boldsymbol{W[A] = \frac{N_{dC\&dA}[A]}{N_{dC}} - \frac{N_{dA}[A] - N_{dC\&dA}[A]}{m - N_{dC}}}$

*diff* is a generalized distance function. In the case of the research outlined in Chapter 4it is set to

$$diff(F,R,I) = \begin{cases} 0 & |F[R] - F[I]| = 0 \\ 1 & |F[R] - F[I]| \geq \max(F) - \min(F) \\ \dfrac{|F[R] - F[I]|}{\max(F) - \min(F)} & otherwise \end{cases} \quad \text{A.1}$$